ENGINEERING GEOLOGICAL INVESTIGATION OF EARTHQUAKE-INDUCED GROUND DAMAGE AND TENSILE CHARACTERISTICS OF LOESS-COLLUVIUM SOILS, EASTERN HILLSBOROUGH VALLEY, CHRISTCHURCH

A thesis submitted in partial fulfilment of the requirements for the Degree

of Master of Science in Engineering Geology

at the University of Canterbury

by

Grace C. O'Sullivan

University of Canterbury

2015

Abstract

Following the M_w 6.2 Christchurch Earthquake on 22 February 2011, extensive ground cracking in loessial soils was reported in some areas of the Port Hills, southeast of central Christchurch. This study was undertaken to investigate the mechanisms of earthquake-induced ground damage on the eastern side of the Hillsborough Valley. A zone of extensional cracking up to 40m wide and 600m long was identified along the eastern foot-slope, accompanied by compression features and spring formation at the toe of the slope.

An engineering geological and geomorphological model was developed for the eastern Hillsborough Valley that incorporates geotechnical investigation data sourced from the Canterbury Geotechnical Database (CGD), the findings of trenching and seismic refraction surveying carried out for this research, and interpretation of historical aerial photographs. The thickness and extent of a buried peat swamp at the base of the slope was mapped, and found to coincide with significant compression features. Ground cracking was found to have occurred entirely within loess-colluvium and to follow the apices of pre-1920s tunnel-gully fan debris at the southern end of the valley.

The ground-cracking on the eastern side of the Hillsborough Valley is interpreted to have formed through tensile failure of the loess-colluvium. Testing was carried out to determine the tensile strength of Port Hills loess colluvium as a function of water content and density, in order to better understand the occurrence and distribution of the observed ground cracking. A comprehensive review of the soil tensile strength testing literature was undertaken, from which a test methodology was developed. Results show remoulded loess-colluvium to possess tensile strength of 7 - 28 kPa across the range of tested moisture contents (10-15%) and dry densities (1650-1900kg/m^3). A positive linear relationship was observed between tensile strength and dry density, and a negative linear relationship between moisture content and tensile strength.

The observed ground damage and available geotechnical information (inclinometer and piezometer records provided by the Earthquake Commission) were together used to interpret the mechanism(s) of slope movement that occurred in the eastern Hillsborough Valley. The observed ground damage is characteristic of translational movement, but without the development of lateral release scarps, or a basal sliding surface - which was not located during drilling. It is hypothesised that shear displacement has been accommodated by multiple slip surfaces of limited extent within the upper 10m of the slope.

Movement has likely occurred within near-saturated colluvial units that have lost strength during earthquake shaking. The eastern Hillsborough Valley is considered to be an 'incipient translational slide', as both the patterns of damage and shearing are consistent with the early stages of such slide development.

Sliding block analysis was utilised to understand how the eastern Hillsborough Valley may perform in a future large magnitude earthquake. Known cumulative displacements of ~0.3m for eastern Hillsborough Valley during the 2010-2011 Canterbury Earthquake Sequence were compared with modelled slope displacements to back-analyse a lower-bound yield acceleration of 0.2 - 0.25g. Synthetic broadband modelling for future Alpine and Hope Fault earthquakes indicates PGAs of approximately 0.08g for soil sites in the Christchurch area, as such, slope movement is unlikely to be reactivated by an Alpine Fault or Hope Fault earthquake. This does not take into account the possible role of strength loss due to excess pore pressure that may occur during these future events.

Acknowledgements

I have been very fortunate to receive the help of many kind people throughout the duration of this thesis. In particular, I would like to thank:

David Bell for his time, advice, encouragement, and for not holding back with the red pen.

Barry McDowell for his expertise and facilitating access to data.

The technical staff at the University of Canterbury, including Cathy Higgins, Matt Cockroft and Janet Brehaut, for their help with everything laboratory and field work related.

Stefan Winkler, for his good humour and for his efficient coordination.

Residents of the Hillsborough Valley who have allowed me on to their land. In particular Stephen Beuzenberg, not only for access to his land but for his support, enthusiasm and encouragement.

Phil Boudreau and Mike Finnemore of Southern Geophysical, for their considerable help with seismic surveying and modelling

Noel Win, James Cowlyn, Jono Mukhtar, Tim Jones and Clem Gibbons for their help with digging holes and sledgehammering.

My office mates – Andrew Walsh, Ryan Tutbury, Joe Cant and Mitch Green - who have supported and distracted me in equal measure throughout the course of this thesis.

Jules, for her support throughout and particularly towards the end.

Mum and Dad for their support and encouragement throughout all of my years of university study, and for understanding when I would forget to call.

My partner Michael, whom I couldn't have done it without.

Table of Contents

List of Figures

List of Tables

1 Introduction

1.1 Project background

Christchurch City is located on the east coast of the South Island of New Zealand (Figure 1.1), occupying some 200 sq. km of the Canterbury Plains and Banks Peninsula (Christchurch City Council 2013). The Mw7.1 Darfield Earthquake occurred at 4.35am on 4 September 2010, 40km west and inland of Christchurch City. Liquefaction and lateral spreading caused extensive damage to the Christchurch built environment, particularly within the low lying coastal suburbs east of Christchurch CBD and in Kaiapoi, 20km north of central Christchurch (Cubrinovski et al. 2010). The ensuing earthquake sequence generated three aftershocks of Mw 5.9 or greater, with the 22 February 2011 Mw 6.2 aftershock causing the greatest damage and loss of life (185 fatalities). The Port Hills suburbs, located on the northern rim of Banks Peninsula, were severely impacted by rockfall, cliff collapse and landsliding during the February 2011, June 2011 and December 2011 aftershocks. Rockfall caused five fatalities in the Port Hills, and hundreds of houses were damaged by rockfall, cliff collapse and ground cracking (Dellow et al. 2011).

In the days following the February 2011 earthquake, emergency response efforts in the Port Hills were initiated by Urban Search and Rescue (USAR) geotechnical specialists, the Port Hills Geotechnical Group (PHGG), and the GNS Science Landslide Response Team. The locations, extent and severity of the different types of ground failure were rapidly determined through aerial and ground reconnaissance, followed by systematic mapping. Buildings at risk of being impacted by rockfall and/or cliff collapse were evacuated and ground damage in other areas, deemed lower risk, was closely monitored (Dellow et al. 2011).

This thesis investigates the ground damage that occurred in the Hillsborough Valley of the Port Hills, during and following the 22 February 2011 earthquake. A zone of extensional cracking up to 40m wide and 600m long appeared along the lower part of the eastern slope, accompanied by compression features near the valley floor. There were no fatalities or injuries arising from the ground damage in the Hillsborough Valley, or from similar deformation in the adjacent valleys. The primary impact of the cracking and compression was to cause damage to structures and services, necessitating demolition/ replacement or repair. The aim of this thesis is to build an understanding of the different geological and geotechnical factors that have contributed to the observed ground damage through field investigation,

laboratory testing and numerical modelling. One aspect of the observed ground damage – extensional cracking – was further explored through development of a test procedure to measure the tensile strength and tensile failure characteristics of Port Hills loess-colluvium soil.

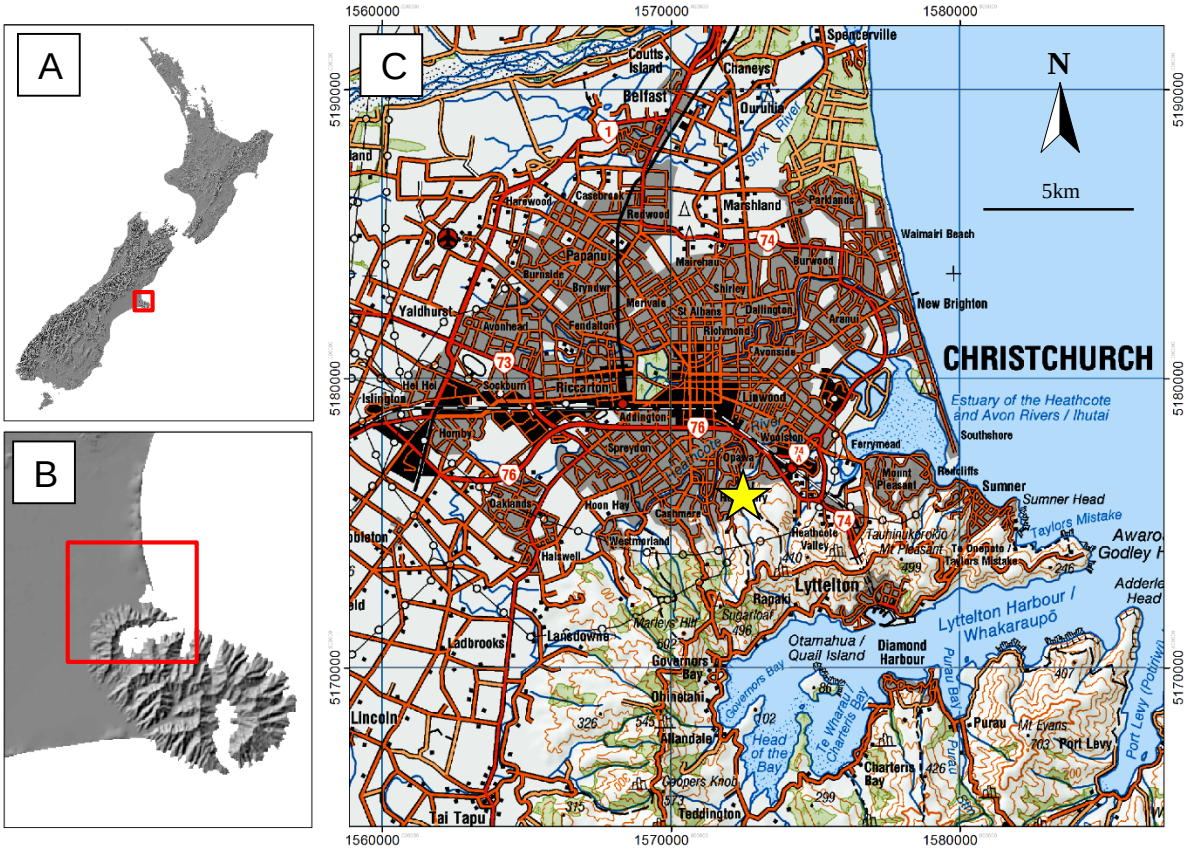

Figure 1.1: Christchurch, New Zealand. Location of the Hillsborough Valley is shown by the yellow star.

1.2 Thesis objectives

This research was undertaken to investigate the factors and mechanisms of earthquake-induced ground damage on the eastern side of the Hillsborough Valley. Specific objectives of this thesis have been to:

- Develop a detailed engineering geological and geomorphological model for the eastern side of the Hillsborough Valley.
- Research, develop a test methodology suitable for measuring the tensile strength of Port Hills loess colluvium, and undertake tensile strength testing of Port Hills loess colluvium.
- Discuss likely failure mechanisms for the eastern side of the Hillsborough Valley, through interpretation of ground damage, geotechnical data and the results of soil tensile strength testing.
- Evaluate and discuss seismic slope performance through application of simple sliding block analyses.

1.3 Geological setting

Christchurch City is located on the Pegasus Bay Coast of the Canterbury Plains, south of the Waimakariri River and at the northern margin of Banks Peninsula (Figure 1.2).

The Canterbury region is underlain by Triassic-age Torlesse Supergroup rocks, consisting of sandstone (greywacke) and mudstone (argillite) (Forsyth et al. 2008). Collision of the Australian and Pacific Plates from the early Miocene (the Kaikoura Orogeny) is responsible for the uplift of basement Torlesse to form the Southern Alps. Plate convergence is largely accommodated by the Alpine Fault to the west of the Canterbury region, and the Marlborough Fault system to the north (Stirling et al. 2008). The remaining component of plate motion is taken up by dextral strike-slip and reverse faulting across the central and southern parts of the Canterbury region (Stirling et al. 2008).

Occurring at the same time as mountain building was the emplacement of the Lyttelton Volcanic Complex (11 – 9.7Ma), followed by Akaroa Volcanic Complex (9.3 – 8Ma) to form what is now known as Banks Peninsula. Lyttelton (northwest) and Akaroa (southeast) are thought to have been built on a NW-SE trending Torlesse Supergroup horst (Ring & Hampton 2012). Volcanism was primarily basaltic, with limited intrusion of trachytic magmas (Ring & Hampton 2012). As volcanic activity waned in the late Miocene, the flanks of the cones were extensively eroded by radial and cone-controlled drainage systems, with the main phase of erosion occurring over a period of 1.5 to 2 million years (Bell & Trangmar 1987; Hampton 2010). The morphology of both volcanoes is discernible from digital elevation models (DEMs) and aerial photographs (Figure 1.1B). Both calderas were breached by the sea during the present interglacial and now form Lyttelton and Akaroa Harbours, respectively (Bell & Trangmar 1987).

The Canterbury Plains are a series of overlapping gravel fans deposited by eastward flowing braided-river systems in the late Quaternary (Brown et al. 1995). The Plains cover an area 160km long and up to 60km wide, with exploration wells across Canterbury encountering gravel thicknesses of up to 500m. The alluvium infills a tectonic depression, made possible by the rate of deposition exceeding the rate of subsidence (Brown & Weeber 1994). Originally an island at the western end of the Chatham Rise, Banks Peninsula was connected to the South Island by progressive deposition of alluvial gravels sometime in the early Pleistocene. Quaternary climate fluctuations mean outwash gravels interfinger with marine and marginal marine sediments below and offshore of Christchurch City. Sea level stabilised at its current level 6500 years ago; since that time the coastline has prograded outward 14km to its present position, at a rate of approximately 2m/yr (Brown et al. 1995).

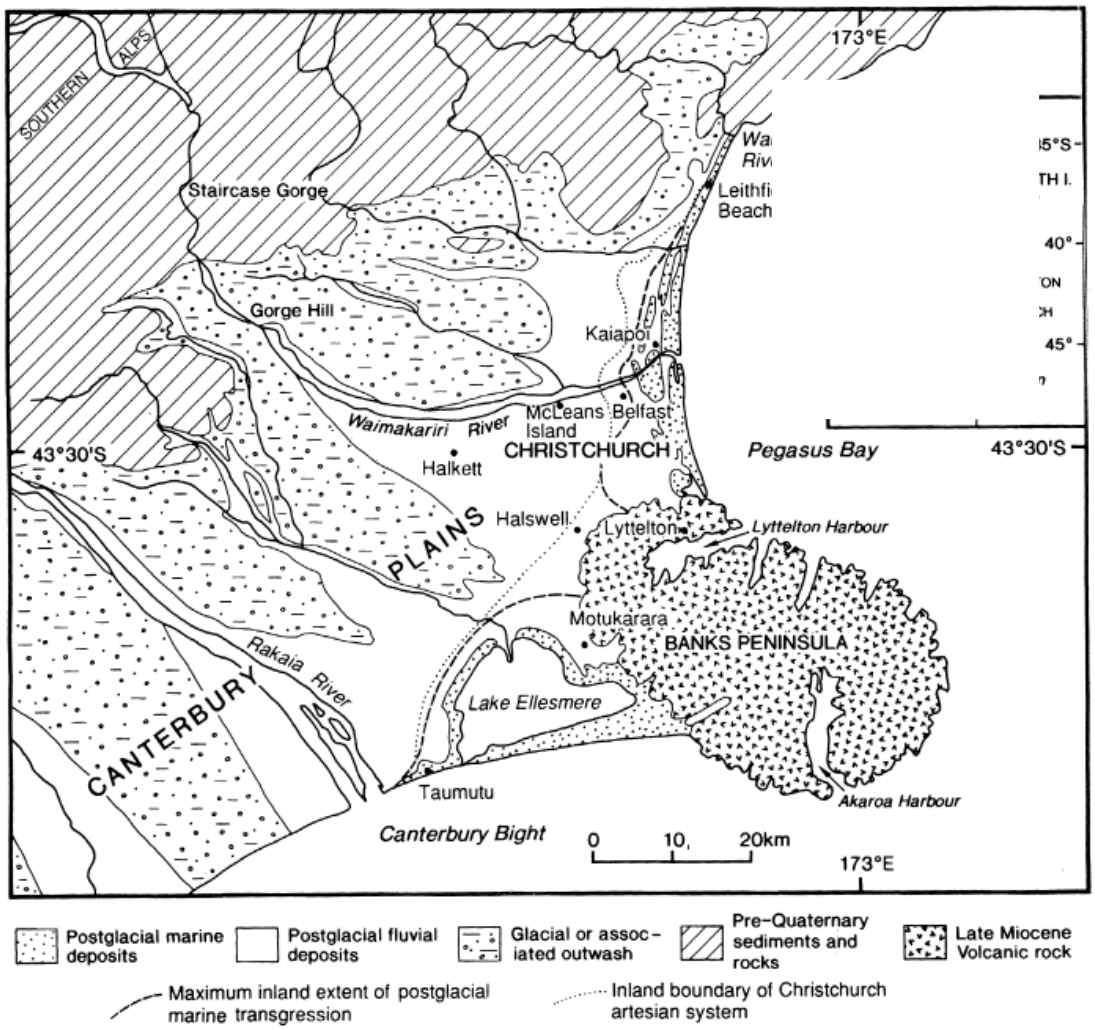

Figure 1.2: Geology of central Canterbury, New Zealand (Brown et al. 1995).

Loess was deposited across the Canterbury Plains and Banks Peninsula during Quaternary glaciations, and Ives (1973) estimates 25% of the land surface of Canterbury is derived from or influenced by loess. The predominantly silt-sized sediment was entrained and transported by northwest winds from glacial outwash surfaces. Raeside (1964) suggests that the exposed continental shelf was a likely additional source region for Banks Peninsula loess. The thickest and coarsest loess deposits occur on the northwestern side of Banks Peninsula and are known as Birdlings Flat loess (Griffiths 1973). The distribution of loess and loess-derived soils across Banks Peninsula is the result of the topography at the time of deposition and subsequent reworking by slope processes. Loess thicknesses on Banks Peninsula typically on the order of 1.0 – >20m (Griffiths 1973), with thick accumulations of loess colluvium and alluvium on the lower slopes and valley floors of the Port Hills.

1.4 2010 – 2011 Canterbury Earthquake Sequence

The September 2010 (Darfield), February 2011 (Christchurch), June 2011 and December 2011 earthquakes, together with more than 10,000 recorded aftershocks (GeoNet 2015), are collectively referred to as the 2010 – 2011 Canterbury Earthquake Sequence (CES). This 16 month time period was selected to include the four largest events, but does not span the entire earthquake sequence.

The M_w7.1 Darfield Earthquake occurred at 4.35am on 4 September 2010, and was centred approximately 40km west of Christchurch City (Figure 1.3). The earthquake event occurred on a fault system comprised of at least seven fault segments, including the strike-slip Greendale Fault which produced a 29.5km-long east-west striking surface rupture (Beavan et al. 2012) (Figure 1.3 and Figure 1.4A). Damage to buildings and services was primarily due to ground deformation associated with liquefaction and lateral spreading (Cubrinovski et al. 2010). Ground damage in the Port Hills was comparatively minor, with some rockfall, valley-floor liquefaction and ground cracking on hillslopes (Dellow et al. 2011; Stephen-Brownie 2012). There were no fatalities and only two accounts of serious injury.

The M_w6.2 Christchurch Earthquake (aftershock) occurred at 12.51pm on 22 February 2011, approximately 6km southeast of the Christchurch city centre and at the eastern edge of the Darfield earthquake aftershock zone (Figure 1.3). The earthquake resulted from the rupture of two to three blind faults, with reverse and right lateral displacements (Beavan et al. 2012). Comparison of digital elevation models (DEMs) generated using 2003 and May 2011 LiDar show the Port Hills and Avon Heathcote estuary (on the upthrown hanging wall block) to have been uplifted by ≤0.4m (Beavan et al. 2012). Extreme ground shaking was experienced, with accelerations of 2.2g (vertical) and 1.7g (horizontal) recorded near the epicentre, and up to 0.8g (vertical) and 0.7g (horizontal) in the city centre (Kaiser et al. 2012). Geodetic and seismological source models show the fault to extend northeast from the suburb of Cashmere towards the Avon-Heathcote estuary and several kilometres offshore (Kaiser et al. 2012).

Shaking damage to buildings, particularly unreinforced masonry structures, was severe. There were 185 fatalities caused by the 22 February earthquake, 169 of which occurred in the Christchurch CBD (NZ Police 2012). As for the Darfield earthquake, widespread liquefaction caused extensive damage to structures, services, roads and bridges, with nearly 15,000 residential properties severely damaged by liquefaction and lateral spreading (Kaiser et al. 2012) (Figure 1.4B). More than half of these properties were deemed uneconomic to repair. The extreme level of damage for a M_w 6.2 earthquake is attributed to the shallow depth and close proximity of the hypocentre to Christchurch, directivity effects, and site amplification (Bradley et al. 2014).

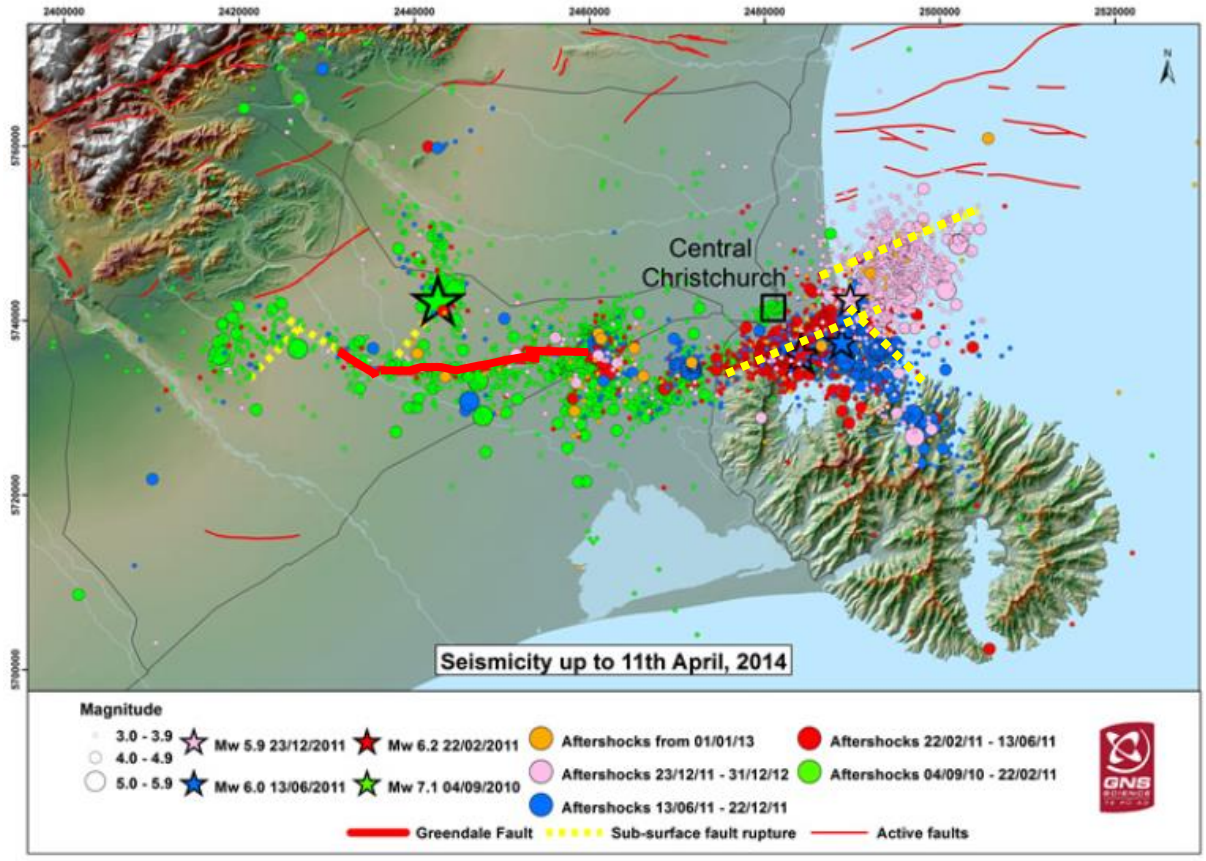

Figure 1.3: GNS Science Canterbury Earthquakes aftershock map. The green, red, blue and pink stars show the epicentres of the Darfield, Christchurch, June 2011 and December 2011 earthquakes, respectively. Source: GNS (2014).

Significant ground failure occurred across the Port Hills, with four types of failure identified by the Port Hills Geotechnical Group (PHGG): rockfall (boulder roll), rockfall (cliff collapse), incipient landslides and fill and retaining wall failures (Dellow et al. 2011). Five people were killed by rockfall, and hundreds of houses were impacted by rockfall and related ground cracking (Dellow et al. 2011; Figure 1.4D).

Aftershock activity increased across the Canterbury region, following the 22 February Christchurch Earthquake, near to both the Darfield mainshock and the February 2011 aftershock. The M_w 6.0 13 June 2011 earthquake took place near the suburb of Sumner, southeast of central Christchurch. Peak ground acceleration (PGA) close to the epicentre reached 2.0g, although the instrument that recorded this acceleration may have been affected by topographic amplification. PGAs reached 0.4g in central Christchurch (Bannister & Gledhill 2012). Earthquake shaking further damaged already vulnerable structures and caused additional liquefaction. Significant cliff collapse occurred at both Whitewash Head and Peacocks Gallop in Sumner, a coastal suburb southeast of central Christchurch. In both instances, failure followed existing (February 2011) tension cracks, with up to 15m of cliff top recession at Peacocks Gallop (Dellow et al. 2011).

An M_w 5.8 earthquake occurred on 23 December 2011, approximately 10km east of central Christchurch, followed several hours later by an M_w 5.9 event. These earthquakes occurred largely offshore, on one or two ENE-striking reverse faults (Beavan et al. 2012). While there was some additional liquefaction and rockfall, these earthquakes were, overall, less damaging than the previous large aftershocks (Gibbons & Kingsbury 2013).

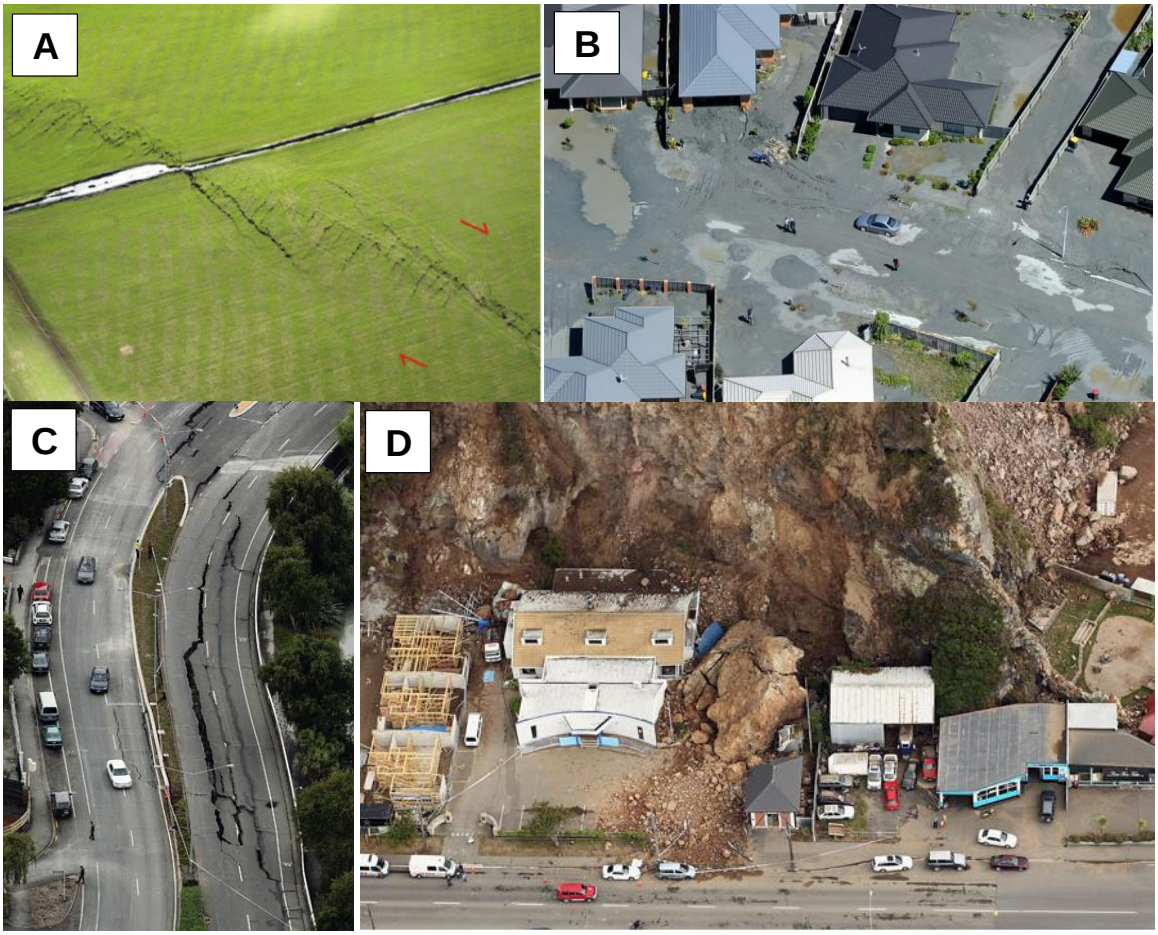

Figure 1.4: A) Oblique aerial photograph of Greendale Fault surface rupture (Darfield earthquake). Red arrows show right lateral sense of movement – approx. 3.5m at this location. The photographed zone of deformation is up to 40m wide (Quigley et al. 2010). B) Severe liquefaction following Christchurch earthquake (Petley 2011). C) Lateral spreading along Fitzgerald Ave between Heywood Terrace and Harvey Terrace, following the Christchurch earthquake. The Avon River is on the right (NZ Herald 2011). D) Cliff collapse along Wakefield Ave, Sumner, following the Christchurch earthquake (NZ Herald 2011).

1.5 Previous work in the Hillsborough Valley

Following the February 2011 earthquake, upward of 200 shallow and deep geotechnical investigations have been carried out across the eastern side of the Hillsborough Valley. Most of these investigations have been conducted for residential purposes, including insurance claims, repair and/or rebuild, and data has been made available through the Canterbury Geotechnical Database (CGD). This information is discussed in Chapters 2 and 3. The remainder of the investigative work has been carried out to

characterise the nature, distribution and extent of the ground damage. The relevant publications are summarised below. Findings are presented in greater detail in Chapter 3.

A paper synthesising the findings of the PHGG, USAR and the GNS Landslide Response Team recognises four distinct ground failure types following the Christchurch Earthquake of 22 February 2011 (Dellow et al. 2011). The ground damage on the eastern side of the Hillsborough Valley is described as an incipient loess landslide, characterised by tension cracks with small amounts of vertical displacement in the 'head-scarp' region and compressional features near the toe. Dellow et al. (2011) postulate the toe of the slope is buttressed by marginal marine sediments which may have liquefied during the February Earthquake.

Stephen-Brownie (2012) documented the extent of the fissuring in the Hillsborough Valley. Based on field mapping and data collation, Stephen-Brownie (2012) hypothesised the ground damage has occurred through a combination of bedrock fracturing, lateral spreading and a trampoline effect. The damage is described as a 'quasi-toppling' style failure, where steeply dipping jointing with the loess has allowed blocks to topple outward. Stephen-Brownie (2012) considers landsliding to be the least likely cause of the observed ground damage.

GNS Science was contracted by the Christchurch City Council (CCC or 'the Council') to carry out detailed investigation of the Port Hills 'mass movements' previously identified by members of the PHGG (Massey et al. 2013). In November 2013, the Council released the GNS 'Stage One Report', which assigned mass movement areas in the Port Hills a preliminary Class I, II or III relative hazard exposure category. The purpose of the report was to aid the Council in its review of the District Plan by providing a list of areas susceptible to significant mass movement. The eastern side of the Hillsborough Valley is categorised as a Class II mass movement, meaning there is potential for critical infrastructure to be affected if the hazard were to occur, although loss of life is unlikely (Massey et al. 2013; Christchurch City Council 2014). The failure is described as a 'toe slump' resulting from undrained loading of hillslope materials.

1.6 Thesis format

The format of this thesis is as follows:

Chapter Two describes the field area for this study, and provides a summary of the thesis methodology and key terminology. The thesis methodology is broken down into desktop study, field work, laboratory analyses and numerical modelling. Terminology used to describe and classify Port Hills soils and mass movements is set out in the latter part of the chapter.

Chapter Three presents an Engineering Geological and Geomorphological model for the eastern side of the Hillsborough Valley. Previous work carried out in the Valley is summarised, before presenting the results of aerial photograph interpretation, trenching and seismic surveying.

Chapter Four is in two parts. The condensed findings of a detailed literature review on soil tensile strength testing are presented in the text. The development of a soil tensile strength test put together for this thesis is then described and results interpreted.

Chapter Five discusses possible failure modes for the eastern side of the Hillsborough Valley. A geomorphological interpretation of the observed ground damage is provided. A geotechnical interpretation is provided using the findings of soil tensile strength analyses, as well as piezometric data and inclinometer data for the Vernon Terrace area. Theoretical models of ground failure are used to provide an interpretation of the 'stage' of ground failure.

Chapter Six presents and discusses the findings of sliding block analyses carried out for the eastern side of the Hillsborough Valley. Numerical modelling techniques commonly used to evaluate seismic slope performance are reviewed.

Chapter seven summarises the findings of this thesis, with specific conclusions and recommendations for future work.

2 Thesis Methodology and Terminology

2.1 Introduction

This chapter introduces the study area for the thesis and provides an overview of how the research objectives set out in the previous chapter have been met. In describing the steps taken to obtain information and collect data at the desktop study and fieldwork stages, subsequent chapters are streamlined. Key sources of information include the Canterbury Geotechnical Database (CGD) and geotechnical information released by the Earthquake Commission (EQC) by way of a confidentiality agreement. The latter part of this chapter outlines key terminology and concepts used throughout this thesis. The terminology outlined in this chapter (and expanded on in later chapters) includes general mass movement and Port Hills soil classification.

2.2 Study area

The Hillsborough Valley is 4km southeast of central Christchurch. This thesis is concerned with the eastern side of the valley, from Hillsborough Terrace up to the shoulder of Glenelg spur - an area of approximately 0.3 km^2 (Figure 2.1). The valley is situated at the northern rim of the extinct Lyttelton Volcanic Complex. Bedrock is comprised Miocene age basalt, which is overlain by Pleistocene age loess and loess-derived soils. The centre of the valley is infilled with upslope-derived loess and volcanic colluvium, together with alluvium and marginal marine sediments.

The epicentre of the M_w 6.3 Christchurch earthquake was 3.8km east of the Hillsborough Valley (Figure 2.1), with the southwestern end of the fault modelled to pass below the valley at a depth of approximately 1km (Kaiser et al. 2012). Seismic instruments located in the adjacent Heathcote Valley, above the hypocentre, recorded peak ground accelerations (PGAs) of 2.21g vertical and 1.41g horizontal (Bradley & Cubrinovski 2011). PGA contours developed by O'Rourke et al. (2012) suggest a peak horizontal acceleration of 0.62-0.64g for the eastern side of the valley during the 22 February 2011 event.

Immediately following the Christchurch earthquake, ground cracking was reported across the hillside between Vernon Terrace and Rapaki Road, with evidence of compressive shortening along the toe of the slope below Vernon Terrace. Similar features were also observed on the western side of the Hillsborough Valley, and in the adjacent Bowenvale and Heathcote Valleys, Stephen-Brownie (2012) and Massey et al. (2013) provide more information on ground damage in these areas. Initial assessment of the Vernon Terrace-Rapaki Road area was in the form of walkover survey by members of the Port

Hills Geotechnical Group (PHGG), at which time crude monitoring devices were installed (Gibbons & Kingsbury 2013). From site walkover, monitoring and survey, it was determined that the risk of imminent failure was low. In addition to fissuring and compression, springs appeared in many locations across the valley floor, the occurrence and distribution of which are being studied by Green (in prep). The western side of the Hillsborough Valley is being studied by White (in prep). The area studied for this research is variably referred to as the eastern Hillsborough Valley or the Vernon Terrace area.

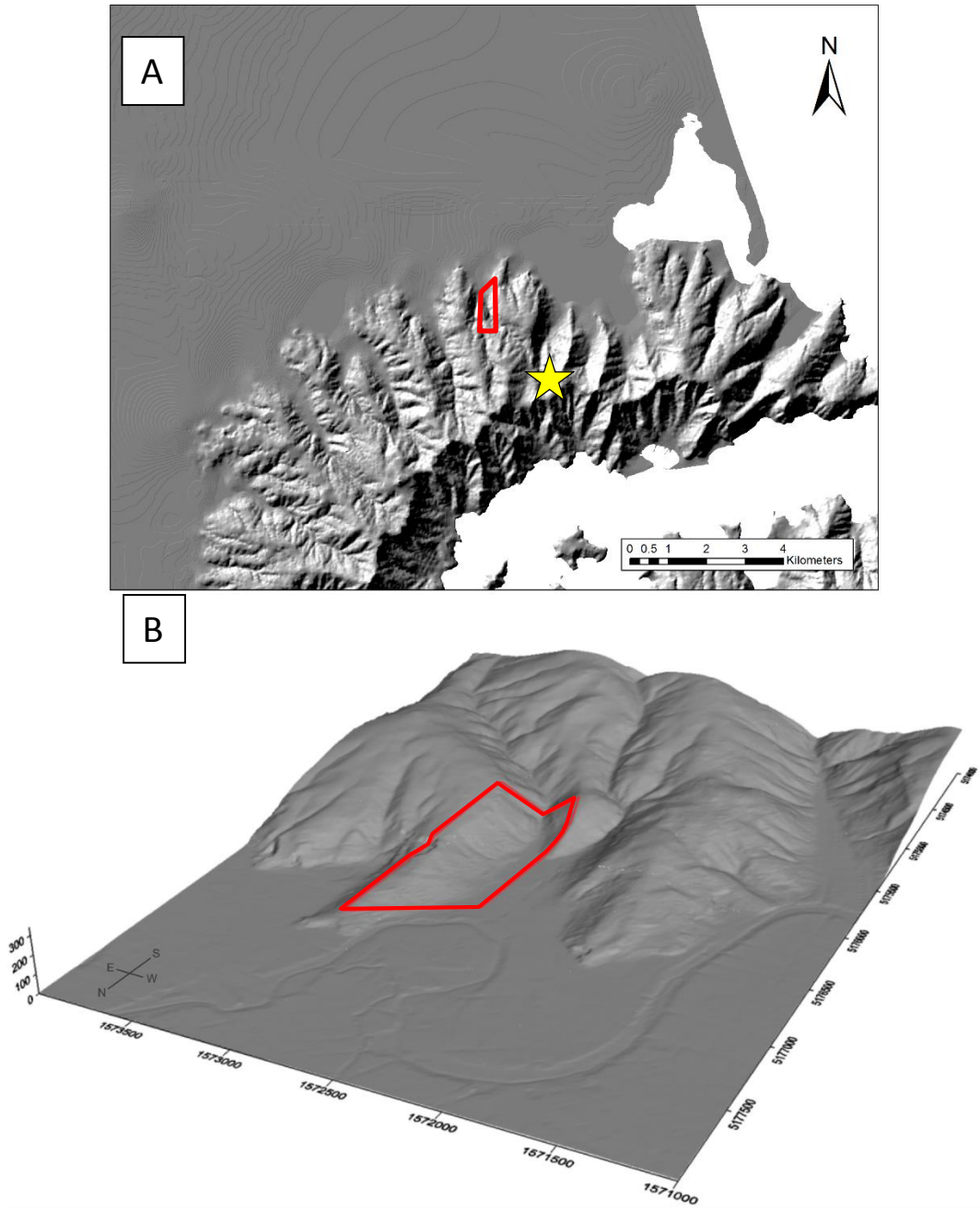

Figure 2.1: A) Map view of field area outlined in red. Epicentre of February 2011 earthquake shown by yellow star. B) Oblique view of field area (outlined in red). The Heathcote River channel can be seen in the foreground. Bowenvale Valley can be seen to the west of the Hillsborough Valley. The spacing between gridline ticks is 500m.

2.3 Port Hills ground damage terminology

The terminology used to describe ground damage in the Vernon Terrace area in this thesis is, where possible, descriptive without being diagnostic. Failure mechanisms are not discussed until Chapter 5, in order to draw on all information presented in the preceding chapters. It is in Chapter 5 that terminology associated with specific failure mechanisms is introduced.

The ground cracking is described as tension cracking by GNS Science (Massey et al. 2013) and is generally referred to as fissuring by Stephen-Brownie (2012). In the following chapters, the ground cracking is referred to as both tension cracking and fissuring, as well as extension. While these terms imply the soil has failed in tension, the terminology is not linked to a particular mode of failure. The features are also referred to as 'deformation' and 'structures'. Both Massey et al. (2013) and Stephen-Brownie (2012) refer to shortening at the toe of the slope as compression or compressional features and that terminology is adopted in this thesis also.

2.3.1 Fissuring description

The fissures on the eastern side of the Hillsborough Valley form a broadly arcuate, discontinuous trace between Vernon Terrace and Rapaki Road (Figure 2.2). The zone of fissuring extends for approximately 600m, and is up to 40m wide at the central section. Individual fissures are up to 50m in length, although are more commonly 5 – 20m. Fissuring is approximately contour parallel, rising to 32m above sea level (masl) at the highest (central) point and tapering down to 15 and 20m above sea level at the northern and southern ends of the valley, respectively (Figure 2.2).

Individual cracks show lateral extension of up to 0.2m (Stephen-Brownie 2012). Some fissures show small amounts of vertical displacement (<0.15m), however it is more common for cracks to show no vertical offset. Where fissures show vertical movement, the down-slope side has dropped relative to the up-slope side (Figure 2.3) with the exception of a small graben at the centre of the zone of fissuring. Actual fissure depths are in most cases not known; internal irregularities made depth measurement difficult and the cracks were often obstructed by loose soil. Cracks on the eastern side of the valley were infilled using a 1:6 mixture of bentonite clay and SAP-20 gravel in mid-2011, meaning depth measurement is no longer possible. Several cracks are known to have been measured to a depth of greater than 2m and in some cases 5m (Stephen-Brownie 2012). Personal communication with residents has indicated that cracking was evident immediately following the initial shaking on 22 February 2011, although the exact timing of the appearance of cracking, relative to shaking, is unknown.

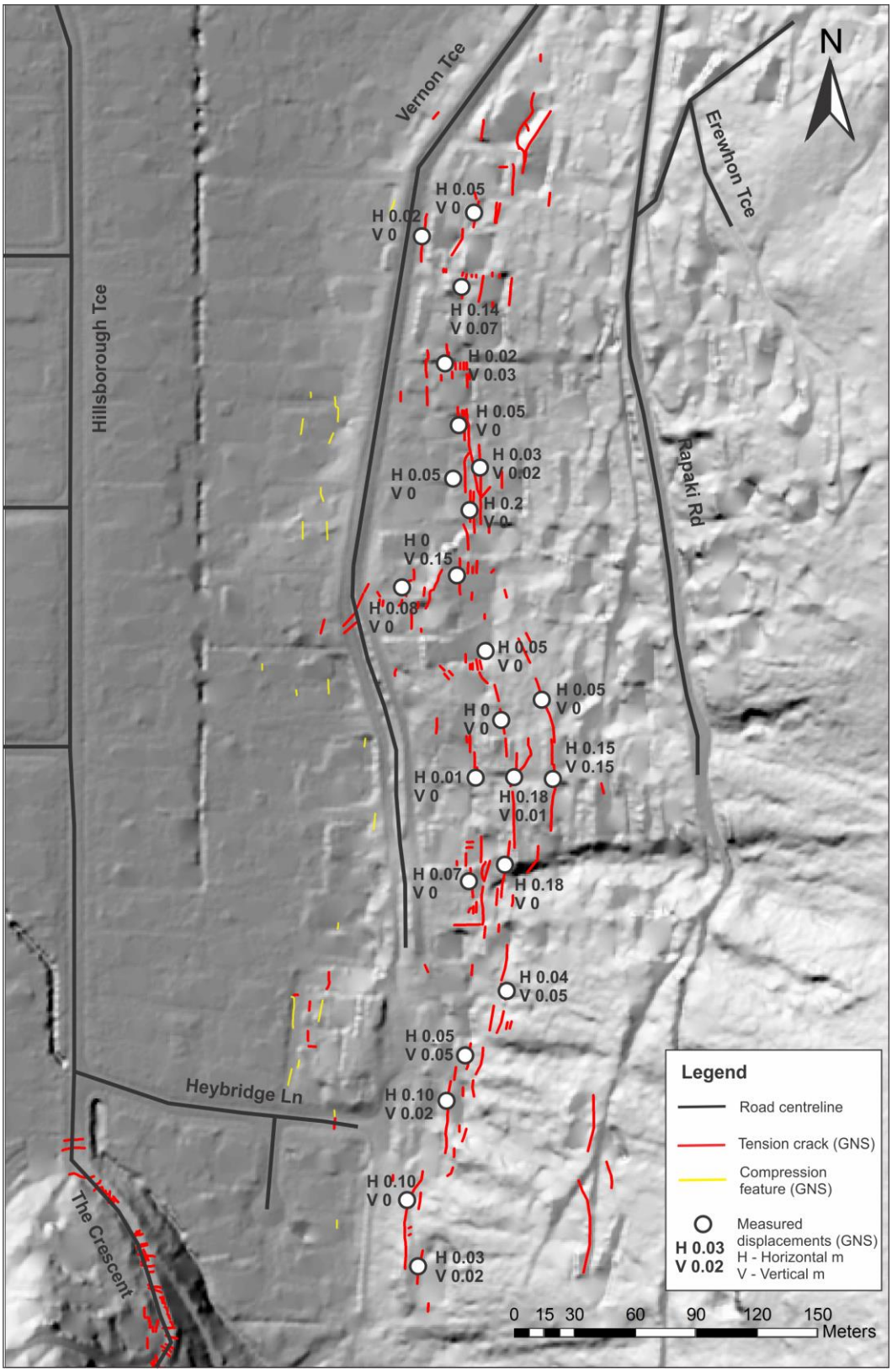

Figure 2.2: Mapped tension cracks and compression features on the eastern side of the Hillsborough Valley; location of tension and compression features downloaded from the CGD (2014). Base map is a hillshade model created using Christchurch City Council LiDar.

Fissuring has caused severe damage to housing and property. Where cracks have formed underneath houses, floor slabs have been cracked and in some instances offsets have been great enough to split the house in two. In many cases, fissures have stepped in front of or behind foundations, creating voids below and around the house.

2.3.2 Compression and spring description

Compressional features have formed directly downslope of the cracking, with the maximum downslope distance between mapped extension and compression approximately 100m. Compression at the toe of the slope is most obvious where rigid structures such as driveways, fences and paving stones have become crumpled or thrust over each other (Figure 2.4). The soil (i.e. lawns and gardens) adjacent to crumpled structures will typically show no sign of damage. As a result, the mapped compression features are short (≤10m) and discontinuous due to only being a patio or driveway wide (Figure 2.2). This is in direct contrast to the mapped fissures. It is assumed that the compression zone extends across the toe of the slope wherever there is fissuring upslope. Compression appears to be of the same order of magnitude as upslope extension, although it is difficult to directly correlate the two features; compression is only obvious where driveways and fencing have been damaged. Surveying would be required to confirm this observation.

A number of springs appeared on Vernon Terrace properties following the Darfield earthquake (Stephen-Brownie 2012). After the February 2011 earthquake, new springs appeared and the flow-rates of existing springs increased (Stephen-Brownie 2012). Springs are distributed along the toe of the eastern hillslope and are confined to the northern end of the valley, primarily below the 5m contour. Their appearance and distribution are being studied by Green (in prep).

Figure 2.3: Examples of tension cracking in the Vernon Terrace area. A) Stephen Brownie (2012), vertical displacement is ~0.12m; B) Dellow et al. (2011); C) Author, vertical displacement is ~0.15m.

Figure 2.4: Examples of compressional features. A, B and D) Author; C) Dellow et al. (2011). A and B show shortening of the same fence at two different locations. C and D show crumpling of paving stones. The asphalt of the driveway at D was also crumpled.

2.4 Desktop study

The engineering geological model presented in Chapter 3 was compiled using the findings of a thorough desktop study, and the results of field investigation carried out for this research. The various data sources are summarised in Table 2.1, and grouped on the basis of availability before or during/following the 2010-2011 CES.

Table 2.1: Summary of data used in this thesis. Pre-CES refers to data available prior to the 4 September 2010 Darfield earthquake and does not include journal publications or university theses. Post-CES refers to data collected or made available during and following the 2010-2011 Canterbury Earthquake Sequence.

	Data	Source	Date	Use in this thesis
Pre-CES	Aerial photographs	Canterbury Maps and D. Bell	1926, 1940, 1973	Assess site history
	Canterbury 'Black Maps'	Compiled by K. Silby of the Christchurch Drainage Board, sourced from (Brown and Weeber (1992)	1856	Assess site history
	Geological maps	Brown and Weeber (1992); Forsyth et al. (2008)		Site geology
Post-CES	Aerial photographs	CCC, supplied by University of Canterbury	24-Feb-11	Base maps
	LiDAR	CCC, supplied by University of Canterbury	24-Feb-11	Generate contours and shade models for maps and cross sections
	Borehole, CPT and hand auger records	Canterbury Geotechnical Database (CGD 2015a)	2011 - 2015	Subsurface information for maps and cross sections
	Piezometer and inclinometer records	Earthquake Commission (EQC)	2011 - 2014	Geotechnical interpretation

2.4.1 Aerial photographs

Historical aerial photographs were used to assess site history. The 1926 images were downloaded from the Canterbury Maps website (www.canterburymaps.govt.nz). The 1940 and 1973 aerial photographs were provided by D. Bell of the University of Canterbury.

Aerial photographs taken by NZ Aerial Mapping on 24 February 2011 for the Christchurch Response Centre (CRC) were supplied by the University of Canterbury. These images were used as base maps, however do not appear in this thesis. The hillshade model created by the author using Christchurch City Council (CCC) LiDar is instead used as the base map on which all data is presented to protect the privacy of residents in the valley.

2.4.2 Canterbury Geotechnical Database (CGD)

The Canterbury Geotechnical Database (CGD) was established by the Canterbury Earthquake Recovery Authority (CERA) in November 2011 to facilitate sharing of geotechnical investigation data. Approximately 200 borehole, CPT and hand auger records for the eastern side of the Hillsborough Valley were extracted from the CGD for this study. Appendix A provides relevant borehole logs. Most of these boreholes were drilled on private property: they have been renumbered and the addresses removed for privacy reasons.

While the information obtained from the CGD has been invaluable for the construction of maps and cross sections, it is noted that the quality of the logging (boreholes and hand augers) is variable. Several borehole logs provide single-word descriptions for soil units, and are perhaps drillers' logs. Although the NZGS logging guidelines are being followed by most, there is clearly a mixed understanding of what the different terms mean (particularly 'plasticity') and, fundamentally, the processes that have led to the formation of the different loessial regoliths. In order to produce meaningful geological maps, judgement was exercised in the review of borehole and hand auger logs sourced from the CGD. It was necessary to reinterpret some logs, while disregarding others. Loess-colluvium, for example, was commonly classified as loess despite the (logged) presence of volcanic gravel, which is widely accepted to be evidence of downslope reworking (Bell & Trangmar 1987; Griffiths 1973).

2.4.3 Earthquake Commission (EQC) piezometers and inclinometers

A series of deep boreholes were drilled on the eastern side of the Hillsborough Valley in May and June 2011. Two piezometers, or a piezometer and an inclinometer, were installed in each of these holes. Data from the instruments are not available through the CGD; a non-disclosure agreement was therefore set up between the University of Canterbury and the Earthquake Commission (EQC) in order to access the data. A spreadsheet containing pressure-corrected piezometric data was supplied to the University of Canterbury on 16 December 2014. Two PDF plots were supplied for each of the five inclinometers, showing tilt change and profile change. Inclinometer monitoring is event-based with readings taken following a significant rainfall event and/or seismic activity defined as >50mm/24hours and M_w 5.0, respectively.

2.5 Field work

Site-specific investigation was carried out in order to develop the desktop model established using data from the CGD. A seismic refraction survey was carried out perpendicular to the eastern hillslope, and a nearby fissure trace was trenched to 1.0m depth for the purposes of soil sampling and observation.

In order to conduct fieldwork in the Hillsborough Valley, it was necessary to contact residents to establish if they had features of interest on their land, and also if they would allow access for data collection. Contact was made through door-knocking, flier distribution and having emails sent out using established post-quake valley-wide communication systems. It became clear during this process that much of the previously visible ground damage had been 'remediated' through the resurfacing of driveways and roads, landscaping, and fixing of fences and gates.

A suitable location was found for the seismic survey in the form of a 100m long driveway running perpendicular to and up the slope in the centre of the zone of fissuring. The trench was dug across an unremediated fissure 30m south of the seismic line on a nearby property.

2.6 Laboratory testing

Laboratory testing was carried out to ascertain selected geotechnical properties of soil sampled from the trench. Undisturbed soil samples were collected using 38mm diameter push tubes and 100mm diameter ring samplers, which were wrapped in cling film and then sealed in 'zip lock' bags to maintain field moisture content. Loose soil was bagged on site and later transferred to 'air lock' containers in the Engineering Geology laboratory at the University of Canterbury.

The testing carried out followed standardised test methods, where available. Loose soil was used for grainsize analyses (pipette and laser particle sizer), Atterberg limit testing and soil tensile strength analyses. It was intended to test soil obtained with the ring samplers for shear strength in the shear box, however damage to the steel mould meant testing could not be undertaken. Push tube samples were used to calculate dry density and moisture content. Push tube samples were also taken with the intention of carrying out triaxial testing, however difficulties arising from laboratory availability due to earthquake repair work meant this also could not be undertaken.

For laser particle sizer (LPS) testing and tensile strength testing there are no standardised test methods available. LPS testing was carried out using 'best practice' methods established at the University of Canterbury. Tensile strength analyses were carried out following a test method developed by the author, which is presented in Chapter 4. The findings of Atterberg Limit, grainsize, moisture and density testing are presented and discussed within the chapters that make use of the data, and not in a dedicated separate chapter.

2.7 Modelling

Seismic slope performance was evaluated using SLAMMER (Jibson et al. 2013). SLAMMER (Seismic LAndslide Movement Modelled using Earthquake Records) is a java program released by the United States Geological Survey (USGS) in 2013 that allows the user to perform sliding block analyses using simplified empirical equations or strong-motion records. The objective of modelling was to compare measured slope displacements from the 2010-2011 CES with modelled slope displacements.

2.8 Terminology used

2.8.1 Port Hills soil classification

The Bell and Trangmar (1987) classification of Port Hills soils is adopted for this thesis. Bell and Trangmar (1987) identify five principal regolith types in the Port Hills: in-situ (or airfall) loess, loess-colluvium (<10% volcanic content), mixed-colluvium, volcanic colluvium (<10% loess content) and residual (volcanic) regolith. Loess and loess-colluvium are classified as loessial regoliths. Mixed- and volcanic-colluvium are classified as volcanic regoliths. The term colluvium is used to describe regolith

materials that have been reworked downslope. The prefix loess-, mixed- or volcanic- indicates the dominant component, based on visual inspection. A typical distribution of the different regoliths types is shown in Figure 2.5.

In this thesis, the term 'loessial' is used to refer to all material with a dominant loess component, irrespective of whether it has been reworked. Primary loess that has not been reworked is referred to as loess, in situ loess or airfall loess. Colluvium without a prefix is used to refer to all material that has been reworked and redeposited downslope (i.e. loess-, mixed- or volcanic-colluvium). Detailed review of the literature on the distribution and geotechnical properties of Banks Peninsula and international loess has been carried out by Stephen-Brownie (2012) and Hughes (2002).

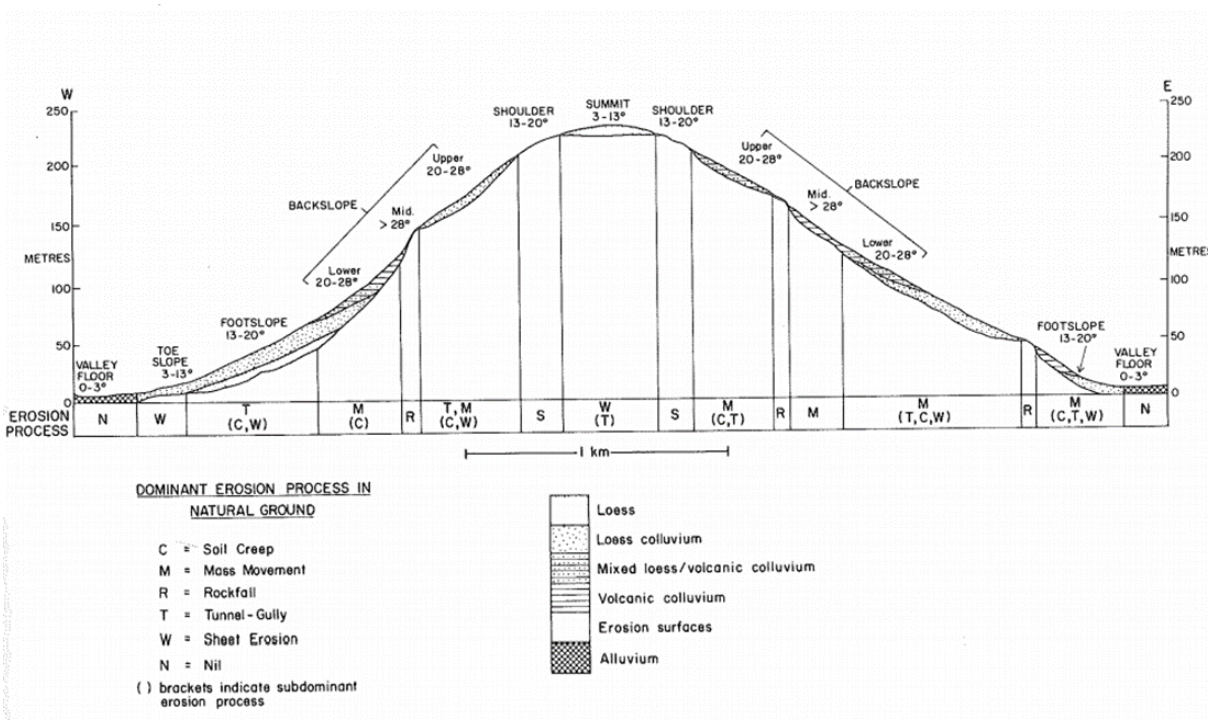

Figure 2.5: Port Hills generalised ridge cross section (Bell & Trangmar 1987).

2.8.2 Mass movement types

Mass movement, or landsliding, is the downslope movement of a mass of rock, debris or earth (Cruden & Varnes 1996). The mass movement classification system and nomenclature developed by Varnes (1978) and refined by Cruden and Varnes (1996) is followed for this thesis. Cruden and Varnes (1996) classify mass movements on the basis of type of movement and type of material involved. Figure 2.6 summarises the six movement types (falls, topples, slides, spreads, flows and complex) together with the three material types (rock, debris and earth). The term 'earth' is used to describe material in which at least 80% of the particles are smaller than 2mm (Varnes 1978).

The six main failure modes according to Cruden and Varnes (1996) are summarised below:

- A fall describes the detachment of soil or rock from a steep slope or cliff, along a surface on which little or no shear displacement occurs. The soil or rock then descends through the air by falling, bouncing, and/or rolling.

- Toppling failure is the forward rotation of a mass of soil or rock about a point or axis.

- A slide is the downslope movement of a soil or rock mass along one or several shear surfaces that are visible or may reasonably be inferred. Slides are subdivided on the basis of translational and rotational movement. Rotational slides move along a surface of rupture that is curved and concave, occurring most frequently in homogenous materials. Translational slides displace along a planar or gently curving rupture surface, and are typically shallower than rotational slides.

- A spread describes the lateral extension of a cohesive soil or rock mass which overlies a softer material. Movement results from liquefaction or flow of the softer material, causing the overlying soil or rock mass to subside, translate, rotate, disintegrate, liquefy or flow.

- A flow is the slow to rapid movement of dry to saturated materials, displacing like a viscous liquid.

- Complex slope movements involve one or more of the principal movement types, either simultaneously or in sequence.

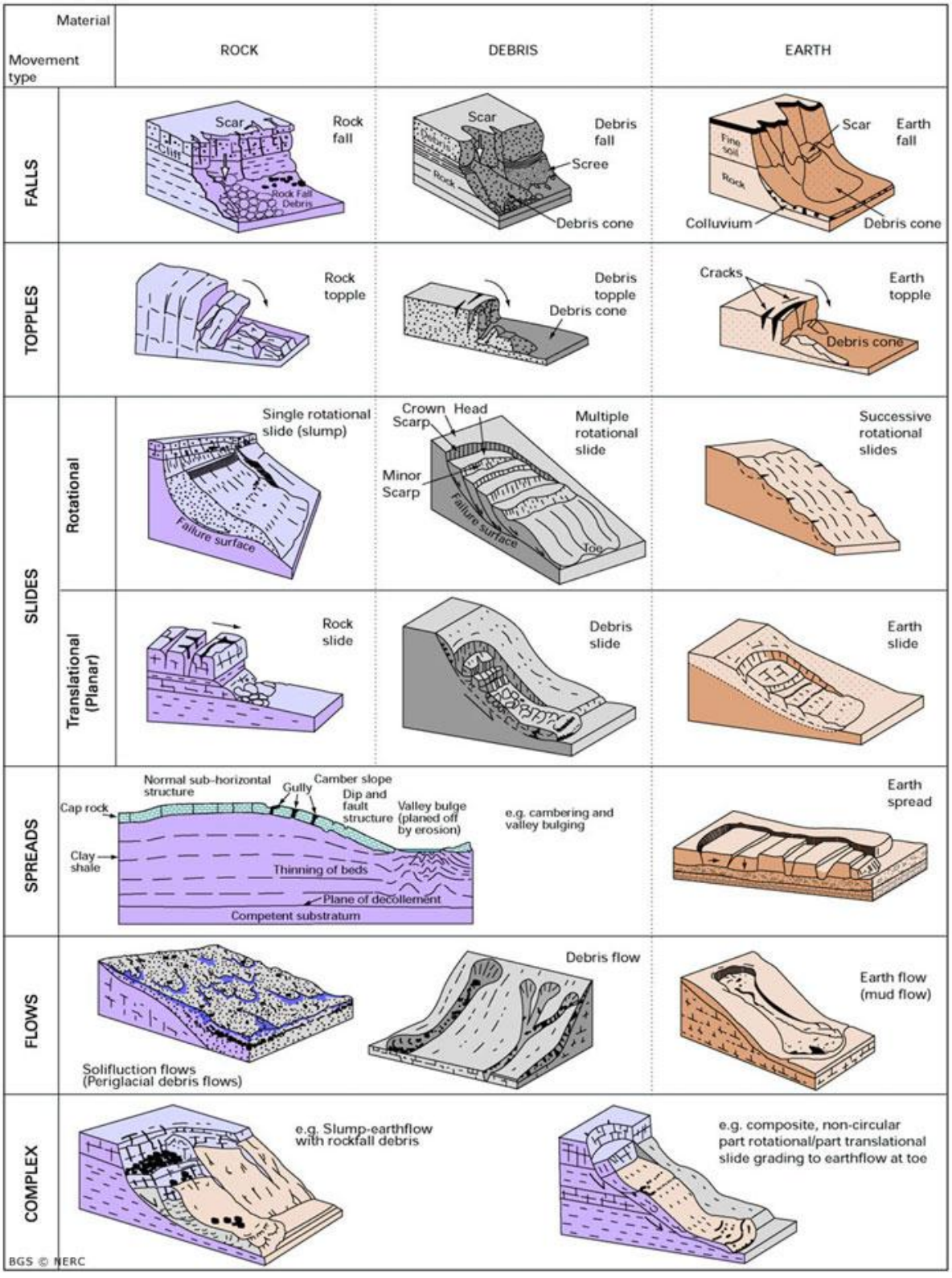

Figure 2.6: Mass movement types (British Geological Survey n.d.).

3 Engineering Geology and Geomorphology

3.1 Introduction

This chapter presents an engineering geological model for the eastern side of the Hillsborough Valley, which is used to place the observed ground damage in the context of its geological and geomorphological evolution. The model incorporates three types of data - that which was available prior to the Canterbury Earthquake Sequence; investigations carried out during and following the Canterbury Earthquake Sequence; and the findings of site-specific investigation carried out for this research. The model consists of geological and geomorphological maps, together with a simplified block model and written description.

Published results of investigations previously carried out on the eastern side of the Hillsborough Valley are included, as are results of aerial photograph interpretation covering the period 1926 - 2011. Field work carried out for this thesis, together with data sourced from the CGD has been used to inform the engineering geological and geomorphological model.

3.2 Previous work

There are three publications that describe and classify the ground damage on the eastern side of the Hillsborough Valley, although it is not a primary focus for either Dellow et al. (2011) and Massey et al. (2013).

3.2.1 Dellow et al. (2011) 'model'

The findings of the PHGG, the GNS Landslide Response Team and Urban Search and Rescue (USAR), are summarised by Dellow et al. (2011) with four distinct ground failure types being recognised. Dellow et al. (2011) classify the Vernon Terrace area as an 'incipient loess landslide', characterised by tension cracks in the head-scarp area and compressional features near the toe of the slope. Minor movements at Vernon Terrace were reportedly observed following the September 2010 earthquake, and the 'slide' is described as having been 'reactivated' by the February 2011 Earthquake(Dellow et al. 2011). It is not made clear where the September 2010 damage occurred. Tension cracks in the headscarp area of the Vernon Terrace 'landslide' were observed to widen in the days after the February 2011 earthquake, which is attributed to continuing creep movement (Dellow et al. 2011). It is suggested that this could be due to the toe of the landslide being buttressed by saturated marginal marine sediments which may

have liquefied during the February 2011 earthquake. It is hypothesised by Dellow et al. (2011) that strength loss in these sediments occurred over a period of several days, which allowed the landslide to keep moving.

3.2.2 Stephen-Brownie (2012) model

Stephen-Brownie (2012) established a fissure classification system based on shared fissure attributes. The Hillsborough Valley fissures, classified as Category A, are characterised by spring formation on the valley floor, fissuring near the loess-loess colluvium boundary, compression features at the toe of the slope, and contour-parallel fissuring on both sides of the valley. Five possible mechanisms were considered to explain the observed fissuring, these being incipient landsliding, bedrock fracturing, toppling failure, the 'trampoline effect', and lateral spreading. Stephen-Brownie (2012) concludes that fissuring is most likely the result of a complex interaction between bedrock fracturing, the trampoline effect and lateral spreading. 'Incipient landsliding' is considered to be the least likely of the five possible fissuring interpretations (Stephen-Brownie 2012). For Category A fissures, it is hypothesised that bedrock fracturing has propagated upward from the fault responsible for the February 2011 earthquake, creating conduits for deep groundwater to travel to the surface and form springs at the valley floors. The trampoline effect, whereby high vertical accelerations cause sedimentary layers to separate and then "slap" into each other during shaking, is proposed to have removed lateral support from the valley walls, resulting in a lateral spreading type movement which had caused the fissuring. The movement is summarised as a quasi-toppling style failure, where steeply-dipping jointing within the loess have allowed blocks to topple outwards (Figure 3.1).

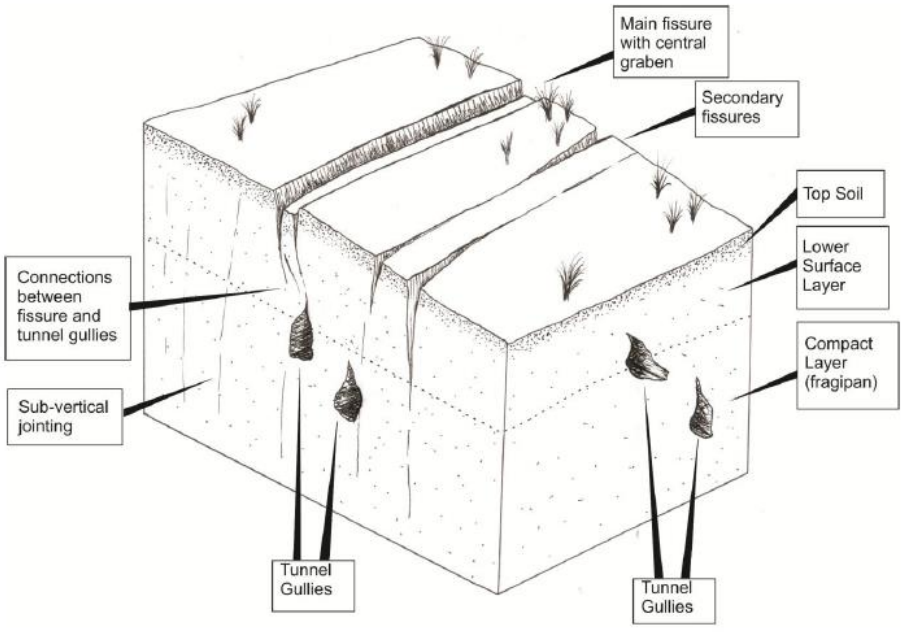

Figure 3.1: Schematic block diagram of fissured section of loess showing toppling within the sub-vertical jointing of the loess body, and interactions of fissures and tunnel gullies (Stephen-Brownie 2012). Depth of land block ~2m.

3.2.3 GNS/Massey et al. (2013) model

Field mapping of the Vernon Terrace area was undertaken by GNS Science between October 2012 and January 2013 (Figure 3.2). Ground damage on the eastern side of the Hillsborough Valley is described as 'toe slump' style failure (Figure 3.3), and is one of many identified in the Port Hills area. Toe slumping is defined as the localised deformation of soil material near the base of low angle (<25°) slopes, and is comprised of zones of compression, translation and tension (Massey et al. 2013). It is suggested that movement is the result of un-drained earthquake loading of locally saturated loess, colluvium and alluvium, and consequent generation of excess pore pressure. Massey et al. (2013) observe that geomorphic evidence exists for movement of several (unspecified) toe slumps prior to the Canterbury Earthquake Sequence, although there are no historical records of damage to dwellings from toe slump movement. It is hypothesised that ground shaking from pre-historic strong earthquakes may have triggered movement prior to the CES (Massey et al. 2013). A simplified cartoon model for toe slumping is provided in the GNS report (Figure 3.3).

The GNS report states that at the time of publication there is limited understanding of the mechanisms of movement of the toe slumps, and it is uncertain as to how they would behave in an Alpine Fault earthquake. Monitoring records from the Vernon Terrace toe slump suggest that large movements of these features are unlikely to be caused by elevated pore pressures resulting from a rainfall event, however records only extend back two years (2011 - 2013) and no systematic assessment had been carried out at the time of the GNS reporting (Massey et al. 2013).

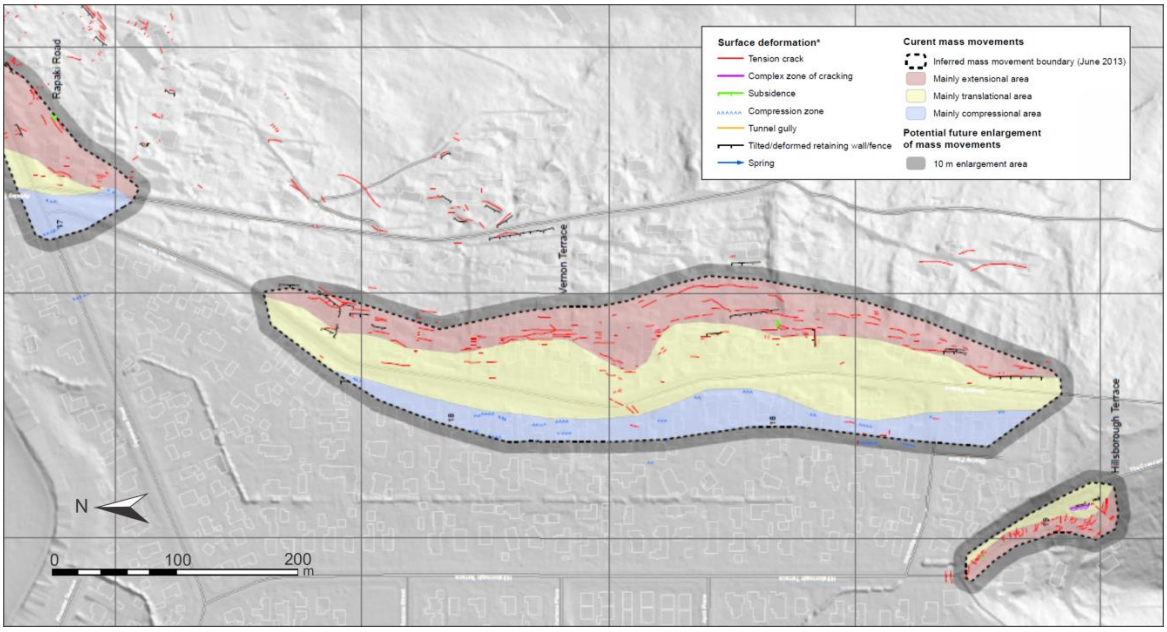

Figure 3.2: GNS Vernon Terrace mass movement map (Massey et al. 2013). Maps C7 and D7 of Appendix 2 (Massey et al. 2013) were merged to create this figure.

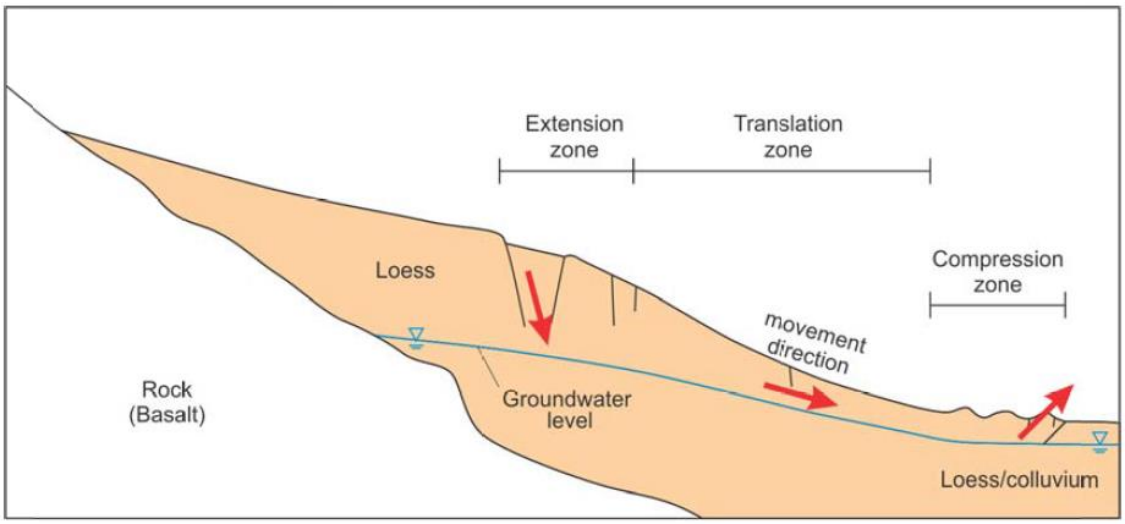

Figure 3.3: Loess toe slump (Massey et al. 2013).

3.3 Aerial photograph and historical map interpretation

European settlement has led to extensive modification of the Hillsborough Valley and surrounding area. Historical maps, photography, and aerial photography were reviewed to assess the recent (post-1850) anthropogenic and geomorphological site history.

3.3.1 Vegetation clearance and effects

Banks Peninsula's forest cover was reduced to approximately 4% of its original extent following Maori and early European burning, together with European logging (Wilson 1994). The removal of vegetation facilitated widespread rill erosion and tunnel gullying across the Port Hills, with prominent collapsed gully features forming on both sides of the Hillsborough Valley. These erosional features were well established by the time of the 1926 aerial survey (Figure 3.5), with individual gullies on the eastern side of the valley up to ~20m wide with a downslope length of approximately 150m.

The 1940 aerial survey stereoscopic images (the earliest stereoscopic images available) show fan debris extending from the base of tunnel gullies onto the valley floor (Figure 3.5). The fans are assumed to have been present at the time of the 1926 aerial survey, although are not easily discernible due to poor image quality. A north-south trending hedge or fenceline at the base of a fan is clearly visible in the 1926 aerial photograph, but partially obscured in the 1940s aerial photograph. It appears the fenceline is covered with sediment, which suggests the upslope tunnel gully system was still active at this time. The surface of the largest 'fan' appears smoothed in the 1973 stereoscopic images, which may indicate the fans were excavated for fill. Currently, the area occupied by the inactive gullies at the south of the valley is covered by vegetation with some housing at the northern end, although they are discernible with LiDAR. A subdivision planning report by (Bell 1980) extends across the rear of the valley. Bell

(1980) mapped a small mass movement and collapsed gully areas with fans and 'aprons' at the base. At the time of mapping this ground was still exposed, and this is the only definitive reference to fan development at the rear of the valley found by the author.

3.3.2 Early development

The 'Black Maps', compiled in 1856, show the waterways, swamps and vegetation cover of Christchurch prior to urbanisation. The Hillsborough Valley is labelled to show 'marshy land' (swamp) at the valley entrance, 'flax and toetoe' in the central part of the valley, and 'fern and flax' to the rear (Figure 3.4A). In 1882 the Hillsborough Valley was subdivided into 163 lots, and within a decade of this subdivision there were more than a dozen farmers settled in the valley (Ogilvie 2009) . The earliest photo of the valley was taken by Robert Beattie pre-1887 from the eastern slope, looking west/northwest towards what is now the junction between Albert Terrace and Roscoe Street (Figure 3.4B). Beattie's farm and can be seen in the foreground, together with a few early residences. To prepare the land for farming, the existing vegetation (flax, toetoe and ferns) would have been cleared and areas of 'marshy land' drained and/or filled. Many of the recent subsurface investigations across the valley identify a silty layer before penetrating the underlying peat. It is likely that extensive filling of the valley has occurred, however Brown & Weeber (1992) note that it is extremely difficult to identify colluvium that has been used as fill in comparison to in-situ or natural colluvium.

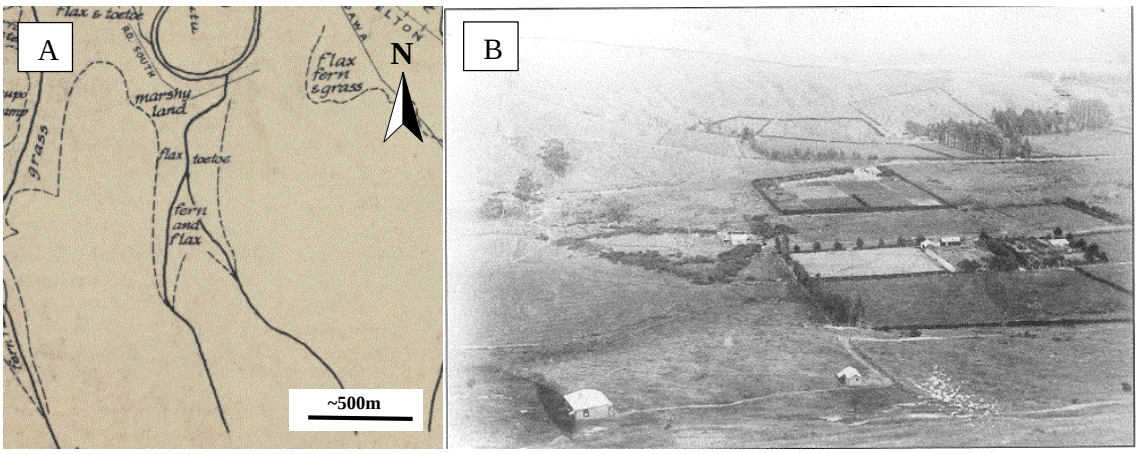

Figure 3.4: A) Replica of the original 1856 Black Maps, showing the Hillsborough Valley (Christchurch City Libraries n.d.). A meander bend of the Heathcote River can be seen at the top of the image. B) Pre-1887 photo taken by Robert Beattie (Ogilvie 2009). View looking west/northwest towards the present-day junction of Albert Terrace and Roscoe Street. Gullying can be made out on the far slope (eastern side of Huntsbury spur).

In 1926 the valley was occupied by market gardens. Erosional gullies and partially collapsed tunnels have the appearance of truncating against planted fields on the lower slopes, suggesting the natural ground was cut and filled for planting (Figure 3.5). According to Ogilvie (2009), early issues with drainage in the valley were not properly addressed until the appointment of the Christchurch Drainage Board in 1875. The 1940 stereoscopic images show the buildings at the base of the eastern slope (also present in the 1926 aerial images) to have been located on topographically higher fan surfaces, which

Figure 3.5: Aerial photographs of the eastern side of the Hillsborough Valley. Images sources are as follows: 1926 (Canterbury Maps 2015), 1940 and 1973 (D. Bell University of Canterbury), 2011 (CCC). Centaurus Road is across the top of the images, Hillsborough Terrace forms the left/western boundary. Of the two roads in the centre, Vernon Terrace is on the left and Rapaki road is on the right. A) Fenceline possibly obscured by sediment. Arrow also indicates toe of main fan surface. B) Gullies truncating against a paddock. C) Smoothed fan surface.

was likely done to get above a high water table on the valley floor . From the 1940s to the early 1950s, land-use in the valley changed from mostly market-garden to mixed residential. By 1963 a single cluster of paddocks remained in the centre of the valley, which had been converted to housing by the time of the 1973 aerial survey. In the 2011 aerial survey vegetation growth at the southern end of the valley had covered the tunnel gullied landscape that was not already covered by residential development sites (Figure 3.5).

3.4 Trenching and logging

3.4.1 Sampling procedure

A trench was hand-dug perpendicular to a fissure trace for the purposes of sampling and observation (Figure 3.6 and Figure 3.7). The excavation was approximately 1 x 1 x 2.6m (width x depth x length). A total of fifteen 10mm diameter shearbox sampling rings and fifteen 38mm diameter sampling tubes were pushed or hammered into the ground. Samples for shear strength analysis were taken from both the vertical and horizontal orientations. The 38mm push tubes samples were collected for measurement of density, moisture content and unconfined compressive strength (UCS). Loose, excavated material was bagged for use in tensile strength analyses of recompacted samples, as it was too difficult to recover suitable blocks for testing. Trenching of the compression zone was considered, however not pursued due to the high water table near the ground surface.

Figure 3.6: View of fissure looking north (left) and close-up view of weathered and infilled section (right), adjacent to the trench.

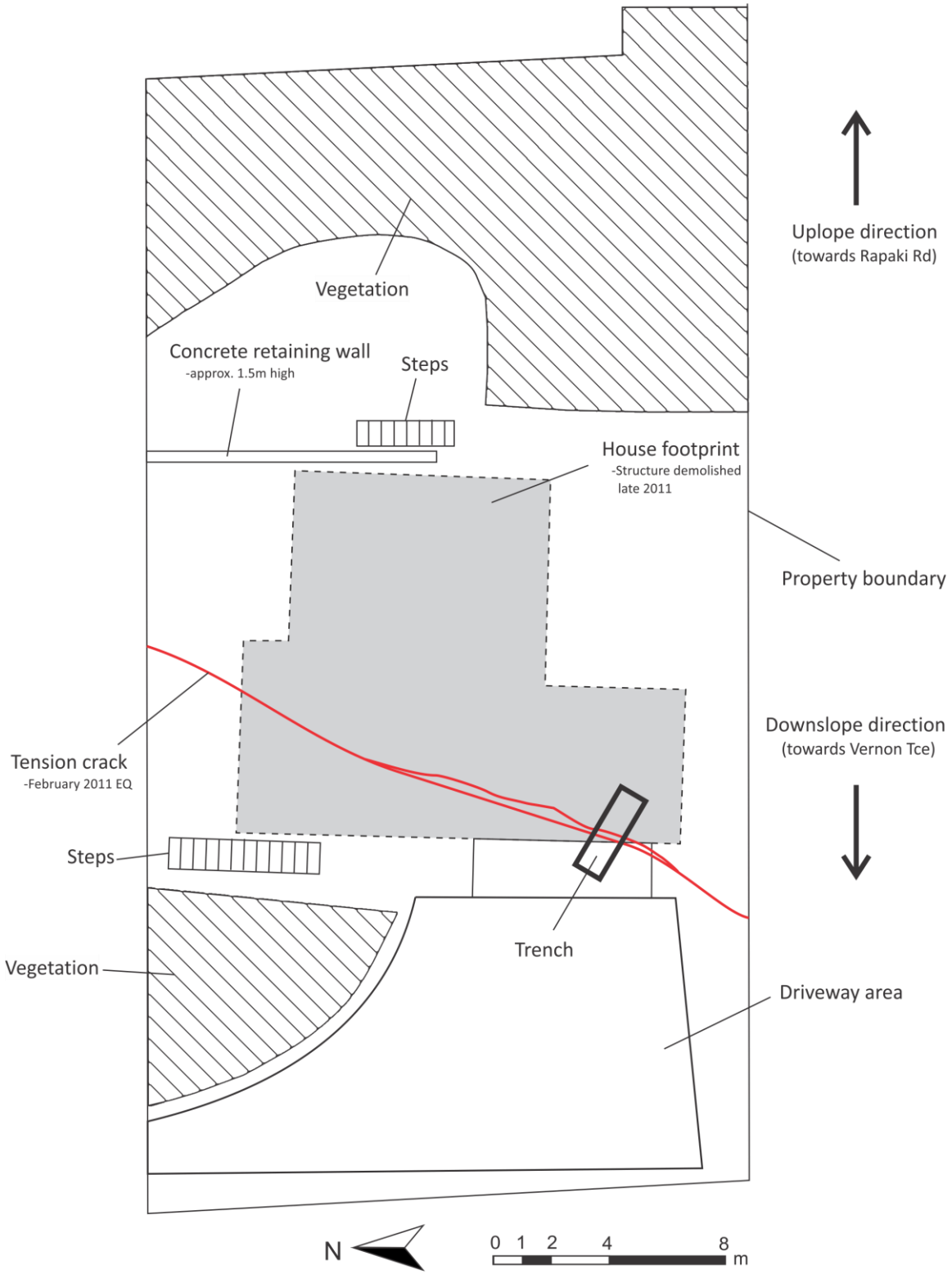

Figure 3.7: Site map showing trench location and tension crack.

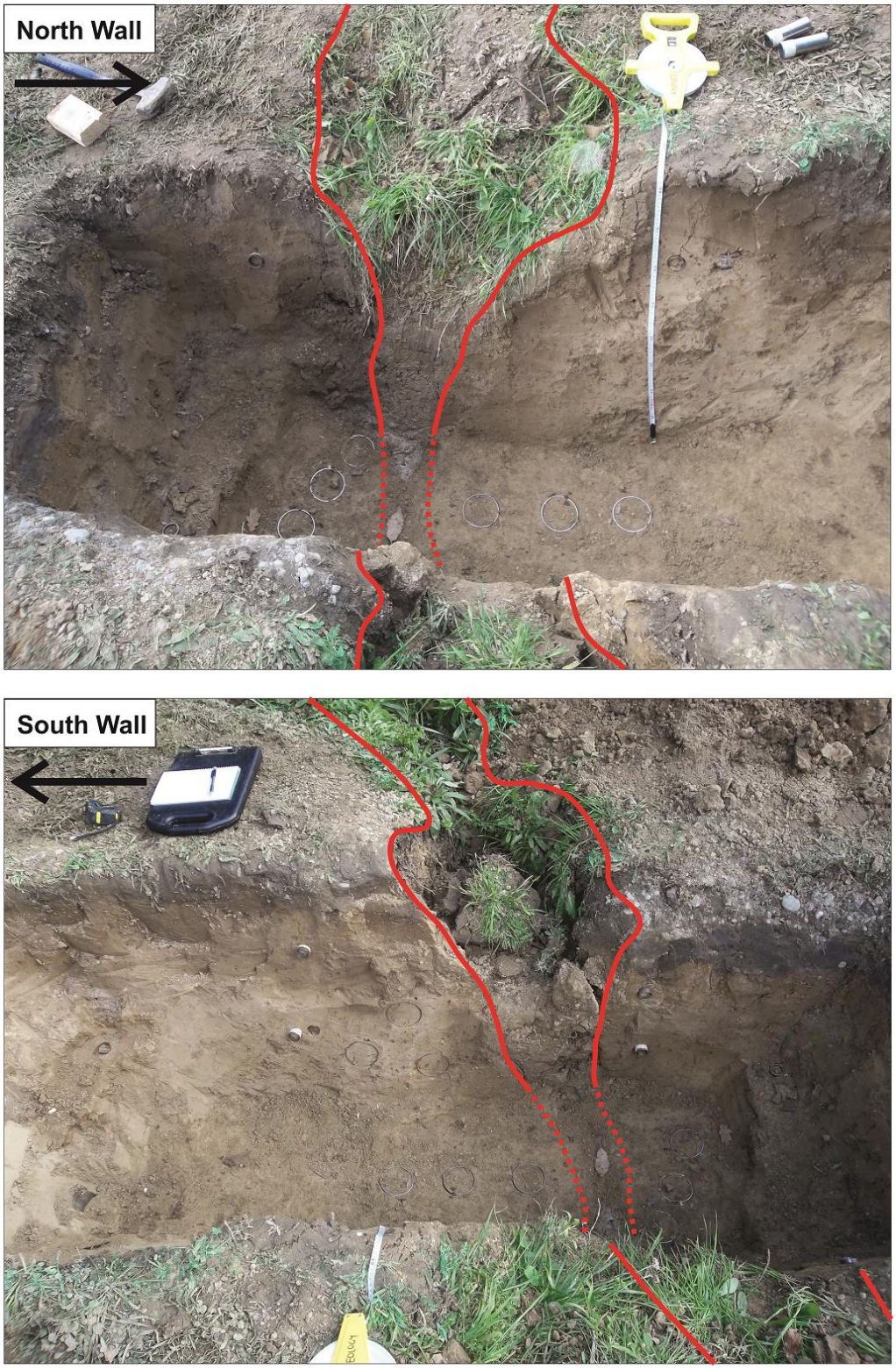

Figure 3.8: Trench walls. Fissure outlined by red and dashed along trench floor. Black arrow indicates upslope direction. Sample rings are 100mm in diameter, measuring tape on north wall reads 0.8m from the base of the excavation to ground level. Note seepage onto floor of trench from north wall fissure.

3.4.2 Trenching observations

The unremediated fissure provided a case study on the short- to mid-term weathering and degradation of the fissured loess. The fissure was 10 – 100mm wide when it first formed. At the time of trenching, three and a half years after formation and two and a half years since demolition of the house, the fissure had weathered open to 1.0m wide in places. 'Open' parts of the fissure were infilled with blocks of moist loess, or saturated loess slurry, with weeds and grass (Figure 3.6). Depth measurement to the base of the fissure was not possible, although it was observed to exceed 1.0m depth during excavation.

During excavation of the trench, it was observed that the soil on the downslope side of the fissure was darker in colour and easier to excavate. Analysis of soil sampled from both sides of the fissure showed a mean soil moisture content of 9% upslope and 14% downslope of the fissure (Figure 3.9). The ground was approximately level on the downslope side of the fissure at the location of the trench, with a thin (<0.2m) layer of gravelley fill. The higher moisture content could be the result of water ingress via the fissure, and/or water perching in the fill and then moving down into the soil below under gravity.

With the exception of fill and topsoil at the ground surface, the trench was excavated through loess-colluvium. Volcanic fragments varied in size from medium sand to cobbles, and consisted of slightly to moderately weathered basalt. The dry density of the loess colluvium ranged from 1460 to 1870 kg/m^3, with a mean density of 1650 kg/m^3 (Figure 3.9).

The nature of the material filling the fissure differed on either side of the trench. The southern side was relatively dry and the sides had weathered inward in large cohesive blocks (Figure 3.7 and Figure 3.8). The northern side was infilled by extremely soft and saturated soil. Water can be seen seeping onto the floor of the trench from the fissure in Figure 3.8.

The depth of the trench did not surpass the zone of weathering and fissure infill. While the exact position of the original fissure walls was in places unclear, the sides were narrowing down towards the base of the trench and were approaching the original aperture of the fissure at the ground surface (at approximately 1.0m depth). The process of excavation (using a pick and then excavating loose material with shovels) meant the section of the fissure on the floor of the trench became in-filled.

As mentioned previously, most of the fissures on the eastern side of the Hillsborough Valley were infilled via a community effort, with a mixture of SAP-20 and bentonite (Stephen-Brownie 2012). The section of fissure that was trenched was located under a house, which had been demolished after

the infilling effort and therefore had been left open. A cutoff drain was dug above and parallel to the fissure to intercept overland flow.

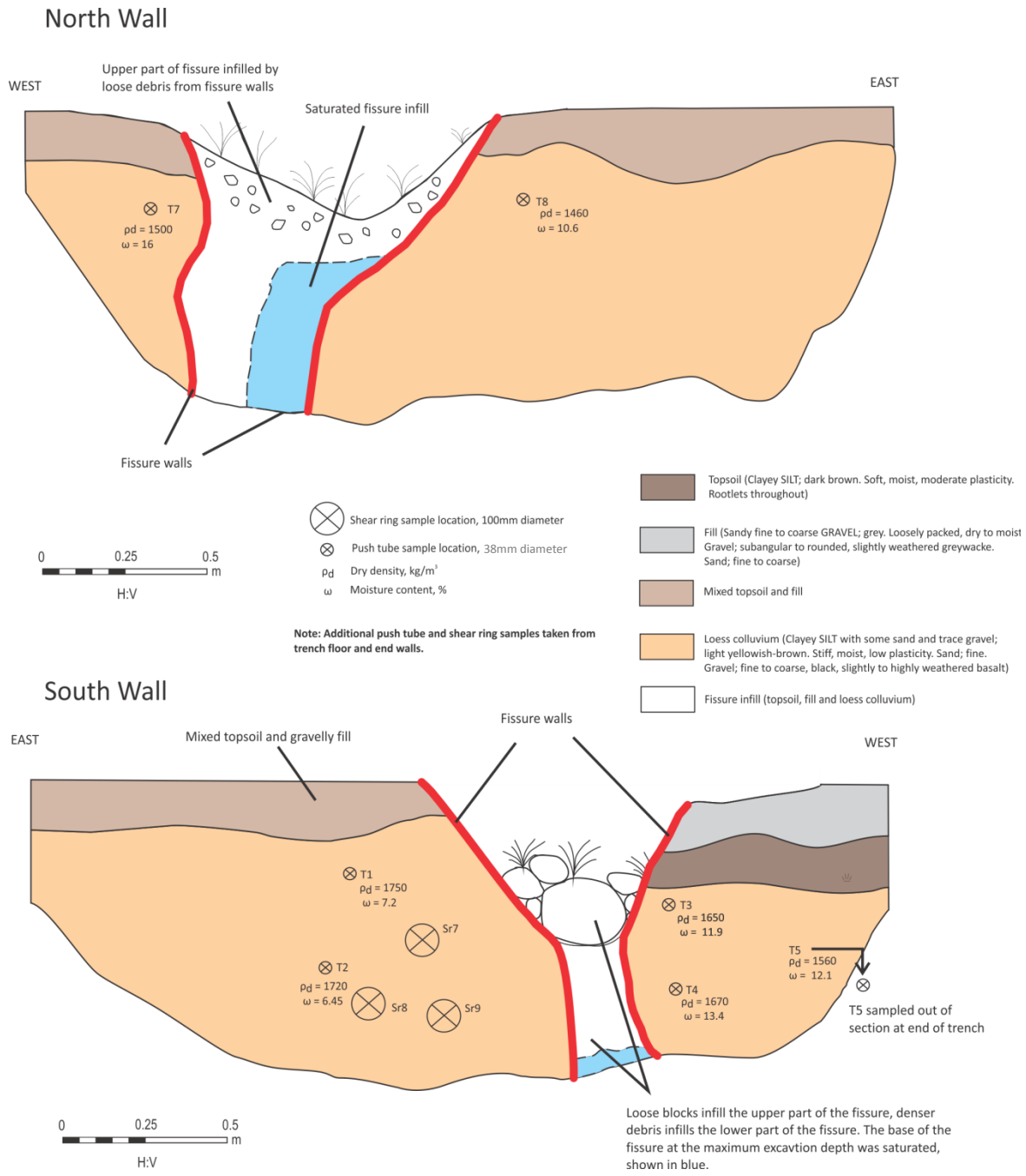

Figure 3.9: Trench logs. Trench was located on flat ground. Uphill direction is east, downhill direction is west. Additional out-of-section push tube samples not shown.

3.5 Seismic refraction survey

A seismic refraction survey was carried out perpendicular to Vernon Terrace (trending east-west), slightly offset from two boreholes (BH08 and BH09). Seismic refraction surveying uses surface-generated seismic waves to infer interface depths and layer velocities. The propagation velocity of a seismic waves depends on the density and elasticity of the medium it is travelling through (Everett 2013). For soil and rock, P-wave velocity increases with saturation, consolidation and homogeneity, and is also greater for geomaterials that are intact and unweathered (Everett 2013). Seismic refraction surveying is commonly used for 'depth to bedrock' and groundwater investigation, when a clear velocity contrast between refractors is expected (Everett 2013).

3.5.1 Survey geometry

The aim of the seismic refraction survey carried out for this research was to model the colluvium-bedrock interface. The survey line was 96m in length with a 2m spacing between each of the 49 vertical 8Hz geophones. An accelerated weight drop and an 8kg sledgehammer (with an inertia switch and steel striker plate) were used as seismic sources. Relative to the first geophone (top of driveway), the weight drop was deployed at -60 (S5), 0 (S4), 45 (S3), 96 (S2) and 146m (S1), see Figure 3.10. The sledgehammer was deployed at 2m intervals along the length of the survey line, starting at -8m and finishing at 104m. Six hammer stacks were taken at each location to increase the signal to noise ratio. Geophone locations were surveyed using real time kinematic (RTK) GPS.

First arrivals were picked by the author using Reflex 2DQuick (Sandmeier 2014), before being transferred to an Excel spreadsheet containing header information for geophone and shot point distances and elevations. Modelling was carried out by Southern Geophysical Ltd using Rayfract seismic refraction software (Rohdewald 2014). An initial 1D gradient model was determined from the imported travel time data using the Delta-t-V method. This model was then refined using 2D Wavepath Eikonal Traveltime (WET) tomography processing. To produce a smooth inversion, 100 WET iterations were performed. The resultant plot is shown in Figure 3.11. Modelled wavepath coverage is shown in Figure 3.12.

3.5.2 Profile interpretation

The model shows a gradual increase of P-wave velocity with depth (Figure 3.11). The area of lowest velocity, 400 - 600m/s, is directly below the geophone spread. These values fall within the expected range for unsaturated Port Hills loess (Table 3.1). The base of this low velocity zone approximately coincides with the water table, as determined from nearby piezometers for the time of the survey

(see section 3.6.5). The velocity increase below this point can be explained by increasing moisture content and increasing density. The bedrock surface, as inferred from nearby boreholes, coincides with the 2400m/s contour. A P-wave velocity of 2400m/s is in good agreement with the findings of McDowell (1989) for weathered basalts in the Port Hills.

The bedrock surface (2400m/s velocity contour) slopes gently through the central part of the hillslope, and steepens towards the valley floor. The model also shows the 2400m/s contour to dip at the 10m mark, although this is probably a modelling artefact. Upslope of the profile, bedrock is expected to rise sharply as it is near to the ground surface above Rapaki Road. The tomogram produced was used to help construct the engineering geological block model presented at the end of this chapter.

Table 3.1: P-wave velocities for Banks Peninsula loess and basalt.

Source	P-wave weathered basalt m/s	P-wave loess m/s	Survey type
McDowell (1989)	2500*	300 - 700	Refraction (shallow)
Crampton et al. (1988)	1718*	387	Refraction (shallow)

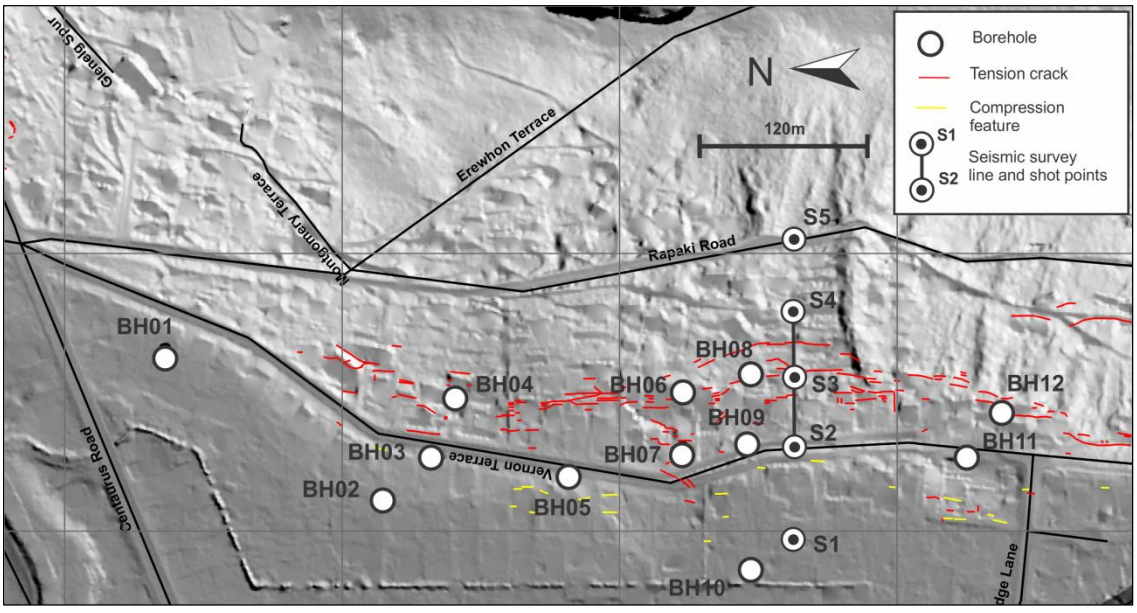

Figure 3.10: Seismic survey line and shot points.

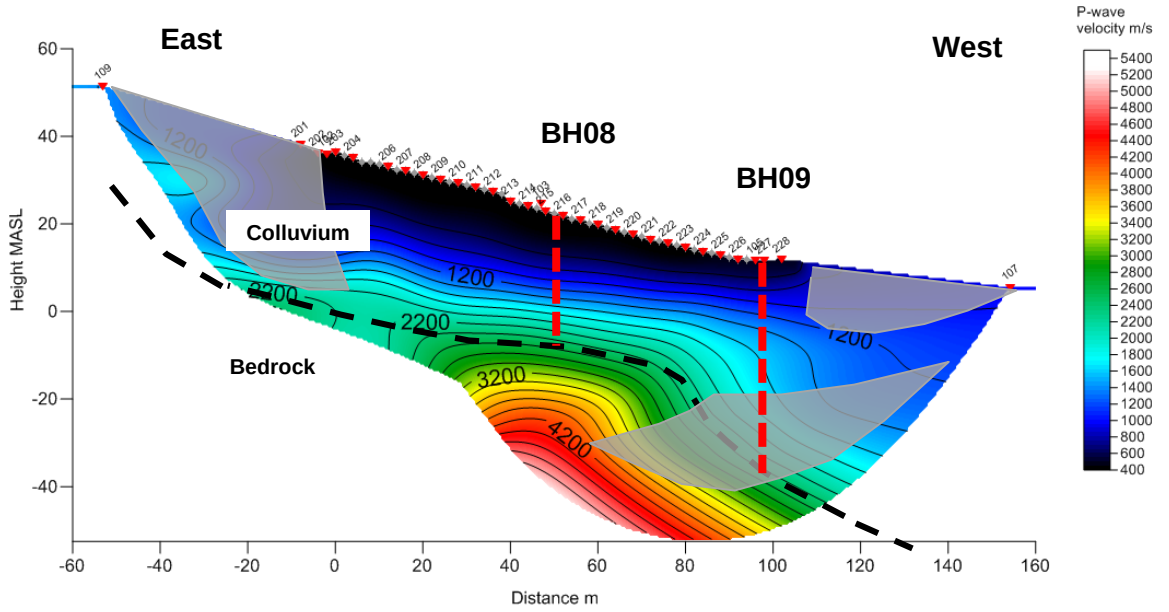

Figure 3.11: Vernon Terrace P-wave tomogram. X-axis shows distance in metres from geophone 1 (shown as 201). The red triangles and grey diamonds are individual geophones. Model information: 100 WET iterations, RMS error 4.6%. Version 3.32, 400/4000 layers, 2 refractors. The greyed areas are those which are modelled to have had little or no wavepath coverage. The two nearby boreholes are shown as dashed red lines, with the inferred colluvium-bedrock contact shown by a dashed black line.

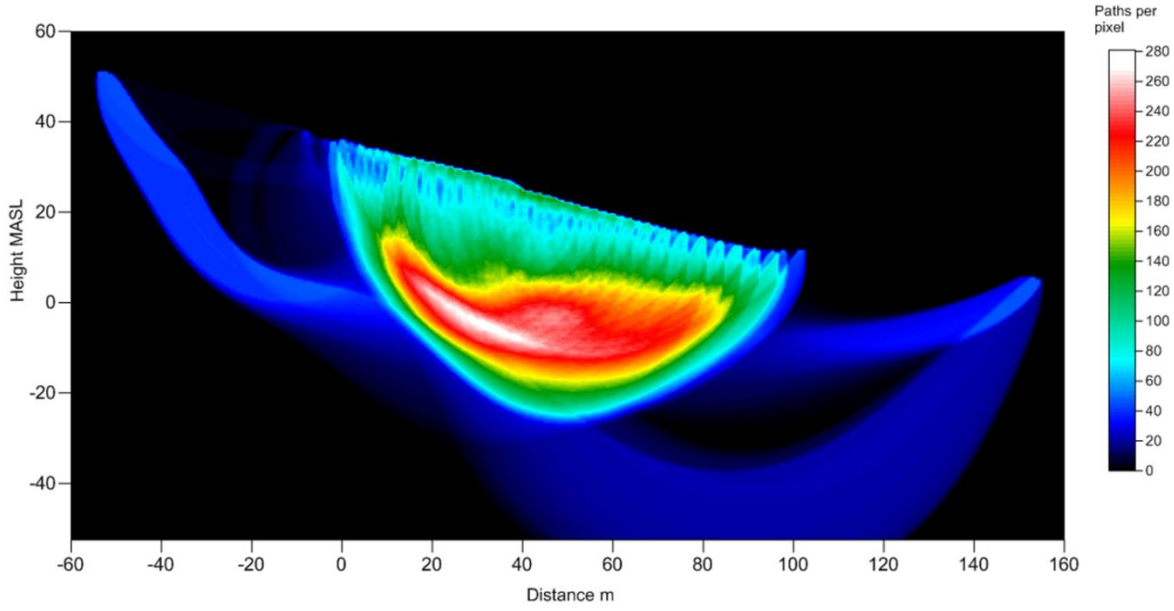

Figure 3.12: Wavepath coverage for Figure 3.11, Vernon Terrace P-wave tomogram. Model information: 100 WET iterations, RMS error 4.6%. Version 3.32.

3.6 Engineering Geological Model

The geology and geomorphology of the Hillsborough Valley is summarised by the map presented in Figure 3.15. Slope morphology was established using LiDar, slope angle maps created using the LiDar and historical aerial photographs. The geology was mapped using borehole and hand auger records sourced from the CGD (2015a) (borehole locations are shown on Figure 3.14) and field observation. Historical photographs were particularly useful for identification of geomorphological features. The mapped locations of extension and compression features were sourced from the 'Port Hills Mass Movement and Surface Deformations' map layer (CGD 2014).

3.6.1 Valley Morphology

The long axis of the valley trends north-south and is approximately 900m long. The adjacent interfluves, Glenelg (east) and Huntsbury (west), are a maximum of 150m above sea level (masl) on either side of the valley and slope gently to the north. The valley floor is 4 – 9 masl and 1km wide at the entrance. Ephemeral drainage lines run down either side of Mt Vernon spur, and pass into the 'Victory Drain' which meets the Heathcote River at the valley entrance. The morphology of the eastern slope is consistent with the model proposed by Bell and Trangmar (1987), where a shallow-angle toe slope (3-13°), steepens through to the foot slope (13-20°) and backslope (>20°), with bedrock outcropping along the mid backslope and along the shoulder of the spur (see Chapter 2). A concave break in slope between Vernon Terrace and Rapaki Road was identified using the 1940 aerial photographs and LiDar (Figure 3.15). This break in slope approximately conincides with the transition from the toe slope to the foot slope.

3.6.2 Bedrock

The Hillsborough Valley is situated on the northern rim of the extinct Lyttleton Volcanic Complex (11 – 9.7Ma) (Hampton 2010). As volcanic activity waned in the late Miocene, the flanks of the cones became incised along radial and cone-controlled drainage lines, with the Hillsborough valley the result of radial incision of the Governors Bay cone (Hampton 2010).

Bedrock consists of Lyttelton Volcanic Group (LVG) basalts, agglomerates and ash (Brown and Weeber, 1992). Flows dip gently to the north, outcropping in the upper reaches of the valley (Figure 3.13), and along the shoulder of Glenelg spur (Figure 3.15). Brown and Weeber (1994) estimated bedrock to be approximately 50m below mean sea level at the northern end of the valley, based on deep drilling in the adjacent Heathcote and Bowenvale Valleys. While depth to bedrock at the centre of the valley is unknown, drilling carried out in mid-2011 encountered bedrock at 44.7m below sea

level at the base of the eastern slope, approximately 150m from the centre of the valley (Figure 3.14). Using the mean bedrock ‘gradient’ calculated from outcrops and boreholes (approximately 1V:2H) it is possible that depth to bedrock at the centre of the valley is greater than 100m below mean sea level. This is not unreasonable given that the valley is thought to have formed as a deep, steep sided erosional feature (Bell & Trangmar 1987). Bedrock contours determined from the boreholes shown in Figure 3.14. Bedrock in these boreholes has variably been logged as unweathered to moderately weathered basalt.

The tomogram produced for Vernon Terrace shows bedrock to dip gently through the centre of the profile below the geophone spread. This buried ‘step’ is consistent with topography observed across the Port Hills, where steep bluffs outcrop in a stepped fashion up a hillslope. The intervening sections of slope are less steep and have been mantled by loess and colluvium.

Figure 3.13: View looking southwest from the carpark at the beginning of the Mt Vernon Valley track. Note the steep slopes and rock outcrops. See Figure 3.14 for photo location.

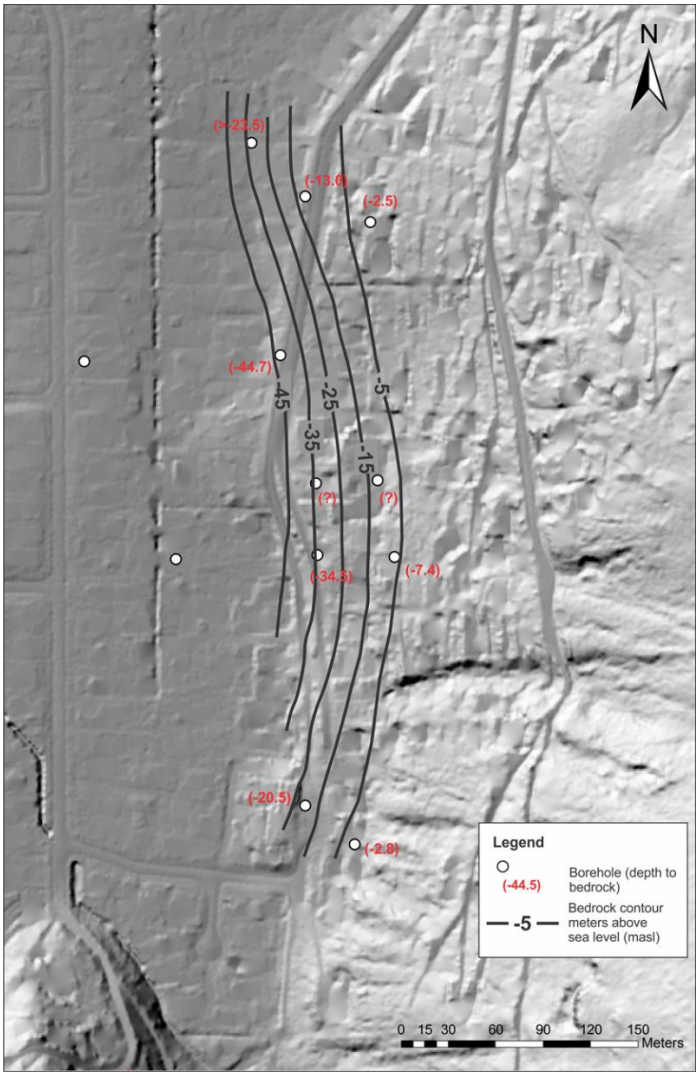

Figure 3.14: Bedrock contours for the eastern side of the Hillsborough Valley. The valley floor is 4 – 9 metres above mean sea level.

3.6.3 Slope cover

Loess was deposited across the Canterbury Plains and Banks Peninsula during Quaternary glaciations. Airfall loess is preserved along the summit of Glenelg spur and forms a thin (<2m) cap over loess-colluvium at the northern end of the spur (Figure 3.15). Borehole logs indicate the material overlying bedrock is primarily loess-colluvium, with volcanic content increasing with proximity to bedrock both at depth and at the ground surface (see Figure 3.15 and Appendix A for borehole logs). Loess-, mixed- and volcanic colluvium are represented on the map (Figure 3.135) by the same colour, with an increasing density of dots to indicate greater volcanic content.

Bedrock is typically overlain by several metres of 'bouldery' volcanic colluvium (BH02, 11 and 12) or capped with a saprolite layer of up to several metres in thickness (moderate to high plasticity silty

clay with minor sand and gravel, encountered in BH03, 05 and 09). The presence of saprolite indicates bedrock was exposed for a considerable period of time before loess deposition commenced. Rare lenses of 'airfall' loess are preserved at depth between layers of loess colluvium, indicating erosion was actively occurring during episodes of loess deposition (Griffith 1973), spanning several glaciations.

Borehole logs describing blocky textures and pinholing at depth within the loess colluvium are evidence for paleo surfaces. Soil is able to form a blocky texture when it contains clay and undergoes cycles of wetting and drying at the ground surface. BH08, for example, is logged as having a blocky texture at 12 different depths (see Appendix A for borehole logs). 'Pinholing' is interpreted as evidence for root casts and also indicative of a paleo-surface.

3.6.4 Valley floor fill

Pleistocene climate fluctuations and associated sea level rise and fall promoted deep valley incision during glacial low-stands and subsequent infilling and 'drowning' during interglacial high-stands (Bell & Trangmar 1987). Brown and Weeber (1992) estimate 25m of postglacial sediment (Springston and Christchurch formations) to have been deposited in the vicinity of the Hillsborough Valley. This postglacial sediment consists of a mixture of marginal marine, peat swamp and overbank material at the northern end of the valley, which interfingers with up-slope or up-valley derived colluvial sediments. BH02, BH03 and BH05 show thicknesses of alluvium and estuarine deposits between -10 and -23.5m below sea level. This material is underlain and overlain by loess-derived soils. The maximum up-valley extent of these sediments is unknown.

Geotechnical investigations are primarily located along the base of the eastern slope and subsurface information for the central valley floor is limited to the upper 20m, with no boreholes or CPTs at the time of writing exceeding this depth. Borehole and hand auger logs show surficial valley fill to be highly variable. Peat deposits are widespread at or near the ground surface, primarily below the 5m contour line (Figure 3.15). The peat is thickest between Leonards and Roscoe Street on the western side of the valley, and this band appears to continue over to the eastern side of the valley, with a thickness ≥4m (Figure 3.13). Peat is also found at the corners of Centaurus Road and Vernon Terrace, with thicknesses of ≥3.5m encountered by hand augers. With the exception of the peat, valley fill has been mapped as 'undifferentiated' and includes all material on the valley floor (Figure 3.15). Up-slope or up-valley derived colluvium is inferred to be make up a significant portion of the valley fill.

3.6.5 Groundwater

The water table at the valley floor is very near to the ground surface (Green, in prep). The springs that appeared following the February 2011 earthquake – most of which are still flowing at the time of writing – can be seen to follow the periphery of the mapped peat (Figure 3.15).

Nine piezometers were installed in boreholes on the eastern side of the Hillsborough Valley to record water levels within the loess and loess colluvium. The piezometers show the water table to follow a near flat gradient into the hillside, from the valley floor. The mean height of the water table above sea level varies from 5 to 8 masl at the northern part of the valley, and 10 to 14.5 masl at the southern end of the valley.

While the piezometers show a single water table, it is expected that groundwater is layered throughout the slope. Different loessial and colluvial units have different grainsizes, densities, etc, and the hydrogeology of the hillslope is inferred to be complex, particularly when the presence of subsurface drainage networks (i.e. tunnel gullies) is taken into account. The borehole logs for the holes in which the piezometers were installed show moisture content to vary from dry to wet. Most of the soil was logged as moist, with moist to wet and wet zones of up to several metres in thickness throughout. Dry zones were also encountered at depth. The slope hydrogeology is discussed further in Chapter 5.

3.7 Earthquake-related features

The location and extent of some of the ground damage can be correlated with geological and geomorphological features. Here, the features are briefly described in the context of the valley geology and geomorphology.

3.7.1 Fissuring

The eastern slope of the Hillsborough Valley has been mapped as loess-colluvium, with fill or made ground within the developed area (unmapped). All fissuring has occurred within loess colluvium. Brown and Weeber (1992) mapped a contact between valley fill and loess, which Stephen Brownie (2012) used to suggest that fissuring had occurred along the contact between the two regolith types. Access to the CGD, together with site investigation, has shown this is unlikely.

The location of the fissuring appears to correlate with geomorphological features identified using historical aerial photography and recent LiDar data. When overlaid on the 1940 aerial photograph, the fissures follow the fan apices visible at the rear of the valley (Figure 3.16). Land modification in

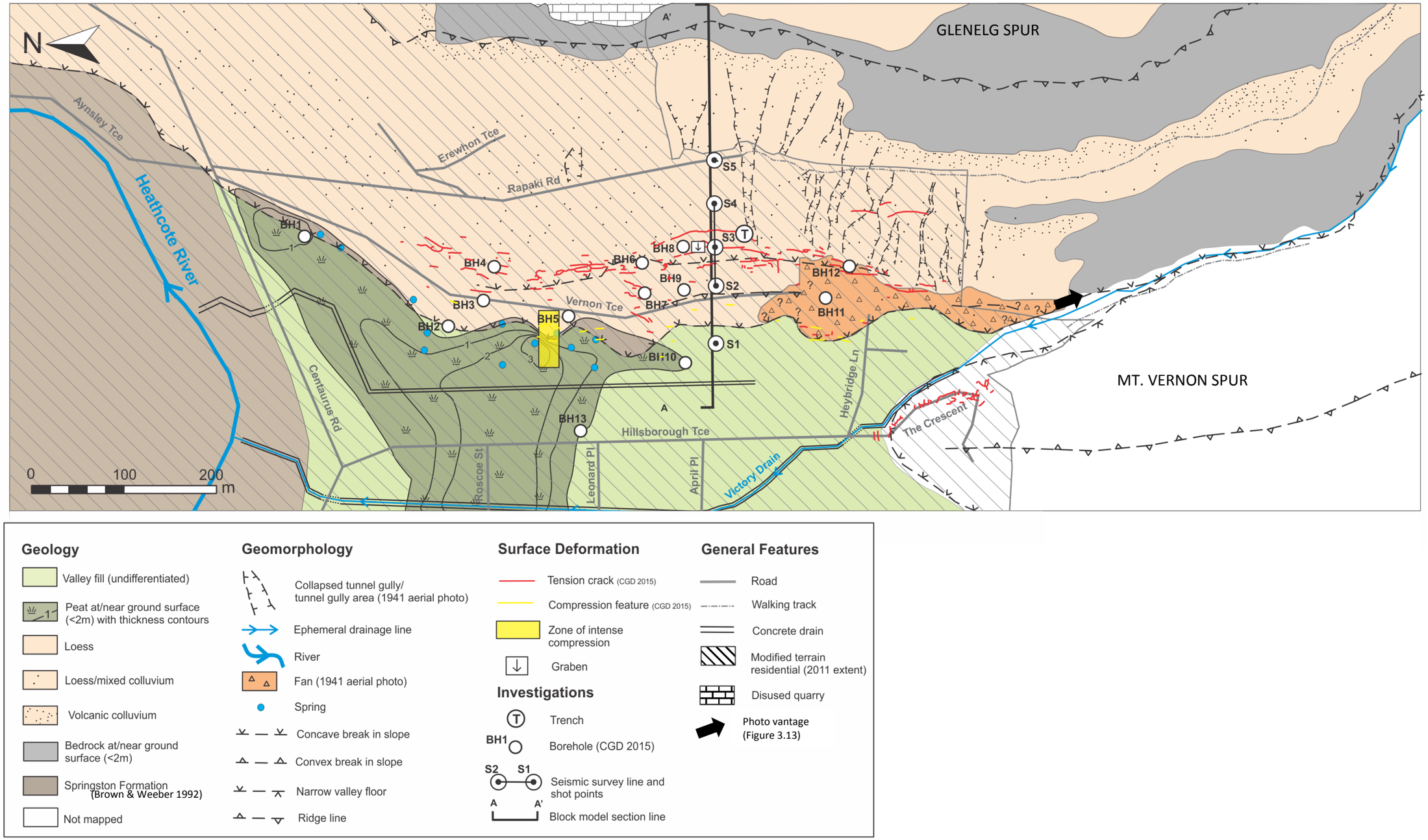

Figure 3.15: Engineering geological and geomorphological map of the eastern side of the Hillsborough Valley.

the central part of the valley has removed obvious signs of fan deposits, however, there is a concave break in slope through the central part of the extension zone (Figure 3.15). The change of slope gradient could indicate the presence of fan material.

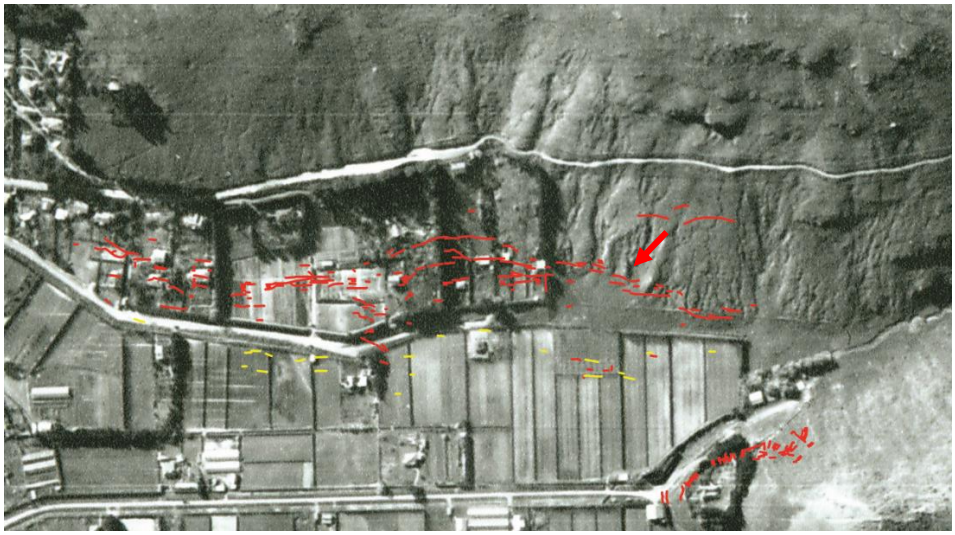

Figure 3.16: Fissure traces overlaid on 1940 aerial photograph. Red arrow indicates where fissure traces follow fan apices.

3.7.2 Compression and springs

There is a zone of significant compression (~0.3m total measured shortening) towards the northern end of the valley (Figure 3.15). This area coincides with the thickest known peat deposits, which are ≥4m, according to hand augers carried out in the area (Figure 3.15). Some compressional features from this area are shown in photographs provided in Chapter 2. Compressional features at the southern end of the valley appear to coincide with the toe of fan material mapped using the 1940 aerial photograph (Figure 3.16).

3.8 Block model

A schematic engineering geological model for the eastern side of the Hillsborough Valley is presented in Figure 3.17. The location of the block is shown by the A – A' section line on Figure 3.15. The model was created to illustrate the extent and scale of the ground damage, relative to the valley geology and geomorphology.

The geology of the model is informed by three out-of-section boreholes: BH08, BH09 and BH10. BH08 and BH09 were both drilled to bedrock and used to constrain bedrock topography, together

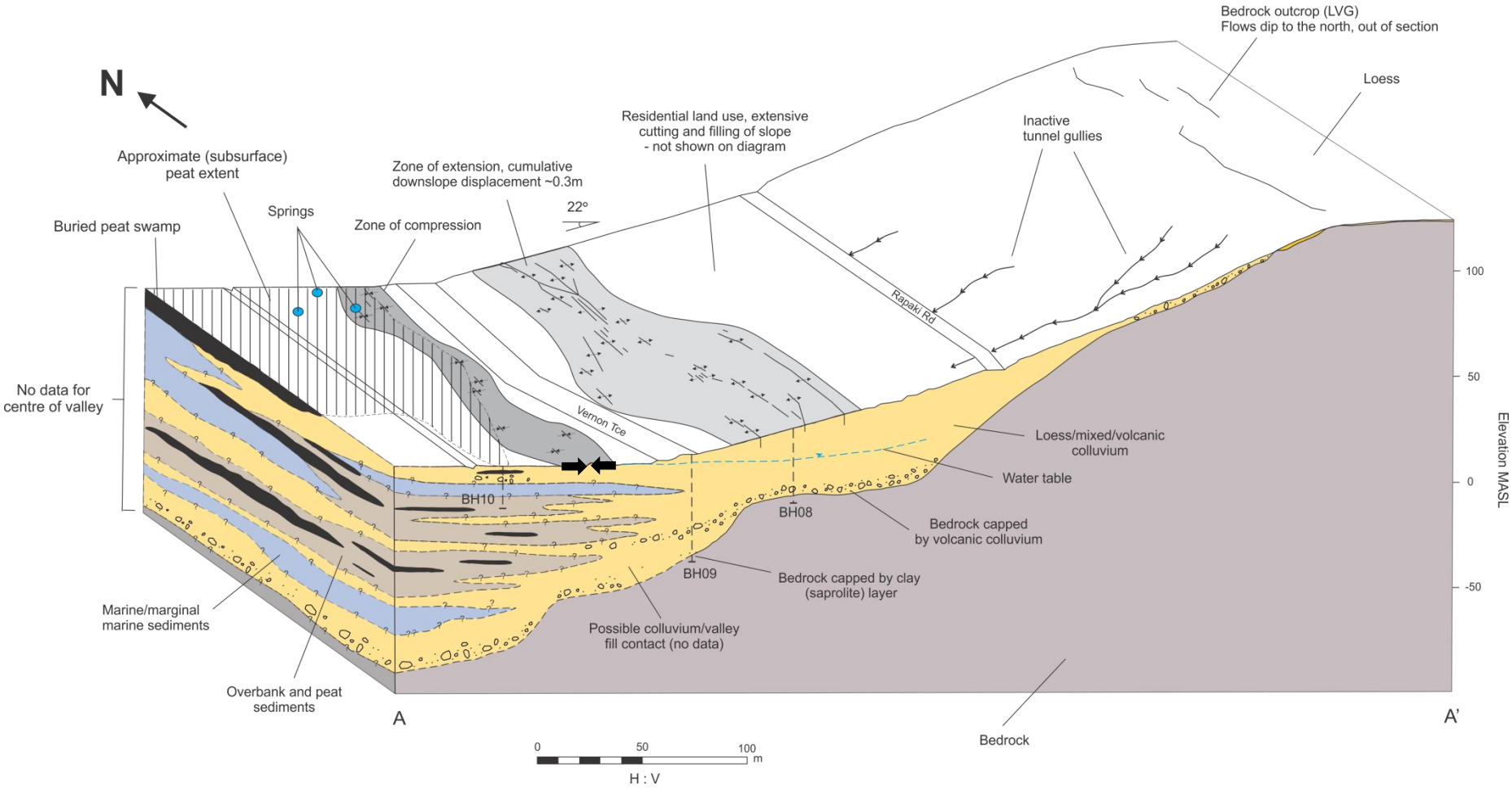

Figure 3.17: Block model of the eastern side of the Hillsborough Valley. BH08, BH09 and BH10 are approximately 30m out of section, to the north. Location shown by section line on Figure 3.14.

with the findings of the seismic refraction survey. Surficial valley-floor sediments, in particular the shallow peat deposits, were mapped using hand auger logs downloaded from the CGD (2015a). As discussed previously, subsurface information for the valley floor is limited to the upper 20m, with no boreholes or CPTs exceeding this depth. The valley is inferred to be infilled by a mixture of upslope and up-valley derived colluvium, marginal marine (interglacial) sediments and overbank (glacial) sediments, as indicated by BH02, BH03 and BH05, located closer to the valley entrance. The actual up-valley extent of these sediments is not known. In addition, the thicknesses of the layers shown is representative only - it is inferred that the actual geology will be much more complex, consisting of thinner, discontinuous units. A simplified water table, as indicated by piezometric data is shown on the model.

The mapped compression and extension features are shown as zones on the diagram, with tension cracks drawn to 5m depth, which is maximum measured according to Stephen-Brownie (2012). Assuming tension cracks are not significantly deeper than what has been measured, the model provides a useful sense of scale for the depth of cracking relative to the thickness and extent of the colluvium.

3.9 Synthesis

- Models accounting for the observed ground damage in the Vernon Terrace area have been presented by Dellow et al. (2011), Stephen-Brownie (2012) and Massey et al. (2013).
- Historical aerial photographs were examined to establish site history. The 1940 aerial photographs show severe tunnel gullying at the rear of the valley (now concealed by vegetation and housing), with fan material extending from the gullies onto the valley floor.
- Field work in the form of trenching and a seismic refraction survey were undertaken. A fissure was trenched for the purposes of soil sampling and observation; undisturbed soil samples and loose soil was bagged for testing. The tomogram produced using seismic refraction data collected for this research shows a bedrock ‘step’ below the geophone array, consistent with outcrop patterns observed across the Port Hills.
- Bedrock is comprised of LVG eruptives and could be as deep as 100m below mean sea level at the centre of the valley. Valley fill is comprised of upslope-derived colluvium, which interfingers with postglacial sediments at the valley entrance. Significant peat swamp deposits are located at the corner of Centaurus Road and Vernon Terrace, and mid-way along Vernon Terrace. Airfall loess is preserved along the summit of Glenelg

spur and at depth within the loess colluvium. Hillslope sediment is primarily loess- and mixed-colluvium.

- Ground cracking has occurred within loess colluvium and follows the apices of fans identified at the rear of the valley. In the central part of the valley cracking broadly coincides with a concave break in slope.
- Compressional features were only observed where rigid structures have been crumpled or shortened. The most significant compression coincides with thick peat deposits.

4 Tensile Strength Analysis

4.1 Introduction

This chapter describes the tensile strength testing carried out for this thesis. The fissures on the eastern side of the Hillsborough Valley are interpreted as tension cracks which have formed through tensile failure of the loess colluvium. Testing was carried out to determine the tensile strength of Port Hills loess colluvium as a function of water content and density, in order to better understand the occurrence and distribution of the observed cracking.

Measurement of soil tensile strength is rarely undertaken at either commercial or academic institutions, and no standards exist for the testing of soils in tension. Testing has not previously been carried out to determine the tensile characteristics of Port Hills loess or loess colluvium, with the existing body of literature focussed on geotechnical properties tested for during routine commercial investigations (e.g. McDowell 1989; Yetton 1986; Glassey 1986; Tehrani 1988; Goldwater 1990; Hughes 2002). In the absence of a standardised test procedure, the literature was reviewed to find a suitable methodology that could be adapted for testing in the Engineering Geology Soil Mechanics Laboratory at the University of Canterbury.

Given that the field of soil tensile testing falls outside mainstream geotechnical engineering, the first part of this chapter summarises the applications and measurement of soil tensile strength. A comprehensive review of soil tensile testing is provided in Appendix B. The direct tensile test procedure developed for this study was adapted from the recent work of Tamrakar et al. (2005 and 2007). The sample preparation and testing procedure are described, with detailed coverage of the development of the test procedure provided in Appendix C. Findings are discussed with reference to the observed ground damage in Chapter 5.

4.2 Engineering applications of soil tensile strength

4.2.1 General basis

Tensile strength is simply the maximum tensile stress (stretch or pull) a material can withstand before failing or breaking. The tensile strength of unsaturated, granular soil is derived from surface tension of pore water, matric suction and cementation if present (Lu & Likos 2006). For cohesive soil,

physiochemical forces (e.g. van der Waals and electric double layer forces) may also contribute. Ignoring cementation, tensile strength of predominantly sandy, silty and clayey soils will generally differ by an order of magnitude. For sandy soils, tensile strength can be up to several kilopascals (kPa), for silty soils tensile strength can be up to several tens of kPa, and for clayey soils tensile strength can be as large as several hundred kPa (Lu & Godt 2013).

4.2.2 Earth dams

Since the 1950s a relatively small number of researchers have sought to understand the behaviour of soils in tension. The majority of the research carried out has been directly or indirectly motivated by the occurrence of earth dam cracking, which can lead to severe internal erosion and/or failure of the structure. As a result, many of the soils tested have been sampled from the borrow areas of earth dams (e.g. Krishnayya et al. 1974; Win 2006; Leonards & Narain 1963). The development of tension cracks on the dam crest is generally the result of differential settlements (Leonards & Narain 1963), and internal cracking of the dam core can act as an initiating site for internal erosion (Vaníček 2013). The onset of cracking is predicted by comparing computed principal tensile stresses and experimentally determined tensile strength (Win 2006). Cracking can also be initiated by desiccation, seismic effects, and deflection of the dam when the reservoir is first filled (Ajaz & Parry 1975; Vaníček 2013).

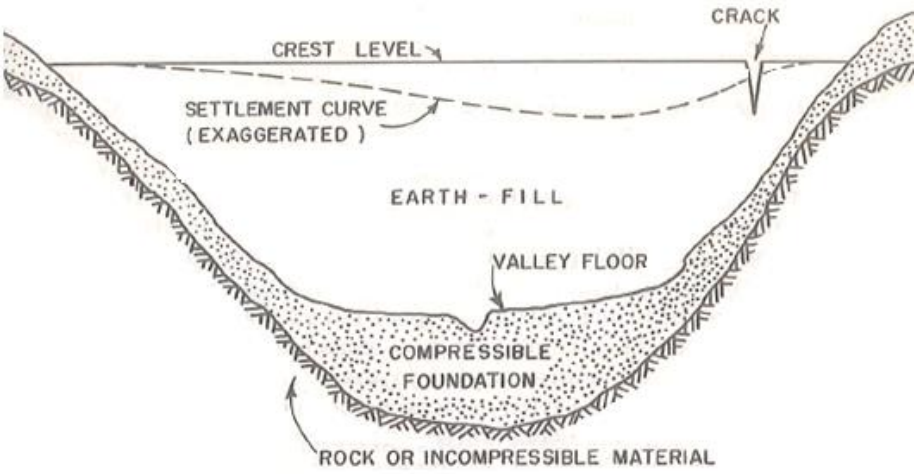

Figure 4.1: Schematic diagram of earth dam settlement and associated tension cracking (Leonards & Narain 1963).

4.2.3 Slope stability

Soil tensile strength is largely absent from traditional slope stability analyses, with limit equilibrium and sliding block methods relying on shear strength to calculate the factor of safety against sliding and critical acceleration, respectively. The role of tensile failure in slope stability is most often considered with respect to how a physical (tension) crack may contribute to the forces driving

movement if the crack was to fill with water (Duncan & Wright 2005). While tensile strength can provide a critical contribution to hillslope stability (Lu & Godt 2013), limited research has been carried out to understand the contribution of tensile strength to the forces resisting movement. Two studies which have explored the role of tensile strength in slope stability are briefly summarised below:

1) Kelzieh (1991) incorporated soil tensile strength into stability analyses for two curved failure surfaces through an idealised slope (Figure 4.2, left). The measured tensile strengths of three soils (ML, CL and CH), together with the calculated horizontal and vertical stresses, were used to assess the impact of tensile strength on the calculated factor of safety. The percentage increase in factor of safety varied from 2.0 - 12.8% depending on the tensile strength of the soil, and the geometries of the slope and assumed failure surface (Figure 4.2, right). It can be seen from Figure 4.2 that tensile strength had a greater influence on factor of safety for the failure surface with the deeper tension crack.

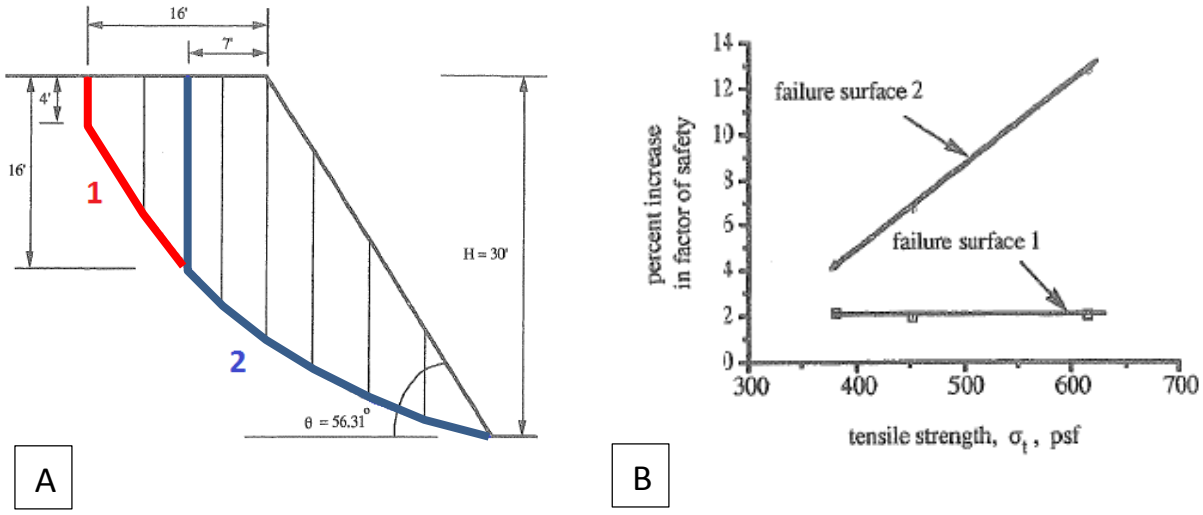

Figure 4.2: Tensile strength in slope stability analysis. A) Slope model and failure surfaces. B) Plot depicting percentage increase in factor of safety vs tensile strength (right) (Kelzieh 1991). Slope dimensions: Height = 9.81m, slope angle = 56.31°, crest to tension crack distances are 2.1m and 4.8m, tension crack depths are 1.2m and 4.8m. 1 kPa ≈ 20psf.

2) Gipprich et al. (2008) developed a limit equilibrium model to assess the role of shear and tensile failure in a slope subjected to seismic shaking. A set of equations was developed to estimate the depth range for each failure mechanism (shear and tensile) using accelerations measured at the ground surface. From the depths at which the modelled failure mechanisms were observed to occur, it was suggested that shear and tensile failure may 'collaborate' to generate slope failure.

4.3 Tensile strength testing

4.3.1 Test classification

Soil tensile strength tests can be classified as either indirect or direct on the basis of loading principle. This means tensile failure is induced either indirectly, through the application of a point or linear compression load, or directly by application of a uniaxial tensile force (Figure 4.3). Indirect tensile tests include the Brazilian (e.g. Krishnayya & Eisenstein 1974; Uchida & Matsumoto 1961), double punch (e.g. Fang & Chen 1970; Kim et al. 2012), and bending (e.g. Ajaz & Parry 1975; Leonards & Narain 1963) methods. Direct tensile testing has been carried out by Tschebotarioff et al. (1953), Ajaz & Parry (1975), Leavell & Peters (1987) and Tamrakar et al. (2005), and others.

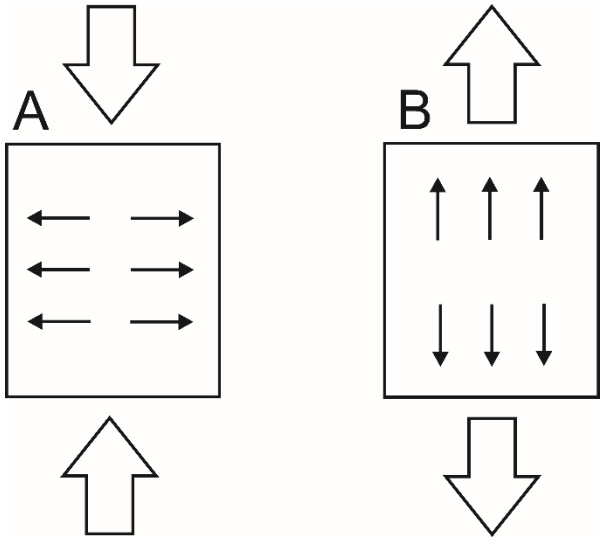

Figure 4.3: Loading principle. Indirect loading (A); direct loading (B). Indirect loading causes the soil specimen to fail parallel to the loading direction; direct loading causes the soil specimen to fail perpendicular to the loading direction. Black arrows show the induced tensile load.

4.3.2 Indirect tensile testing

Indirect tensile tests induce failure by application of a compression force or bending moment which generates tensile stresses perpendicular to the direction of loading, causing the sample to split (Figure 4.4). Together with specimen dimensions and peak load, assumptions are made about the stress-strain properties of the soil in order to calculate tensile strength. Measurement of tensile strain is complex, as a portion of the total strain measured in the 'failure zone' has been caused by the applied compressive stress. This phenomenon is called the Poisson effect and is measured by Poisson's ratio (Greaves et al. 2011). The portion of strain attributable to the compressive stress must either be measured or calculated, and then deducted from the total strain. Tensile strains are also typically very small (~0.1%), meaning strain gauges must be both sensitive and well positioned. Indirect testing methods were popular throughout the 1960s and 1970s, in large part due to their simplicity

and expediency. Specimen dimensions and testing equipment meant indirect tests could be carried out alongside conventional laboratory tests using widely available laboratory equipment. Direct tension testing techniques at the time were also not well developed (Suklje 1969).

The Brazilian test, also known as the split tensile test, was initially developed for testing of concrete specimens. In the Brazilian test, a disc shaped specimen is placed horizontally between two platens and loaded until failure, which manifests as a vertical crack (Figure 4.4a). Elastic theory is used to calculate tensile strength, together with specimen dimensions and the peak load at failure.

In a series of technical reports and papers published between 1969 and 1972, Fang and Chen presented their double-punch technique as a simple alternative to the Brazilian tensile test. A cylindrical specimen is installed in a load frame with two steel discs (punches) centred top and bottom (Figure 4.4B). As a vertical load is applied, cone shaped rupture surfaces form below each disc, displacing the surrounding material as they move towards each other. Failure is in the form of two to three simple tension cracks along the radial direction of the specimen and two cone shaped rupture surfaces beneath the punches. Tensile strength is calculated using peak load at failure, specimen dimensions and the theory of perfect plasticity (Fang & Chen 1970).

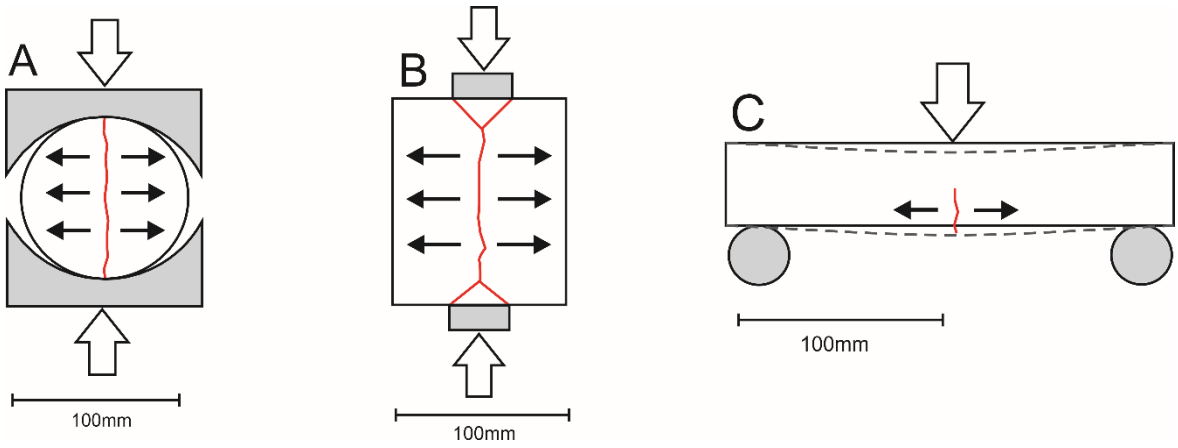

Figure 4.4: Schematic showing the three main indirect tensile tests: A) Brazilian, B) Double Punch/Unconfined Penetration and C) Bending/Flexure. The grey areas in the images are testing equipment. The red line indicates where failure is expected to occur. The white arrows show loading direction and the black arrows show the orientation of the induced tensile stress/load. All tests are carried out in the vertical orientation.

The bending test, also known as the flexure test, is usually carried out on rectangular, beam-shaped specimens (Figure 4.4c). The beam is supported at each end and loaded either at the centre (three point test) or at two points equidistant from the centre (four point test). Loading causes the beam to deflect, with the greatest compressive and tensile stresses occurring at the very top and bottom of the beam, respectively. If strains are measured, the stresses corresponding to the measured strains and applied bending moment can be calculated using the differential method (Ajaz & Parry 1975). If

strains are not measured then the stresses can be calculated using either the elastic bending method or the direct method (Ajaz & Parry 1975). In the bending test, the calculated tensile strength is actually the flexural strength (modulus of rupture); for a perfectly homogenous material, the flexural and tensile strengths will be equal, but if the test specimen has defects, the flexural strength will usually be greater (McKenzie et al. 2002).

4.3.3 Direct tensile testing

In direct testing, the tensile force is applied directly to the specimen until failure occurs. The maximum applied load divided by the area of the tension crack gives the tensile strength of the soil. Direct tensile testing has the advantage where stresses and strains are theoretically homogenous, meaning they can be calculated from direct measurements without making assumptions about the stress-strain response of the soil (as is the case for indirect testing methods). In practice, however, it is very difficult to grip and 'pull apart' a soil specimen. Test specimens tend to have a reduced cross-sectional area at the centre to generate higher tensile stresses, and thus control where failure will occur (Figure 4.5). Care also needs to be taken to design the end clamps or grips in a way that will uniformly transfer a tensile load. Difficulty applying the tensile force and measuring strains has led to the development of a wide range of test procedures and configurations (Figure 4.5). Early testing methodologies employed end clamps or grips to pull the test specimen apart (e.g. Tschebotarioff et al. 1953; Hasegawa & Ikeuit 1964); more recently there has been a focus on the use of specially shaped moulds to apply the tensile load (e.g. Tang & Graham 2000; Nahlawi et al. 2004; Tamrakar et al. 2005; Tamrakar et al. 2007). Strains can be measured optically, radiographically, photographically, or with a suitably-placed strain gauge (Ajaz & Parry 1974). With the exception of mould-based testing, the soil must be self-supporting in order to be tested. Excluding the work of Leavell and Peters (1987) and Win (2006), no direct tensile test configuration has become established and then improved upon by subsequent researchers, as has been the case for indirect tensile tests such as the Brazilian and double punch methods.

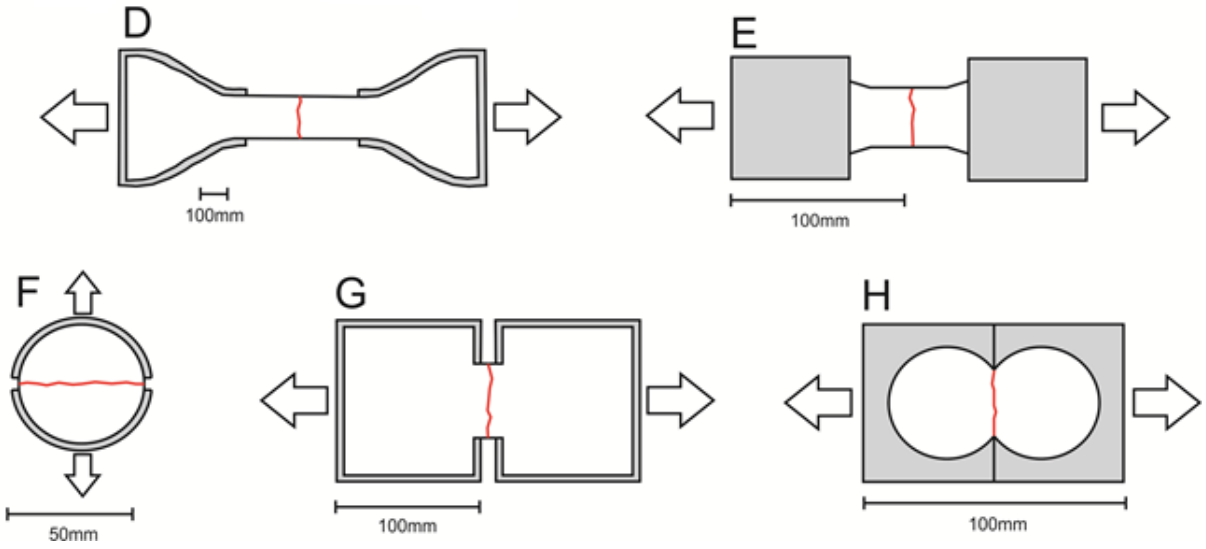

Figure 4.5: Schematic showing selected direct tensile tests. The grey areas in the images are testing equipment, the red line indicates where failure is expected to occur and the arrows show loading. Tests D, E, G, and H are carried out horizontally; the cartoon is showing a plan view. Tests F is carried out vertically; the cartoon is showing an orthographic view. Loading arrows indicate the orientation of the test (i.e. vertical arrows mean the test is carried out in the vertical orientation and the cartoon is therefore an orthographic view). D = Tschebotarioff et al. (1953); E = Leavell and Peters (1987); F = Tang and Graham (2000); G = Nahlawi et al. (2004); H = Tamrakar et al. (2005, 2007).

4.3.4 Factors influencing tensile strength

The key studies reviewed for this thesis are summarised in Table 4.1. Direct comparison of test results is made difficult by the wide range of test procedures and tested soil types. Most of the research has, however, focussed on the tensile characteristics of compacted, unsaturated soil due to its use in the construction of earth dams (e.g. Krishnayya et al. 1974; Win 2006; Leavell & Peters 1987; Ajaz & Parry 1975) and landfill liners (e.g. Tang & Graham 2000; Jessberger & Stone 1991). Most studies have sought to determine the relationship between tensile strength and key test variables such as moisture content, density, suction, rate of loading, and unconfined compressive strength (Table 4.1). The key trends from the literature are summarised below:

Moisture content and tensile strength

- Observations regarding the influence of moisture content on tensile properties of soil are in good agreement, with tensile strength found to decrease with increasing moisture content.
- This drop in strength is accompanied by an increase in the observed tensile strain at failure (Krishnayya et al. 1974; Ajaz & Parry 1975; Leavell & Peters 1987; Tang & Graham 2000; Nahlawi et al. 2004).

- Moisture content relative to the optimum moisture content (OMC) is also significant. Leavell and Peters (1987) observed soil strength to fall off rapidly wet of the OMC, while dry of optimum strength was nearly constant.
- Krishnayya et al. (1974) noted strains were 'disproportionately' high (<3%) at moisture contents greater than optimum and observed a linear relationship between strength and water content dry of the OMC. Vaníček (2013) also reported a marked increase in the tensile strain at failure for small changes in moisture content wet of the optimum.

Density and tensile strength

- Krishnayya et al. (1974) and Leavell and Peters (1987) found tensile strength to increase with compaction effort dry of optimum, and decrease with compaction effort wet of optimum.
- Win (2006) compacted test specimens to 95, 98 and 100% of the maximum dry density (MDD) at optimum moisture content. Maximum strength was achieved at approximately 98% of the MDD; Win (2006) suggested the drop in strength at 100% compaction could be due to distortion of the soil macro and microstructure, which would create defects that act as crack initiators.

Suction and tensile strength

- The literature indicates the relationship between tensile strength and soil suction is complex, with most researchers having found tensile strength to increase non-linearly with suction (e.g. Tang & Graham 2000; Leavell & Peters 1987; Win 2006).

Rate of loading and tensile strength

- It is important for the rate of loading to be taken into account when considering tensile failure of earth structures subjected to different loading conditions. The stress-strain response of an embankment dam subjected to seismic shaking, for example, is expected to differ from that of a dam that is slowly filled over a period of several months.
- The rate of loading (or test duration - faster rates of loading will result in shorter tests) has been found to greatly influence observed tensile strength and strain. When considered together, the findings of Tschebotarioff et al. (1953), Leonards and Narain (1963) and Krishnayya et al. (1974) indicate there is a critical rate of loading at which minimum tensile strength and strain is observed. Tests carried out faster and slower than this critical rate will yield higher tensile strengths. For a low plasticity silt (ML classification), Krishnayya et al. (1974) observed the critical rate of loading to be approximately 0.0025 mm/min.

- For very rapid tests lasting seconds to minutes, varying the rate of loading does not appear to affect the measured tensile strength (Tamrakar et al. 2007; Fang & Chen 1970).

Ratio of compressive to tensile strength

- Establishing relationships between compressive and tensile strength is of interest to engineers due to its practical uses (Fang & Fernandez 1981).
- It has been widely observed that the ratio of compressive to tensile strength increases with water content (Krishnayya 1974; Fang & Fernandez 1981; Leavell & Peters 1987). This relationship reflects the critical influence of water content on the tensile strength of unsaturated soil; as water content increases, tensile strength drops sharply compared to the reduction in compressive strength.
- The σ_t/σ_c ratio ranges from 0.16 - 0.53 for clayey soils, and from 0.03 - 0.09 for predominantly sand and silty soils tested using both direct and indirect methods (Table 4.1).

Table 4.1: Summary table for some of the literature reviewed for this study. The column 'Remoulded' refers to whether soil specimens were remoulded for testing; the column 'Strain' indicates whether strain was measured during testing. All tests are total stress analyses carried out on unsaturated soil. *Sand and/or bentonite has been added to soil to alter plasticity index, exact quantities and effect on USCS classification not known.

	Test Method	Author/s	Soil Type (USCS)	Test Variables	Remoulded	Strain	σ_t / σ_c
Direct	Classical	Tschebotarioff et al. (1953)	CH, CL	Clay mineralogy, moisture content, strain rate	Y	Y	-
		Hasegawa & Ikeuti (1964)	CH	-	Y	Y	-
		Ajaz & Parry (1974)	CH	-	Y	Y	0.20
		Satyanarayana & Rao (1972)	CL	Moisture content, density	Y	N	0.16 - 0.22
		Leavell & Peters (1987)	CL	Moisture content, density, suction	Y	Y	0.20 - 0.40
		Win (2006)	CL, SM	Moisture content, density, suction, strain rate, drying and wetting following compaction	Y	Y	-
	Mould	Tang & Graham (2000)	CH	Suction	Y	Y	-
		Nahlawi et al. (2004)	CH	Moisture content, curing time	Y	Y	-
		Tamrakar et al. (2005)	MH	Moisture content, density, strain rate, suction	Y	Y	0.08 - 0.09
		Tamrakar et al. (2007)	CH, CL, MH, ML, SC, SM	Moisture content, density, strain rate, no. of compaction layers	Y	Y	0.06 - 0.22
Indirect	Flexure Test	Leonards & Narain (1963)	CH, SM (?)	Moisture content, density, strain rate	Y	Y	0.08 - 0.42
		Ajaz & Parry (1975)	CH, CL	Moisture content	Y	Y	0.18 - 0.53
	Brazilian Test	Uchida & Matsumoto (1961)	ML, SC	-	N	N	0.14
		Krishnayya et al. (1974)	ML*	Moisture content, density, strain rate, plasticity	Y	Y	0.03 - 0.08
		Satnarayana & Rao (1972)	CL	Moisture content, density	Y	N	0.16
	Unconfined Penetration/Double Punch Test	Fang & Chen (1972)	CL*	Moisture content, strain rate, plasticity, specimen and punch size	Y	N	0.08 - 0.17
		Fang & Fernandez (1981)	CL*	Moisture content, plasticity, punch size and alignment	Y	N	0.04 - 0.32
		Kim et al. (2012)	SM, SP, SC	Plasticity, strain rate, punch size	Y	N	-

4.4 Selection of test methodology

4.4.1 Tamrakar et al. (2005) approach

The test procedure used in this study is adapted from the recent work of Tamrakar et al. (2005) and Tamrakar et al. (2007), in which a figure-of-eight shaped mould was developed for direct tensile testing. The authors sought to develop an apparatus that could be used to quickly and accurately measure the tensile strength of very soft and/or saturated soils. The mould consists of two halves that fit within a split box (Figure 4.6). One half of the box is held fixed, while the other is pulled at a constant rate of displacement (strain) until the soil fails. The tensile load is measured by a load cell positioned between the movable box and the motor. Through careful testing and a well-designed setup, Tamrakar et al. (2005) and Tamrakar et al. (2007) avoided many of the shortcomings associated with direct tensile testing. The mould was modified and tests were run to check for possible stress-concentrations at the constricted central section; test results from the two moulds were identical, and it was deemed that the original, simpler mould should be used for future testing. Testing was also carried out to confirm the perpendicularity of the deformation, and therefore tensile force, to the failure plane (Figure 4.6, right). Friction was addressed by placing linear rollers between the moving box and the platform on which it rests.

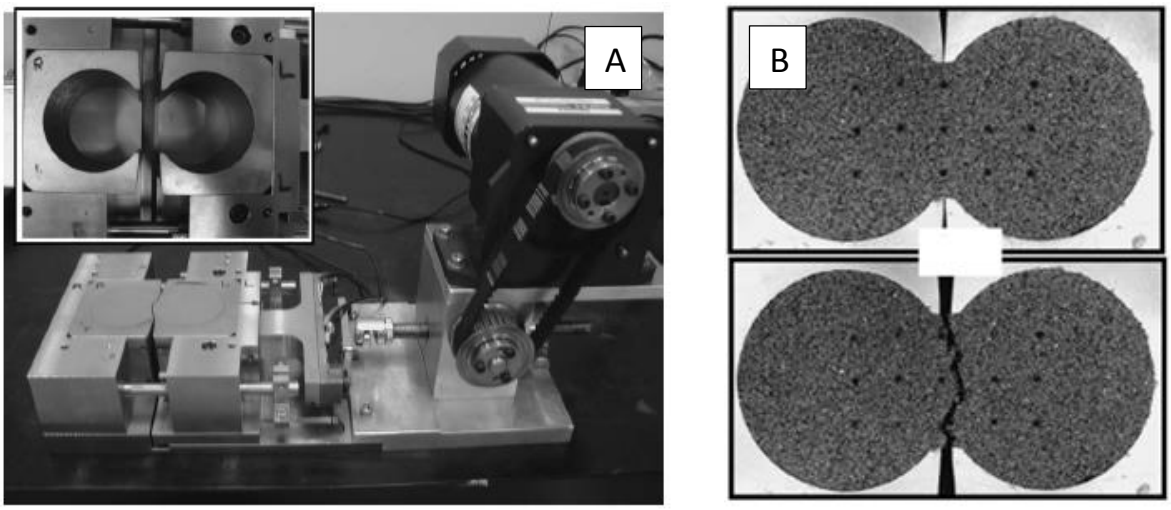

Figure 4.6: A) Tensile test apparatus/load frame (Tamrakar et al. 2007). B) Failed test specimen in mould (Tamrakar et al. 2007). Note strain marker grid on test specimen has a 10mm spacing.

Tamrakar et al. (2005) presented the results of testing an unsaturated clayey silt ('Kanto loam') and a saturated silty clay ('NSF-clay'). The ratio of tensile to compressive strength was approximately 0.08 for the Kanto loam. The maximum tensile strength was obtained at 50 - 60% water content, which is below its plastic limit of 75. Tensile and compressive strength were found to increase with increasing dry density.

Tamrakar et al. (2007) tested 14 mixtures of Kanto loam, NSF-clay and a fine-medium sand ('Toyoura sand'). Together with varying the sand/silt/clay ratios, test specimens were prepared at a range of moisture contents and dry densities. The tensile pulling rate and number of compaction layers were also varied to assess their influence on tensile strength. The weakest and strongest mixtures had the greatest proportions of sand and clay, respectively. Tensile strength varied from 1.4 to 11.7 kPa and tensile to compressive strength ratios ranged from 0.22 to 0.06. Increasing the number of compaction layers was found to increase the tensile strength; the authors recommend compacting specimens in 3 or 4 layers.

4.4.2 Test method selection

The merits and shortcomings of direct and indirect soil tensile tests are summarised in Table 4.2, below.

Table 4.2: Summary comparison of advantages and disadvantages of direct and indirect soil tensile testing techniques.

	Advantages	Disadvantages
Direct	· Tensile strength is measured directly · Strains easily measured · Moulds can be used to accurately test very soft and/or saturated soil	· Require specialist lab equipment to be made or existing equipment to be modified · Potential for misalignment of moving parts · Potential for stress concentration where soil is gripped · Limited potential for testing undisturbed soil specimens
Indirect	· Testing is straightforward and quick · Tests use readily available lab equipment · Potential for testing undisturbed soil specimens	· Tensile strength is calculated based on assumed elastic or plastic soil behaviour and cannot be measured directly · Difficult to measure strain · Soil needs to be self-supporting

A direct tensile testing method was selected for this research as no assumptions need to be made regarding soil properties in order to obtain meaningful results. Strength is simply calculated by dividing the peak load by the failed area, which also limits the potential for calculation error.

The decision to adapt the figure-of-eight shaped mould was influenced by the resources available for this testing. Using a mould over the more 'classical' end gripping techniques meant an unmodified Wykeham Farrance shear rig could be utilised as the load frame. In addition, limited resources were available for the fabrication of testing equipment, and the available materials were better suited to making a mould over 'classical' end grips or clamps. The load frame also requires specimens to be tested horizontally, which eliminates any issues associated with self-weight of the specimen.

The major shortcoming of the direct tensile mould approach is that there is limited potential for testing of undisturbed or natural soil, the behaviour of which is the focus of this research. In order to address

this limitation, it was planned to carry out indirect testing using the unconfined penetration test procedure described by Fang and Fernandez (1981). This is one of the few tests in which tensile strength of undisturbed soil could easily be tested; comparison of the two sets of test results would provide insight as to how remoulding the loess-colluvium affects tensile strength. Early trials showed test specimens to be failing correctly by development of two to three radial cracks with cone formation under the punches. Due to difficulty obtaining undamaged samples from the sampling site, however, it was decided to discontinue this line of testing and focus on development of the direct testing technique.

4.5 Test equipment, specimen preparation and test procedure

4.5.1 Test equipment

The test equipment consists of a conventional Wykeham Farrance direct shear apparatus (Model No. 25300) and a plywood mould. One half of the mould is attached to the load cell and held fixed in place; the other half is clamped to the carriage (Figure 4.7). During testing the carriage moves horizontally away from the fixed half of the mould and failure is made to occur at the narrowed section where the two halves of the mould join. Tensile strength is obtained by dividing the measured tensile load at failure by the failed area (40 x 50mm). Details of the mould fabrication and development of the test procedure for this research can be found in Appendix C.

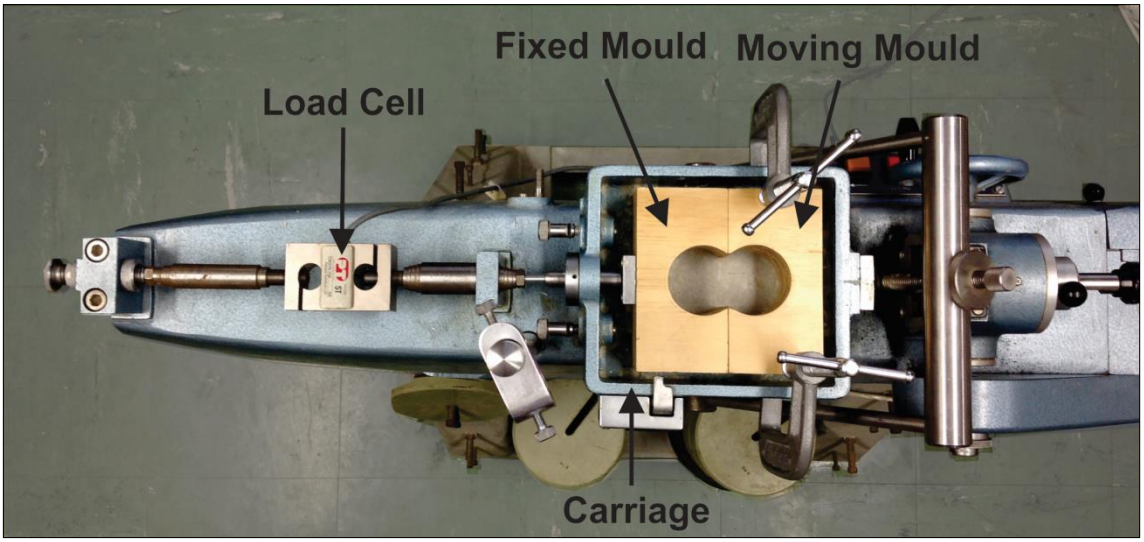

Figure 4.7: Tensile mould in load frame. Mould cavity is 40mm wide at the constricted central section. Carriage moves to the right of the image, towards the rear of the apparatus.

4.5.2 Materials

Loess-colluvium for testing was collected from the eastern/uphill section of the trench at approximately 0.5m below the ground surface. Soil was kept sealed in airtight bags and stored in a cool dark cupboard to retain field moisture content.

An engineering geological description for the sampled colluvium following New Zealand Geotechnical Society (NZGS) guidelines is as follows:

Clayey SILT with some sand and trace gravel; light yellowish brown. Stiff, moist, low plasticity. Gravel is fine, reddish brown weathered basalt. USCS: ML.

Atterberg Limits were determined in accordance with NZS 4402.2.5:1986 Tests 2.3 and 2.5. Results are presented in Table 4.3, together with Atterberg Limits from previous studies. The cone penetration limit (coincident with the liquid limit for low plasticity soils) is 25, and the plastic limit is 15, giving a plasticity index of 10. Typical values for Banks Peninsula loess range from 18-33 for the liquid limit, 16-22 for the plastic limit, with a plasticity index of <12. The values for the sampled loess-colluvium are within the ranges for local soils, with the exception of the plastic limit being slightly lower.

Table 4.3: Atterberg Limits for this study and previous studies. Note that the 'Typical values for Banks Peninsula Loess' are for airfall loess; the testing carried out for this study was on loess colluvium. LL = Liquid limit; PL = Plastic limit; PI = Plasticity index; NP = Non-plastic.

Source	LL	PL	PI
This study	25	15	10
Typical values for Banks Peninsula loess (Yetton 1986; Glassey 1986; Tehrani 1988; McDowell 1989; Goldwater 1990; Hughes 2002)	18-33	NP or 16-22	<12

Laser particle sizer (LPS) analysis was carried out following standard laboratory procedures established at the University of Canterbury. Results showed all test specimens to have approximately 60% silt, 32% fine sand and 8% clay, by volume (Table 4.4). Given that the low clay content was not consistent with either the measured plasticity index or the field description, it was decided to re-test using the pipette analysis as set out by NZS 4402.2.8.3:1986 (Figure 4.8, left). Results showed the clay fraction to make up 24% of the sample by weight, with 63% silt and 13% sand of which 10% is ‘very fine’ sand (Table 4.4 and Figure 4.9). The sample contained approximately 0.5% medium to coarse sand, a significant proportion of which was black in colour when washed clean and inferred to be of colluvial/volcanic origin (Figure 4.8).

Comparing the results of the two grain size analyses, the estimation of silt content was very close (at 60% and 63%), however clay and sand contents were significantly different. This is because the LPS

gives proportions by volume, while the pipette and hydrometer techniques give proportions by weight. The laser sizer is also known to underestimate the clay fraction due to non-sphericity of particles (Konert & Vandenberghe 1997). LPS results from this study are similar to those obtained by Stephen-Brownie (2012) for loess colluvium sampled from a nearby property, while pipette results fall within the (pipette and hydrometer) ranges given by Yetton (1986), Glassey (1986) and McDowell (1989) for loess.

Figure 4.8: A) Pipette analysis carried out for this study. B) Medium sand fraction sieved out before pipette analysis, note black volcanic sand.

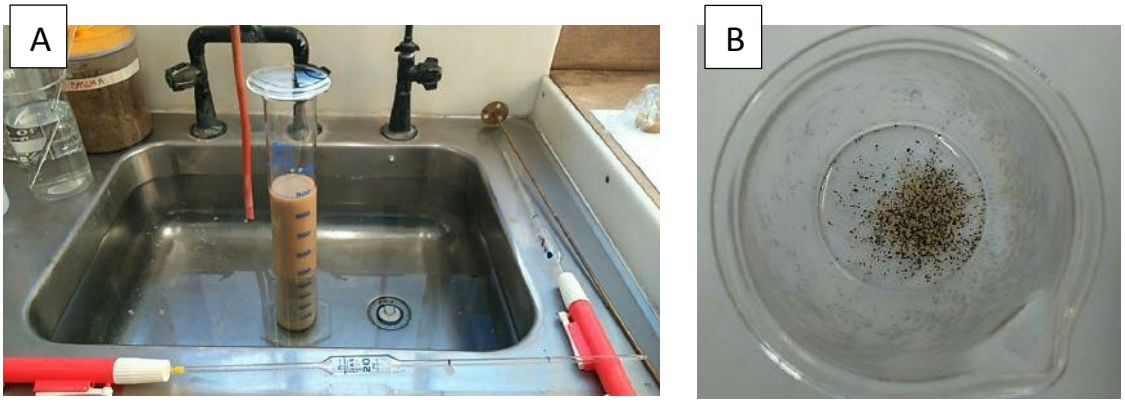

Table 4.4: Results of grain size analyses for this study (loess colluvium) and previous studies (loess). Testing for this study was carried out on one bulk sample of loess colluvium. Laser sizer results are by volume percentage, pipette results are by weight percentage. Previous testing has been carried out on loess using the pipette or hydrometer techniques. Testing for this study has been carried out on loess colluvium using the pipette and laser sizer techniques.

Analysis type	Source	Clay	Silt	Sand
LPS	This study	8	60	32
	Stephen-Brownie (2012)	5	50	45
Pipette or hydrometer	This study	24	63	13
	Yetton (1986)	11-25	65-80	10
	Glassey (1986)	21	65	14
	Tehrani (1988)	14	76	10
	McDowell (1989)	8-25	60-80	10
	Goldwater (1990)	14-31	63-77	6-9

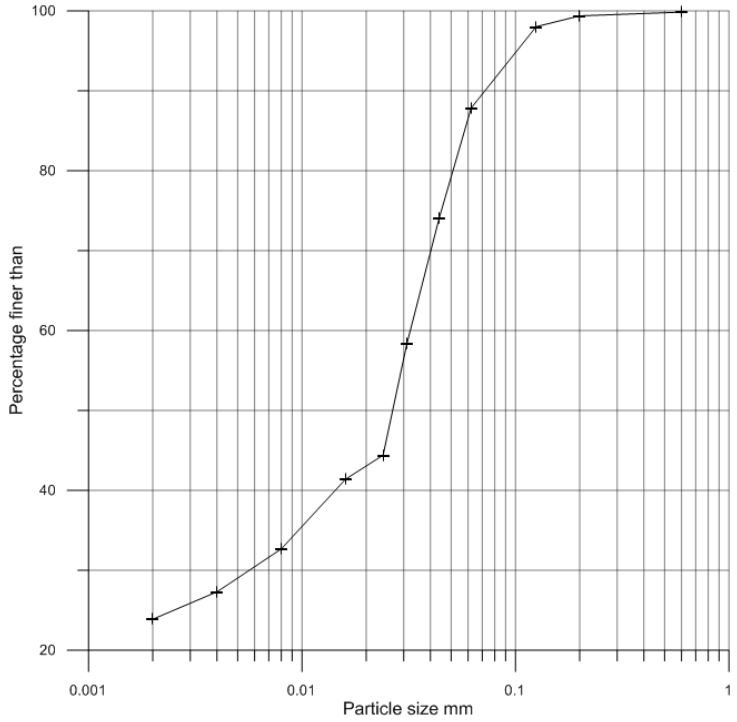

Figure 4.9: Cumulative grain size distribution from pipette analysis of bulk sample (this study).

In-situ dry density and moisture content were determined for loess colluvium sampled from the trench dug for this study (Table 4.5). Thin walled steel tubes were used to sample from the walls and floor of the trench, both up- and down-slope of the fissure. Dry density and moisture content were determined in accordance with NZS 4402.5.1.3:1986 and NZS 4402.2.1:1986, respectively.

Table 4.5: In-situ dry densities and moisture contents for samples collected from trench. Fifteen tube samples were collected and analysed from up- and down-slope of the fissure.

Parameter	Range	Mean ± 1 Std Dev
In-situ dry density range (kg/m^3)	1460 - 1870	1640 ± 0.16
In-situ moisture content (%)	6.5 - 15.5	9 ± 2.24

4.5.3 Specimen preparation

Soil clods were broken up using a mortar and pestle and then passed through a standard 2mm sieve to remove volcanic gravel and rootlets. Batches of soil were prepared at 10, 12.5 and 15% water content, by weight. It was intended to test specimens at 5, 10 and 15% water content to reflect field conditions (Table 4.5), however the soil was too dry below 10% moisture content to successfully compact into the mould. Following the addition of water, soil batches were thoroughly mixed and then stored in airtight containers to equilibrate for at least 24 hours. Soil moisture content was checked prior to testing and adjusted if outside the acceptable ± 0.5% of target. If further wetting or drying was necessary, the soil was re-mixed afterward and then left for a further 24 hours.

4.5.4 Soil installation and test setup

Prior to the installation of soil, the mould was taped together on the upper surface and sides with masking tape. This was to keep the arrangement together with minimal disturbance to the specimen when being transported to the electronic scales and shear rig. The mould was weighed before being clamped together with two vices and then clamped to a solid surface with a third vice (Figure 4.10). Compaction within the shearbox carriage was trialled and deemed unsuitable (see Appendix C).

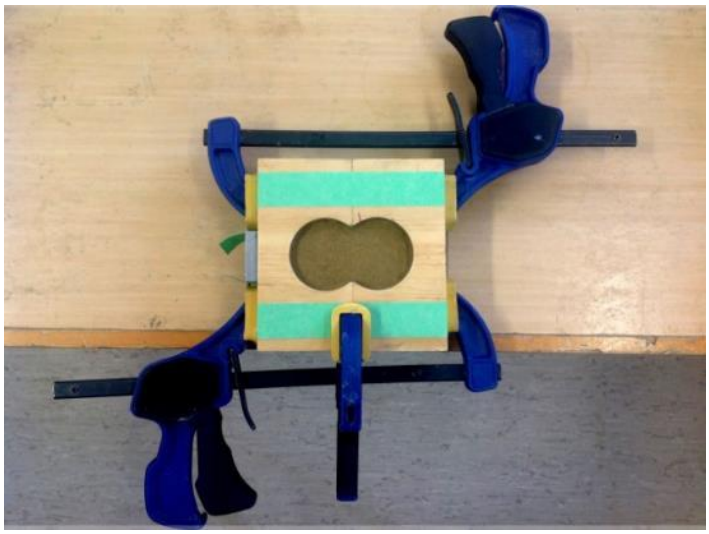

Figure 4.10: Plan view of tensile mould and compacted soil specimen. The mould is taped and clamped together to prevent movement during compaction and transport. The third clamp is securing the mould to the bench.

Soil was compacted into the mould using a 49mm diameter steel cylinder and a rubber mallet. Soil was compacted in four layers, as recommended by Tamrakar et al. (2005). The quantity of soil required to achieve the target dry density was split amongst four containers, one for each compaction layer. Specimens were compacted to a dry density of 1650, 1800 or 1900 kg/m^3 in keeping with the measured mean and maximum field densities (Table 4.5). The inside of the mould was marked to show the level to which each quantity of soil needed to be compacted. Loose soil was inserted into the mould using a funnel before being levelled with a spatula. The steel cylinder was then used to gently tamp down each side mould, going back and forth between the two sides to avoid the development of a 'free face' near the centre. If compaction by hand was not sufficient, the rubber mallet was used to tamp soil down further, again moving from side to side every 2 - 3 blows. When complete, the mould was unclamped, weighed and the soil height checked to ensure the target density had been achieved.

Following compaction, the mould was carefully placed in the shearbox carriage, hooking the front end over the load cell rod. The back half of the mould was carefully clamped to the carriage and the masking tape slit with a craft knife where the two halves join.

4.5.5 Test procedure

The programme TracerDAQ was used to digitally log readings from the load cell using a sampling interval of 3 seconds. A strain rate of 0.3mm/minute was used, as recommended by Tamrakar et al. (2005). For short duration tests, it has been found that strain rate does not affect results (see section 4.3.4). Failure generally occurred within approximately 30 seconds and tests were run for 2 - 3 minutes to establish baseline friction. If the failure plane was observed to follow where the steel cylinder had compacted the sample, the test was considered to be invalid and results were discarded. Following testing, the mould was reweighed and moisture content of the soil checked to ensure the specimen had not experienced moisture loss.

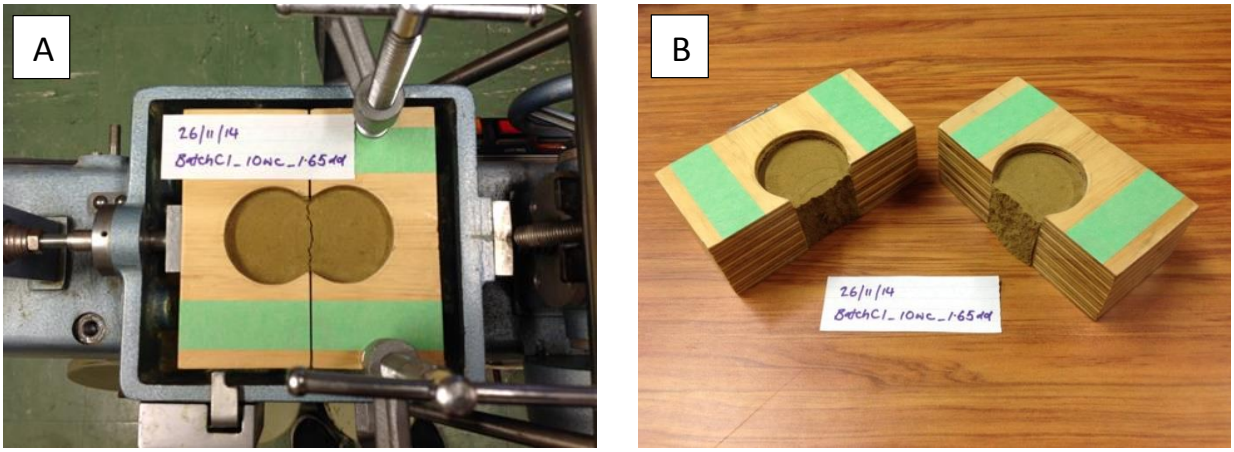

Figure 4.11: A) Failed specimen in shearbox carriage. The left side of the mould is attached to the load cell (out of view) and the right side is clamped to the carriage and displaced to the right. B) View of failure surface; crack is planar with an uneven surface.

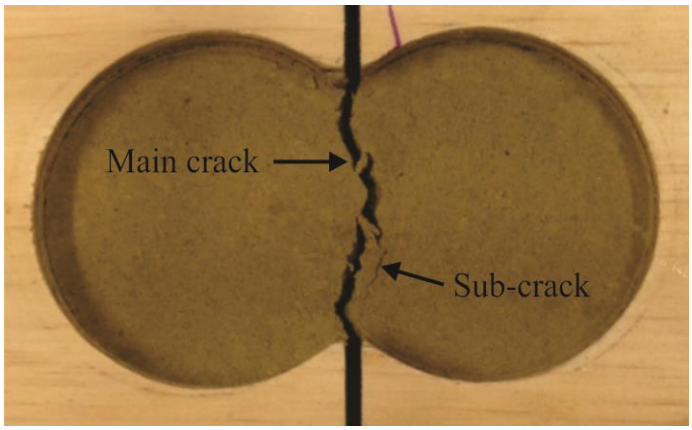

Figure 4.12: Failed tensile test specimen showing subsidiary (‘sub’) crack and main crack.

4.6 Results

Failure occurred as a rough planar crack where the two halves of the mould join, normal to the direction of the applied tensile stress (Figure 4.12). Specimens typically failed in less than one minute. Small subsidiary cracks appeared first, which would then coalesce to form the main tensile fracture (Figure 4.12).

The data for the two sets of direct tensile tests are presented in Table 4.6. During the first set of tests, specimens were compacted to a dry density of 1650 kg/m^3 at moisture contents of 10, 12.5 and 15%. For the second set of tests, specimens were compacted to dry densities of 1800 and 1900 kg/m^3 at 10% moisture content. For the range of test conditions, tensile strength was found to vary from 6.6 - 27.6 kPa. Each test was carried out two to three times to ensure consistency of results. Due to the nature of the testing, minor variations in stress at failure were expected, and the observed differences are attributed to slight variations in density and moisture content at the time of testing. The 3 second sampling interval in TracerDAQ may also account for some of the variability.

Table 4.6: Mean tensile stress at failure for the range of test conditions. Results are graphed in Figures 4.14 and 4.15.

Moisture content %	Dry density kg/m³	Mean tensile stress at failure kPa
10	1650	17.5
10	1800	25
10	1900	27.6
10	1650	17.5
12.5	1650	14.1
15	1650	6.6

Test multiples are shown in Figure 4.13 as tensile stress plotted against displacement. The flattened tail of each stress-displacement curve represents baseline friction. For each test, the average baseline friction force was subtracted from the peak tensile force, which was then divided by the area of the tension crack to calculate the tensile stress at failure. The graphs shown in Figure 4.13 have not been corrected for baseline friction and must be read carefully. Each stress-displacement plot is labelled with the corrected mean tensile stress at failure to aid interpretation. The graphs have been left uncorrected to avoid unnecessary manipulation of data, as baseline friction cannot simply be subtracted from all test readings because any values greater than baseline friction would then become positive. The stress-displacement curves plot below the x-axis as tensile stress is negative (compressive stress is positive). The convention is to quote values of tensile strength as positive, which has been followed for this thesis.

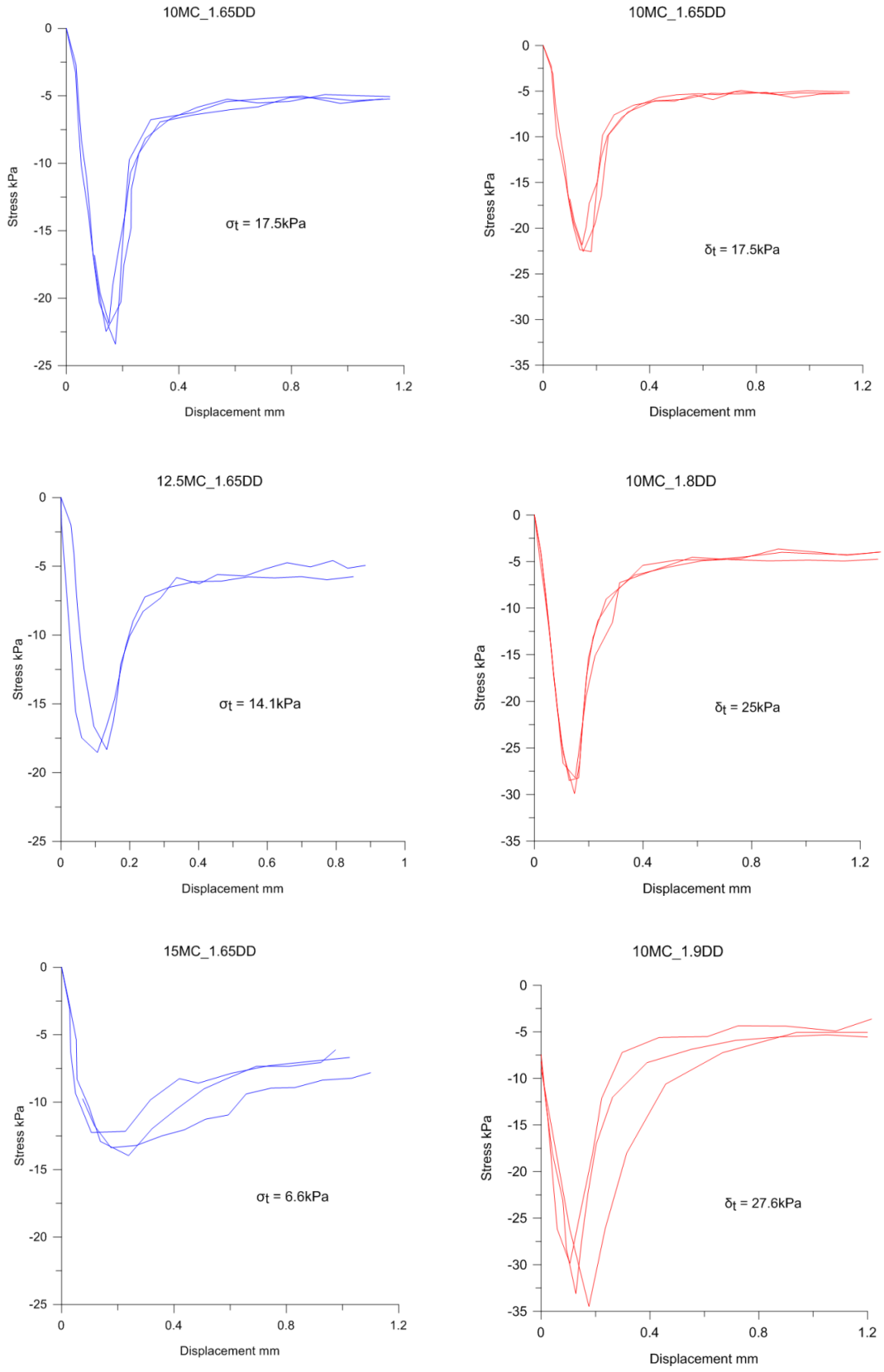

Figure 4.13: Stress vs. displacement plots of test multiples. MC = moisture content; DD = dry density. The blue plots show the effect of varying moisture content, the red plots show the effect of varying dry density. Mean tensile strength corrected for friction is shown on each graph (σ_t).

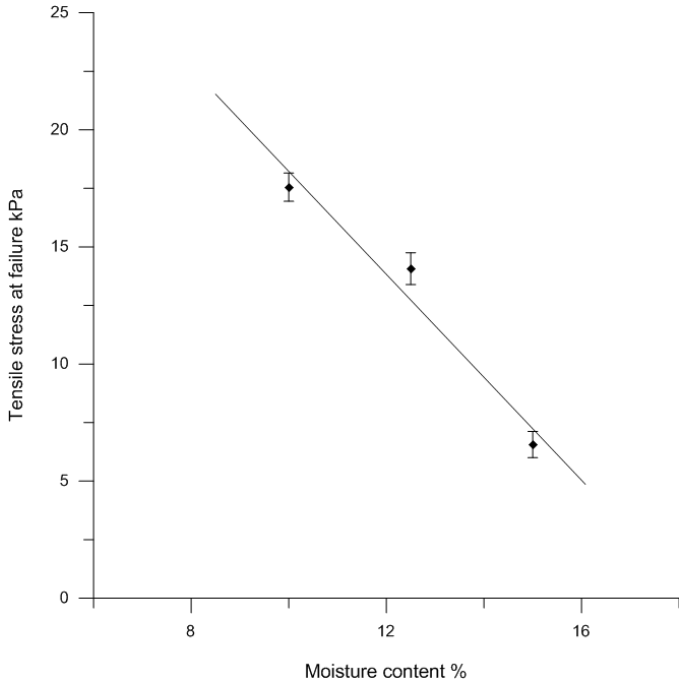

Figure 4.14: Tensile Stress vs. Moisture content for Port Hills Loess Colluvium. All test specimens compacted to 1650 kg/m^3. Error bars show the range of test results.

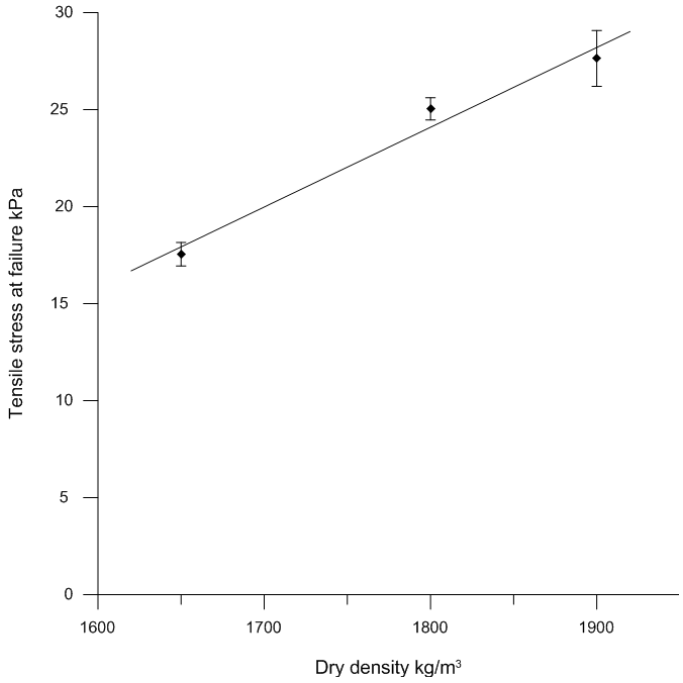

Figure 4.15: Tensile Stress vs. Dry density for Port Hills Loess Colluvium. All test specimens prepared at 10% moisture content. Error bars show the range of test results.

Comparing the three moisture content plots (Figure 4.13), post-peak behaviour is fairly consistent for specimens tested at 10 and 12.5% moisture content, but is variable for the specimens tested at 15% moisture content. The width of the peak can also be seen to increase with increasing moisture content. The tests carried out at a dry density of 1900 kg/m^3 also show some variability in post peak behaviour, while the stress-displacement curves for the specimens compacted to 1650 and 1800 kg/m^3 are reasonably consistent.

Figure 4.14 shows an increase in tensile strength as moisture content decreases. Each data point on the plot represents the average of the two or three tests carried out at that moisture content. Figure 4.15 shows an increase in tensile strength as dry density increases. As for Figure 4.14, each data point on the plot represents the average of the two or three tests carried out at that moisture content.

4.7 Interpretation of results

4.7.1 Tensile strength

The range of recorded tensile strengths is consistent with the limited literature for low plasticity silts (USCS 'ML' classification). Specimens tested for this research yielded strengths ranging from 6.6 to 27.6 kPa. Krishnayya et al. (1974) tested a low plasticity silt and reported strengths varying from 3.5 to 25 kPa for the range of test conditions. Kelzieh (1991) recorded a maximum tensile strength of 33 kPa for an ML soil, as did Fang & Fernandez (1981).

4.7.2 Moisture content

The negative linear relationship between strength and moisture content (Figure 4.14) is in good agreement with the findings of previous studies (e.g. Win 2006; Nahlawi et al. 2004; Krishnayya et al. 1974). The tensile strength of unsaturated, recompacted soil is largely derived from suction, as evidenced by the almost total loss of tensile strength when these soils are saturated (Leavell & Peters, 1987). Suction is strongly influenced by the percentage of pore space occupied by water or degree of saturation (Fredlund & Rahardjo 1993). While matric suctions were not measured for this study, increasing the moisture content while compacting specimens to the same dry density is inferred to be increasing the degree of saturation. A tensile strength of 17.5 kPa was measured for the lowest moisture content, compared to 6.6 kPa for the highest moisture content at the same dry density. It is concluded that greater suctions were experienced by the drier test specimen, contributing to greater tensile strength.

The relationship between suction and shear strength of loessial soils in Canterbury has been documented by several researchers (e.g. McDowell 1989; Hughes 2002). Cohesion and apparent cohesion of loess soils are derived from calcite cementation and negative pore water pressures, respectively. The factors that contribute to cohesion - the stress-independent component of shear strength - also contribute to soil

tensile strength (Snyder & Miller 1985; Lu & Godt 2013), although this connection is rarely discussed in the literature. McDowell (1989) attributed high cohesion values at moisture contents of 6-8% to soil suction, and inferred the rapid drop in cohesion towards 12-13% moisture to be a consequence of open connections between pore spaces decreasing. A similar trend has been observed in this study for tensile strength and moisture content.

The shape of the tensile stress-displacement curve is observed to change with moisture content (Figure 4.13). For the specimens tested at 10% moisture content, the stress-displacement curve is approximately linear before and after the 'narrow' peak. For the specimens tested at 15% moisture content, the stress-displacement curve shows non-linearity before and after the peak, which is also much broader than that of the drier stress-displacement curves. The changing curve shape is indicative of a transition from relatively brittle tensile failure at 10% moisture content to a more ductile or plastic tensile failure at 15% moisture content. The 15% moisture content curve shows a clear post-peak softening behaviour. This means tensile resistance is lost gradually after the peak, which is a basic feature of quasi-brittle materials (Zhang et al. 2015). The 10% moisture content curve, by contrast, shows a fairly rapid drop in stress after the peak which is indicative of brittle fracture. According to Bell and Trangmar (1987) loessial soils are known change from a brittle failure mode to one of plastic or ductile deformation at moisture contents of greater than 15%, which is in good agreement with the findings of this study.

4.7.3 Dry density

A positive linear relationship is observed between tensile strength and dry density (Figure 4.15). As for moisture content, this relationship has been observed in previous studies (Tamrakar et al. 2005; Krishnayya et al. 1974). The maximum recorded stress (strength) in this study was for the specimens tested at a dry density of 1900 kg/m^3 with a moisture content of 10%. According to Terzaghi et al. (1996), the mechanical effects of the contact pressure arising from suction depends on the relative density of the material. This supports the observed tensile strength increase with increasing dry density.

There is some variability in the test results for 1900 kg/m^3 dry density (Figure 4.13), where recorded stress at failure ranges from 25 - 30 kPa. This has been observed in other studies, where strength of the soil is found to drop when compacted to the maximum dry density for a given moisture content (e.g. Win 2006; Krishnayya et al. 1974). Win (2006) suggests that this is due to damage to the soil structure which creates flaws that can act as crack initiators. McDowell (1989) suggests a maximum dry density of 1800 - 1900 kg/m3 with an optimum moisture content of 13-14% for Port Hills loess. The specimens compacted to 1900 kg/m^3 at a moisture content of 10% for this study (using a non-standard technique) is likely very close to the maximum dry density; damage to the soil structure would explain the variability of results compared to the other tests carried out for this research.

4.7.4 Remoulding

In order to apply findings to fissuring in the Port Hills (Chapter 5), consideration must be given as to how remoulding the loess-colluvium for testing may have influenced its ability to withstand tensile stress. It is suggested that the results of this testing can be used as a conservative estimate of the tensile strength of undisturbed loess-colluvium, within the tested range of moisture contents and densities. While cohesive soils are known to lose strength upon remoulding (Ranjan & Rao 2007), testing carried out by McDowell (1989) indicates that Port Hills loess does not experience significant strength loss on reworking. Through graphing of test results, McDowell (1989) inferred the cohesive strengths of in-situ loess and recompacted loess fill to be similar, with the high cohesions at low moisture contents (6-8%) attributed to suction. Given that suction is also a major contributor to tensile strength, McDowell's findings are used to infer that the remoulding of loess-colluvium for testing will not have greatly changed its ability to withstand tensile stress.

4.7.5 Application of findings to tunnel gullying and slope creep

Tensile strength characteristics of Port Hills loess and loess-colluvium may also be used to better understand the conditions under which tunnel gullies develop and slope creep movements take place. Tensile strength must be overcome in order for shrinkage cracking to occur, which is thought to be the starting point for tunnel gully development (Bell & Trangmar, 1987). Drying and shrinkage, the processes that lead to desiccation cracking, also increases suction and therefore tensile strength (Peron et al. 2009). This means high tensile (shrinkage) stresses will need to be generated in order for cracking (mode I tensile fracture) to occur.

In the future work section of his 1990 MSc thesis, Goldwater recognises the significance of soil tensile strength and recommends detailed study of tension crack formation and propagation in Banks Peninsula 'C layer' loess to better understand the initiation of slope creep.

4.8 Synthesis

Tensile strength testing was carried out in order to better understand the occurrence and distribution of tensile failure on the eastern side of the Hillsborough Valley. Following a detailed review of the soil tensile testing literature (see Appendix B), a direct, mould-based approach was selected for this study. The test methodology was developed through process of trial and error over a period of several months and is documented in Appendix C. Suggested improvements in the event of future testing are also summarised in Appendix C.

The tensile strength of loess colluvium was tested for over a range of moisture contents and dry densities. Test results show a negative correlation between moisture content and tensile strength;

increasing moisture content from 10 to 15% reduced tensile strength by 65%. Test results show a positive correlation between dry density and tensile strength; increasing dry density from 1650 kg/m^3 to 1900 kg/m^3 increased tensile strength by 57%. Stress-displacement curves show a transition from brittle to ductile-type failure when moisture content is increased from 10% to 15%. This is in agreement with observations made by Bell and Trangmar (1987) and McDowell (1989) for shear failure.

The significance and implications of tensile failure for the Hillsborough Valley are discussed in the following chapter.

5 Geomorphological and geotechnical review of ground damage

5.1 Introduction

This chapter presents an interpretation and discussion of the observed ground damage on the eastern side of the Hillsborough Valley. In the context of slope movement, the nature and distribution of surface damage provides insight into the processes and mechanisms occurring at depth (Terzaghi 1950). The observed ground damage (Chapters 2 and 3), findings of tensile strength testing (Chapter 4), and available geotechnical information (inclinometer and piezometer records provided by EQC) are used to present a geomorphological and geotechnical interpretation of the type of ground failure that has occurred in the Vernon Terrace area.

Theoretical models which relate observable ground damage to the formation and propagation of rupture surfaces are applied to the Vernon Terrace area to propose a 'stage' of slope failure. The mechanisms of previous models for the eastern side the Hillsborough Valley (introduced in Chapters 1 and 3) are then reviewed and with the conclusions drawn in this chapter.

The term 'failure' is used throughout this chapter to describe the ground damage that has occurred and does not imply, unless otherwise stated, 'catastrophic' or 'total' failure. The Vernon Terrace slope is considered to have 'failed' on the basis of downslope movement having occurred.

5.2 Geomorphological interpretation

5.2.1 Geomorphological aspects of ground damage

The mechanism or mechanisms of slope failure are usually identified through recognition, classification and mapping of diagnostic surface features such as tension and en echelon cracking, back tilting, rotation, shortening, and bulging. Ground damage on the eastern side of the Hillsborough Valley consists of extension cracking between Vernon Terrace and Rapaki Road, and compression features along the toe of the slope below Vernon Terrace. The distribution of extension and shortening is characteristic of translational sliding, where there are multiple tension cracks which follow the contours of the slope, little or no vertical displacement across cracks, 'pressure ridging' at the toe of the slope, and no sign of rotation or back-tilting at the head (Rib & Liang 1978; Cruden & Varnes 1996; Keefer 1984). A small graben feature was mapped mid-valley, which is also indicative of translational

(extensional) movement (Cruden & Varnes 1996; Keefer 1984). Cumulative downslope displacement can be estimated by summing tension crack apertures along a line of section, and is on the order to 0.2 – 0.3m for much of the Vernon Terrace area. This estimate is based on CGD (2014) mapped tension crack apertures (Figure 2.2). Summing crack apertures does not take strains into account and is therefore considered to be a lower bound estimate.

Fundamental to the kinematics of translational sliding is the presence of a planar or gently curved rupture surface along which the sliding mass has displaced (Cruden & Varnes 1996). Drilling carried out across the Vernon Terrace area in mid-2011 failed to locate a shear surface along which the ~0.3m of displacement may have occurred (Stephen-Brownie 2012). One possible explanation is that shearing has occurred along multiple fractures of limited extent, instead of a single, discrete failure surface. Multiple small fractures could be difficult to detect in rotary drilled core, and there was also appreciable core loss in the upper 10-15m of several boreholes (e.g. BH03, BH05, BH09, see Appendix D), which would likely occur if the soil has been disturbed across this depth. Shear (en echelon) cracking along the sides of the mapped deformation zone are also associated with translational movement, but are absent from the Vernon Terrace area (Stephen-Brownie 2012).

Although spring formation at the toe of landslides is not uncommon, the Hillsborough Valley springs are unlikely to have been caused by slope movement. Spring formation associated with slope movement usually occurs when water-bearing layers are disrupted by rotational sliding (Sowers & Royster 1978). The inferred style and magnitude of ground damage in the Vernon Terrace area is unlikely to have caused spring development: rather slope movement and spring formation are both considered to be the product of strong earthquake shaking. The isotopic signature of the springwater is also volcanic (deep), meaning it is unlikely to have been sourced from disruption of shallow sediments (Green, in prep). The hydrogeology of the Hillsborough Valley is being studied by others (e.g. Green, in prep), and is not a component of this thesis.

The presence of peat at the base of the slope was discussed in Chapter 3. A zone of marked compression coincides with the thickest (known) extent of the peat deposits (≥4m), which illustrates the compressibility of these sediments prior to movement. Although the dynamic response of peat subjected to cyclic loading has not been widely studied, it is postulated that peat, although non-liquefiable, is a poor slope buttress during seismic shaking. The geotechnical characteristics of peat sampled from the Vernon Terrace area are currently being assessed by engineering geology students at the University of Canterbury.

No signs of previous, similar slope movements on the eastern side of the valley were found through study of historical aerial photography (Chapter 3). There may be evidence of past failures observable by site inspection, although this type of mapping was not undertaken for the current research. It is

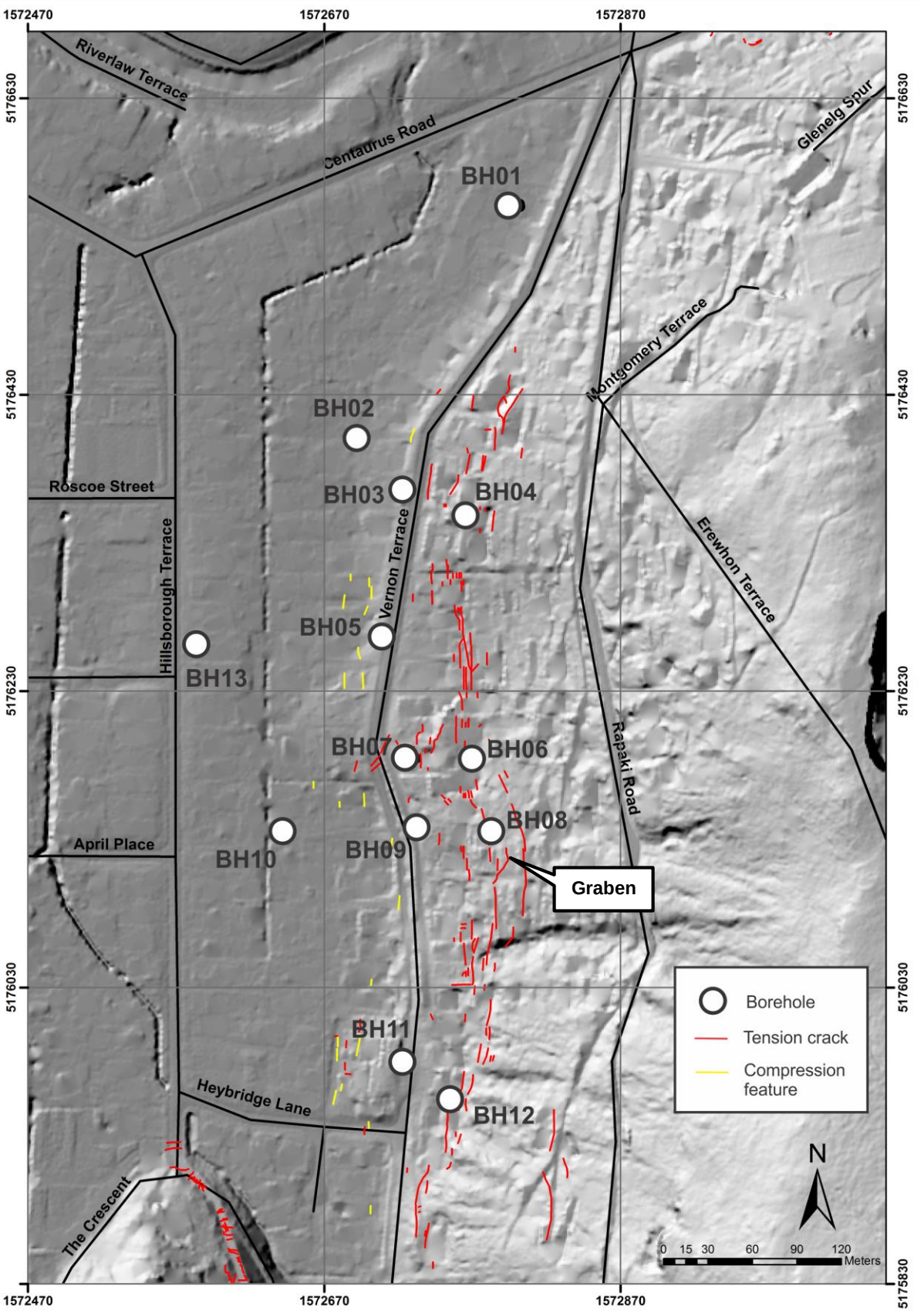

Figure 5.1: Borehole/piezometer/inclinometer location map. Tension cracks and borehole locations sourced from CGD (2014) and CGD (2015a), respectively. Borehole and piezometer numbering is the same.

possible that the eastern Hillsborough slope has failed in the past, likely in response to strong, proximal earthquake shaking, although the geological setting of the valley (i.e. coastal and therefore subjected to cyclic drowning and incision during climate fluctuations) means that evidence for past movement could easily be removed or buried. Slope failure deposits on the valley floor would be almost indistinguishable from 'normal' colluvial deposits, sourced from periodic reworking of upslope colluvium and/or airfall loess, which have been infilling the valley since loess deposition commenced in the early Pleistocene.

5.2.2 Failure dimensions

There are a number of 'rules of thumb' for estimating sliding mass dimensions using the geometries of deformation structures. An approximately 10m-wide graben feature was mapped mid-valley, consisting of a down-dropped block bordered by extensional fractures (Figure 5.1). Graben formation is associated with translational movement, and can be used to estimate depth to the 'failure surface' (Cruden & Varnes 1996; Keefer 1984). Using geometric data obtained from a large number of translational landslides, Cruden et al. (1991) found graben width to be approximately 90% of the depth to the failure surface. Applying this to the Hillsborough Valley indicates a sliding mass thickness of ~10m.

Translational slides are typically shallow, with a depth to length ratio of <0.1 (Cruden & Varnes 1996). The downslope length between tension cracking and compression features ranges from 50-100m, which suggests a sliding mass thickness of 5-10m, with the implication that the mass is thickest in the centre and thins towards the edges. Although a throughgoing shear is not present in the Vernon Terrace area, the estimates of ~10m (graben) and 5-10m (depth to length ratio) may provide an indication of the depth to the base of the deformation.

5.3 Geotechnical data interpretation

The acquisition of inclinometer and piezometer data for the Vernon Terrace area via a non-disclosure agreement with EQC was addressed in Chapter 2. The following section describes the most important aspects of the data, and uses the information to refine conclusions drawn from the previous section on the geomorphology.

5.3.1 Inclinometer data

Inclinometers are used to determine the magnitude, depth and direction of slope movement by measuring deformation normal to the axis of the borehole casing (Stark & Choi 2008). Five inclinometers were installed on the eastern slope of the Hillsborough Valley during May and June 2011, in boreholes 03, 08, 09, 11 and 12. Monitoring is event-based, with readings taken following heavy rainfall (≥50mm/24hours) or moderate earthquakes (≥Mw 5.0).

Profile and tilt change plots for all inclinometers are provided in Appendix D. Information connecting the instruments to the properties on which they are installed has been removed for privacy reasons. Profile change plots compare the measured profile to the initial profile, showing cumulative displacement. Tilt change compares the reading at a given depth to the initial reading at the same depth, and is particularly useful for identifying the depth at which deformation is occurring (Stark & Choi 2008). The profile and tilt change plots for BH03 and BH08 are shown in (Figure 5.2). A0 and B0 are the two measurement axes. The A0 measurement axis is oriented in the upslope/downslope direction (east/west); B0 is oriented perpendicular to A0 along the slope. Movement is recorded as positive in the direction of bearing. If the A0 axis is 270°, for example, westward (downslope) movement is recorded as positive.

Only the BH03 inclinometer was installed and a baseline reading made prior to the M_w 6.0 June 2011 earthquake. The A0 tilt change plot for BH03 shows 2.5mm downslope movement at 9.75m depth, 7mm downslope movement at 6.75m depth, and 8mm downslope movement at 3.5m depth, following the June earthquake (Figure 5.2). The uppermost 1.5m of the inclinometer casing shows 5mm of uphill movement, which may be caused by rotation or deflection of the casing at the ground surface. The total cumulative downslope displacement resulting from the June 2011 earthquake is 50mm (as shown by the cumulative displacement plot), and the readings show a pattern of reducing displacements with depth between 3.5 and 9.75m below ground. In addition to the downslope (westward) movements detected on the A0 axis, the B0 tilt change plot shows 5mm of southward movement following the June 2011 earthquake.

The remaining four inclinometers were installed by the time of the December 2011 earthquake. No movement is recorded by the tilt change plots for this event. There has also been no movement recorded following significant rainfall, with the possible exception of BH08. Inclinometer readings were taken following the March 2014 rainfall event when 118mm of rain fell over a three day period (Massey et al. 2013). The A0 tilt change plot for BH08 shows 2.5mm of movement to the northwest (downslope and slightly towards the valley entrance) at 9.75m depth. There is also a small amount of deep movement recorded at 20.75m depth. No movements were recorded by the other inclinometers at this time.

The profile change plots for BH08 (Figure 5.2), BH11 (Appendix D) and BH12 (Appendix D), show the measured profile to step in and out up the height of the borehole, the meaning of which is unclear. It is understood that there were difficulties with some the inclinometer installations and the profile change readings could reflect buckling or deformation of the inclinometer casing. The readings for BH08, which was installed in the graben, step in and out on both sides of the measurement axis (i.e. shift from positive to negative) for both the east/west and north/south directions. This could be related

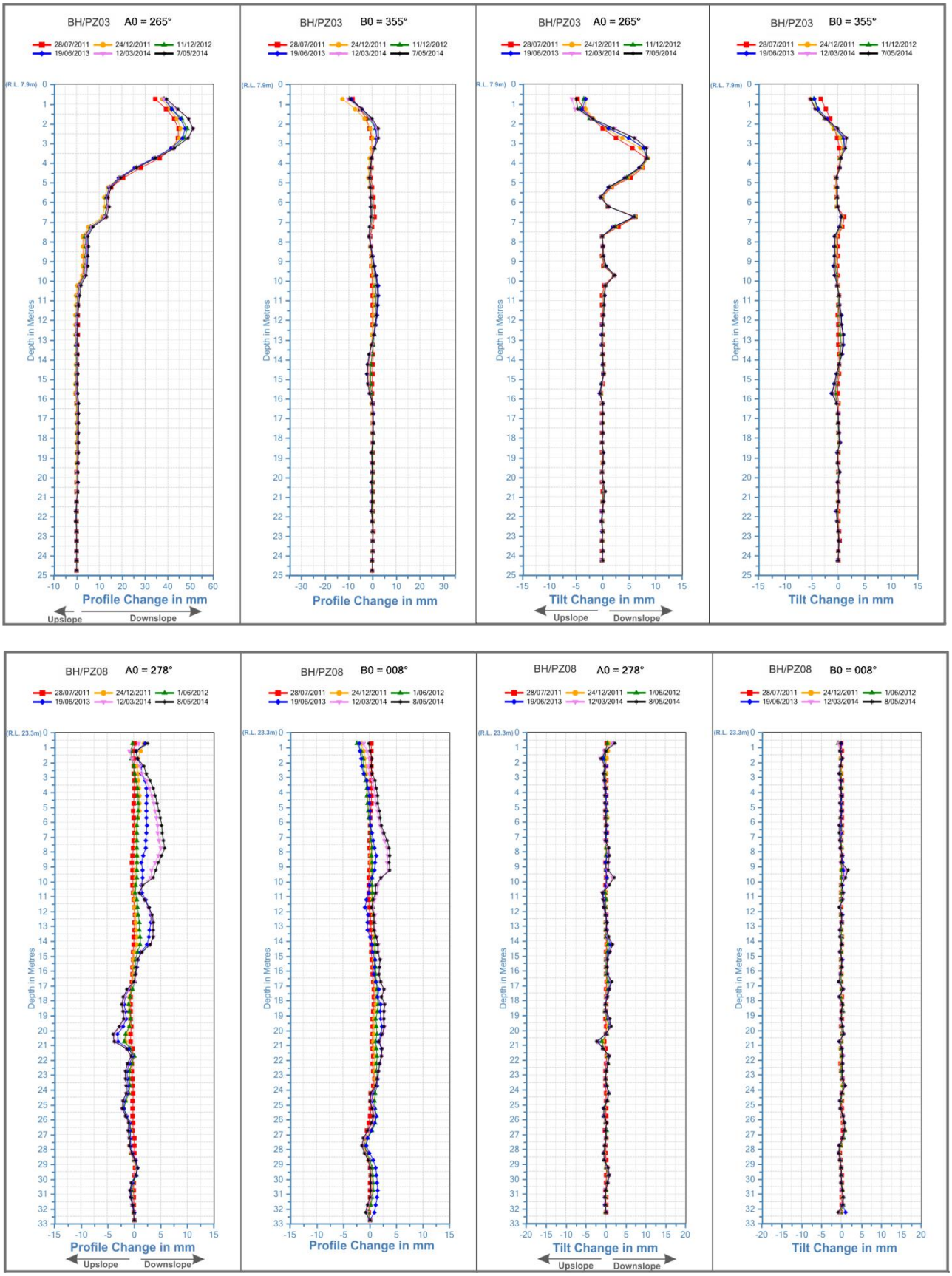

Figure 5.2: Inclinometer profile change (left) and tilt change plots (right) for BH03 (top) and BH08 (bottom). The upslope and downslope directions are indicated on the A0 axis plots.

to settlement of the graben over time. As the tilt change plots for boreholes 08, 11 and 12 show no clear movement, the unusual profile change readings have been disregarded.

The movements recorded in BH03 for the June earthquake support the hypothesis of displacement being accommodated by multiple shears, as opposed to a single failure surface, and the recorded depths of movement are consistent with the crude 'rule of thumb' depth estimates made using slope and graben geometries. The June 2011 movement recorded in BH03 and the lack of movement recorded following the December 2011 earthquakes and March 2014 rainfall event indicate that strong earthquake shaking is required for slope mobilisation.

5.3.2 Piezometric data

Nine piezometers were installed in the eastern slope of the Hillsborough Valley in boreholes 02, 03, 04, 05, 08, 09, 11 and 12 (Figure 5.1). The water level and rainfall plots are provided in Appendix D and the salient features are summarised in Table 5.1. All piezometers are screened in loess-colluvium, well above bedrock (Figure 5.3). Three piezometers (PZ04, PZ04A and PZ05) are manually dipped; the remaining six are monitored by down-hole loggers which provide continuous water level readings (Table 5.1). Monitoring records provided for this research date from June 2011 (the time of installation) to between April 2012 and March 2014.

Five piezometers recorded a head increase of between 0.5 and 1.5m at the time of the 23 December 2011 earthquake, which took up to 7 days to dissipate (Table 5.1). Of the remaining piezometers, three were being dipped manually (and infrequently), and the fourth (PZ12) does not appear to be measuring a true water table. Increased pore pressure due to cyclic loading from earthquake shaking has the effect of reducing effective stress and therefore shear strength (Hack et al. 2007), and slope movements commonly initiate within locally saturated layers that have lost strength due to excess pore pressure. Although no soil has been logged as saturated (Appendix A), there are zones of 'wet' soil up to several metres in thickness and the distinction between 'wet' and 'saturated' when logging is not always clear. The presence of a measurable water table (probably one of several) indicates there is saturation within the slope, and this is reinforced by the observed head increase during the December 2011 earthquake.

Table 5.1: Summary table of groundwater response to rainfall and earthquake shaking. All piezometers are screened in loess colluvium. Where the data are unclear or there are insufficient data, the cell is populated with an '-'.*Following 23 December 2011 earthquakes, aftershocks not taken into account which may maintain head or extent dissipation time.

Piezometer	Data collection	Screened interval (RL) Top	Base	Mean water level (RL)	Seasonal fluctuation	Rainfall response	Earthquake response (height m)*	Pore pressure dissipation (days)*
BH/PZ03	Logger	4	2	6.3	Yes	Yes	Yes (+0.65m)	7
BH/PZ02	Logger	1.3	-1.7	5	No	-	Yes (+1.34m)	5
BH/PZ04	Manual	4.8	2.3	7.2	-	-	-	-
BH/PZ04A	Manual	8.8	6.8	7.7	-	-	-	-
BH/PZ05	Manual	-1.7	-3.7	6.5	-	-	-	-
BH/PZ08	Logger	6.3	3.3	7.8	Yes	-	Yes (+0.45m)	7
BH/PZ09	Logger	5.5	3.5	8.2	-	-	Yes (+0.54m)	3
BH/PZ11	Logger	6.3	2.3	9.9	Yes	Yes	Yes (+0.85m)	4
BH/PZ12	Logger	15.3	12.3	14.6	No	Yes	No	-

It is inferred that movement has occurred within these wet (saturated) zones, which is supported by the BH03 inclinometer plots and borehole logs. The movement recorded by the BH03 inclinometer for the June 2011 earthquake occurred at 3.5, 6.75 and 9.75m depth. The soil, logged one month prior, is recorded 'wet' at 9.75 and 6.75m depth, and was not logged at 3.5m depth due to coreloss, which commonly occurs when the soil is saturated. Although no movement was recorded by the inclinometers for the December 2011 earthquakes when piezometric head increased, it is probable that the magnitude of pore pressure increase was greater during the larger magnitude February and June 2011 earthquakes, facilitating initiation of slope movement.

Piezometers 03, 11 and 12 show a rainfall response and are inferred to be influenced by intra-slope drainage (tunnel-gully) systems, as the response time is too fast for surface water to be infiltrating down through the soil profile. As discussed in Chapter 3, the piezometers show a near-flat water table extending back into the hillside from the valley floor. BH08, for example, has a mean annual water level of 7.8m and BH09, directly upslope, has a mean annual water level of 8.2m (Figure 5.3). While the piezometers show a single water table, this is considered to be an oversimplification of the slope hydrogeology. This was noted in Chapter 3 and is discussed in greater detail below.

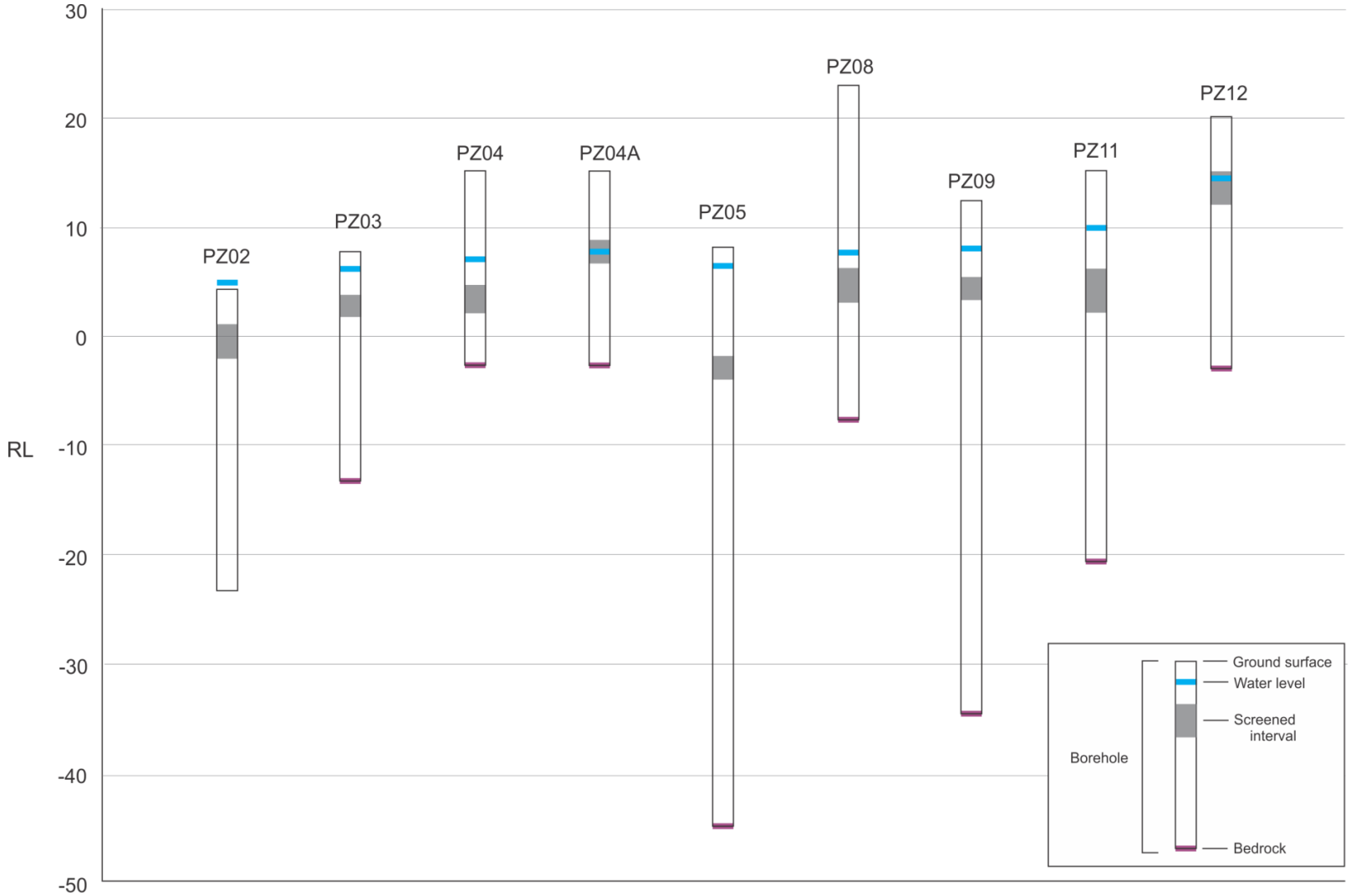

Figure 5.3: Piezometer summary diagram. RL (reduced level) is relative to Lyttelton Vertical Datum (MSL1937). Piezometers are arranged approximately north (left) to south (right), however the x axis has no relevance to the spatial distribution of the piezometers. Piezometers 04 and 04A are in the same borehole. All boreholes except BH/PZ02 were drilled to bedrock. All piezometers are screened in loess-colluvium. See Figure 5.1 for piezometer locations.

5.3.3 Layering within the slope

Translational sliding occurs along surfaces of weakness, such as where there is a variation of shear strength between two layers (Varnes 1978). Bell and Trangmar (1987) state that layering within loess-colluvium has a significant influence on slope stability in the Port Hills. Different colluvial packages display differences in permeability, moisture retention, density, texture and strength characteristics. As such, contacts between layers can provide a surface for shear displacement, particularly where water is able to perch above a layer of lower permeability such as clayey silt.

To illustrate the variability within the slope, pocket penetrometer readings (converted to undrained shear strength) were plotted against logged moisture condition for BH08 and BH09 (Figure 5.4). Moisture condition is represented by a step plot, with drier soil at a particular depth shown by a greater step to the right (i.e. more of the brown colour). While undrained shear strength is indicative only, and logged moisture condition is probably subjective (the boreholes were logged by different engineers), the plots show considerable variability within the slope, despite being almost entirely silty loess-colluvium (see Appendix A for borehole logs). It is probable that slope movement has been accommodated within wet (probably saturated) units where there has been strength loss due to increased pore pressure. Loessial soils of the Port Hills are also highly sensitive to moisture content, losing strength (both shear and tensile) with increasing moisture content. The relationship between shear strength and moisture content for Port Hills soils is explored by McDowell (1989) and Goldwater (1990), and is summarised by Massey et al. (2014). The dependence of tensile strength on moisture content is illustrated in Chapter 4 of this thesis.

It is worth noting that the boreholes for which undrained shear strength and logged moisture condition have been plotted form a line of section perpendicular to the slope (Figure 5.1), however the ground is too variable to correlate units between the two boreholes. The colluvial wedges that form the slope will be discontinuous both laterally and downslope. It is believed that this variability (captured by Figure 5.4) has played a role in the development of multiple shears within the slope, as the geotechnical heterogeneities do not provide a through-going weakness along which a rupture surface can readily develop, as is normally the case for translational slope movement. The inferred distributed shearing may also be reflected in the distributed nature of tension cracking across the hillslope.

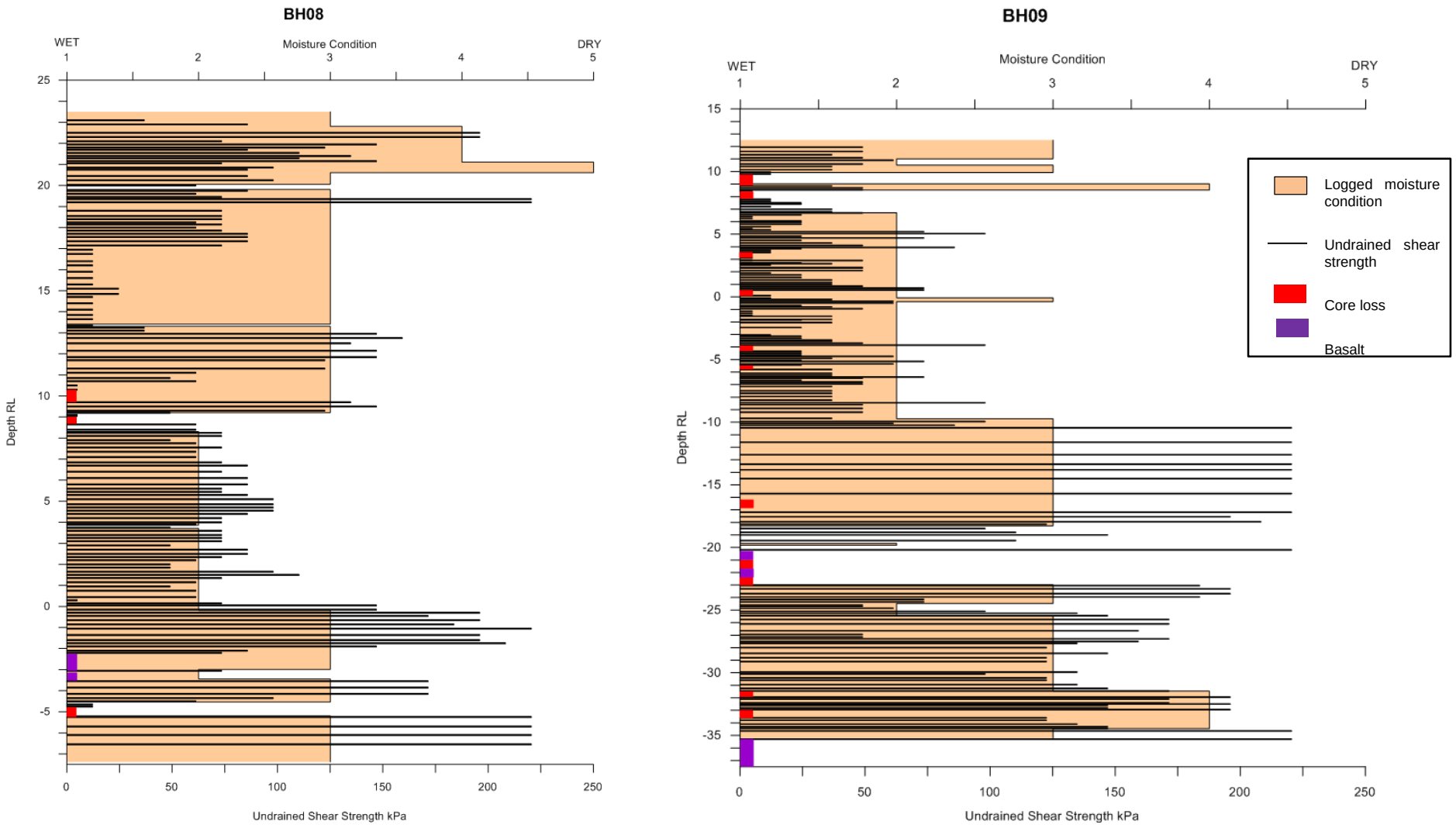

Figure 5.4: Down-borehole plots showing undrained shear strength (calculated from pocket penetrometer readings) and logged moisture condition. Logged moisture conditions are wet (1), moist-wet (2), moist (3), moist-dry (4) and dry (5). Undrained shear strength is indicative only.

5.4 Application of tensile data

The most important conclusion drawn from tensile strength testing (Chapter 4) is that Port Hills loess-colluvium possesses measureable tensile strength over the tested range of moisture contents (10-15%) and dry densities (1650 – 1900 kg/m3). This strength was mobilised during seismic shaking in order for tensile failure to occur. Tensile fracturing on hillslopes decreases the overall strength of the slope, due to the loss of (tensile) strength along the plane of the crack (Duncan & Wright 2005; Muller & Martel 2000), which could be providing a critical contribution to hillslope stability (Lu & Godt 2013). It is noted that in the context of sliding failure, this only applies to translational movement and not to rotational movement, for which the entire slip surface theoretically fails in shear (Figure 5.5).

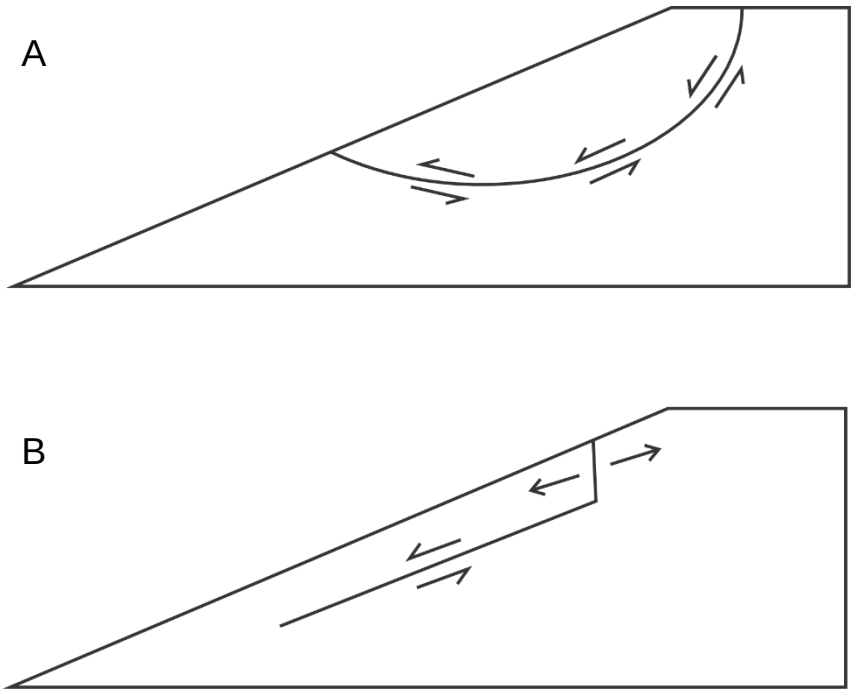

Figure 5.5: Failure mode for rotational and translational slides. A) Rotational failure, showing shearing along the entire rupture surface. B) Translational failure showing tensile failure at the head of the sliding mass and shearing along the base.

Observations made throughout the course of tensile testing (Chapter 4) can also be used to understand the development of tension cracks at a hillslope scale in the Hillsborough Valley. The test methodology followed in this study was developed through a process of trial and error over a period of several months. In the early stages of testing, it was observed that any notches or impressions made on the surface of the test specimen during compaction would be followed by the tension crack when the specimen was loaded. The resultant crack would be curved or irregular instead of planar, and would pass through the centre of the mould. While the results of these tests were disregarded (due to invalid failure), the behaviour of the tension cracks is considered to model the development of cracks in the field, whereby they propagate up through or towards weak zones or topographic irregularities. Tension cracks on the

eastern side of the Hillsborough Valley have been observed to step out around house foundations (e.g. the boundary between fill or foundation slab and natural ground), follow breaks in slope, pass through backfilled service trenches, and along the upper contact between recent fan material and undisturbed slope at the southern end of the valley. The passage of tension cracks through notches on slopes is supported by finite element modelling carried out by Muller and Martel (2000).

Phase2, a commercially available 2D finite element programme, was trialled to carry out a tensile strength sensitivity analysis for a homogenous loess slope. The objective of the sensitivity analysis was to model the possible contribution of tensile strength to slope stability. Although the programme allows the user to specify tensile strength of the soil or rock mass, analyses did not yield realistic results. It is concluded that specialist modelling would need to be undertaken to quantify the contribution of soil tensile strength to slope stability in the Hillsborough, such as the early work carried out by Kelzieh (1991).

5.5 Stage of slope 'failure'

It is believed that the observed ground damage on the eastern side of the Hillsborough Valley has resulted from the early stages of translational sliding. Ground damage is characterised by a zone of extension cracking (tensile failure), with compression features evident along the toe of the slope. It is inferred that the downslope movement required to create these features has been accommodated by multiple discrete shears, rather than a single rupture surface, which is normally the case for translational sliding. This inference is based on the inclinometer tilt change plots for BH03, the lack of a shear surface detected during drilling and logging of boreholes, and the variability of moisture content, strength and density within the slope, which would provide multiple surfaces of limited lateral and downslope extent along which movement could occur. The Vernon Terrace slope movement is therefore considered to be in a state of 'incipient failure', which could precede large-scale translational movement.

The processes of incipient sliding are poorly understood (Muller & Martel 2000). Although many authors have identified the need for research which relates the styles and patterns of surface deformation to the processes of rupture surface formation and propagation (Petley et al. 2005; Petley 2004; Carey & Petley 2014), progress in this field remains "surprisingly" limited (Carey & Petley 2014). The two models presented below are applied to the Vernon Terrace area in order to provide an interpretation of the 'stage' of ground failure, and to assess the likelihood of multiple shear surfaces accommodating ~0.3m of cumulative downslope displacement, without development of a throughgoing shear surface.

Muller and Martel (2000) applied boundary element techniques and fracture mechanics to analyse the growth and development of a translational landslide rupture surface. It was observed that, in general, conditions promoting translational sliding are enhanced near the base of slopes. This could have

implications for the initiation of slope failure in the Hillsborough Valley, particularly as the toe of the slope is buttressed by peaty and/or saturated sediments which are inferred to lose strength during earthquake shaking by pore water ejection.

Muller and Martel (2000) present an idealised model of the stages of rupture surface development and incipient landsliding (Figure 5.6). Although there are aspects of the model that do not fit the hypothesised 'failure' of the Vernon Terrace area, such as the dimensions of the 'slip patch', the stages are a useful representation of the development of common landslide structures. Stage 'c' depicts the onset of tensile failure, as it propagates up towards the ground surface. Stages 'd' and 'e' show tensile failure to have occurred prior to en echelon cracking down the flanks of the slope. This supports the idea of tension cracking representing an early (incipient) 'stage' of failure, and en echelon cracking indicating a more advanced stage of 'failure', which is not observed on the eastern side of the Hillsborough Valley.

Crack propagation is one mechanism by which rupture surfaces are postulated to form. Petley et al. (2005) propose that during the early stages of loading (in this case earthquake shaking), cracking begins to develop within the slope. At some critical point, cracks begin to interact and coalesce, forming the shear surface. Failure occurs when the shear surface is fully developed, bounding the sliding mass on all sides (Petley et al. 2005). Elements of this hypothesis may be used to interpret the 'stage of failure' of the eastern side of the Hillsborough Valley, where displacements have occurred without development of an obvious slip surface. It is proposed that the multiple shears indicated by the BH03 inclinometer represent an early stage of rupture surface development and the 'critical point' at which fractures begin to coalesce has not been reached. Petley et al. (2005) suggest that slope displacements are able to occur from the onset of cracking, which would account for the apparent downslope movement in the absence of a through-going basal rupture. Although the model was initially developed to explain failure in hydrologically triggered landslides (Petley et al. 2002), the model is also considered to be applicable to seismically triggered landslides.

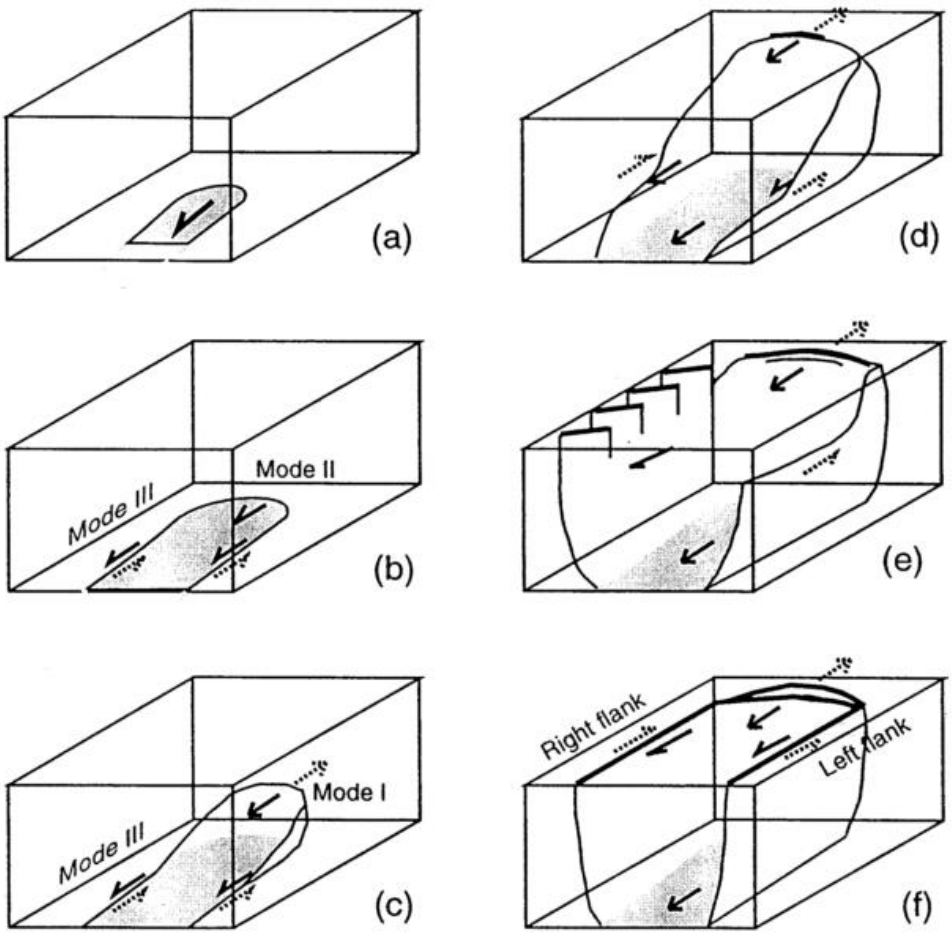

Figure 5.6: Idealised stages of translational rupture surface development (Muller & Martel 2000). A) Initial slip occurs. B) Fracture enlarges via mode II ('sliding') and mode III ('tearing') fracture. C) Upslope tip of rupture surface begins to propagate up towards ground surface in mode I (opening/tensile) fracture. D) Tensile fracture daylights, with continued downslope displacement. E) En echelon cracking develops as tension crack enlarges. F) En echelon cracks become rupture surfaces.

5.6 Discussion of Dellow et al. (2011), Stephen-Brownie (2012) and Massey et al. (2013) ground failure models

'Incipient loess landsliding' (Dellow et al. 2011), 'quasi-toppling' (Stephen-Brownie 2012) and 'toe slumping' (Massey et al. 2013) are the three ground failure models that have previously been proposed for the eastern side of the Hillsborough Valley. Both Dellow et al. (2011) and Massey et al. (2013) provide an overview of earthquake-induced ground failure in the Port Hills, and the failure mechanisms presented for the Vernon Terrace area are not the primary focus of the publications. As such, detailed explanation is limited. It is also worth noting that the model presented by Stephen-Brownie (2012) was made without the density of geotechnical investigation data currently available through the CGD, and without the inclinometer and piezometer records utilised in this thesis.

Dellow et al. (2011) infer liquefaction (or near liquefaction) at the toe of the slope below Vernon Terrace during the February 2011 earthquake. This liquefaction, possibly of marginal marine sediments, is

postulated to have caused a loss of support at the toe of the slope, thereby causing cracking and movement in the 'head area' (Dellow et al. 2011). There was no liquefaction observed on the eastern side of the valley floor (Stephen-Brownie 2012), which is likely due to the presence of peat and peaty soils. The conclusions drawn in this chapter are in agreement with the hypothesis that loss of support at the toe of the slope has facilitated movement, although it is more likely to do with peat providing an inadequate buttress during earthquake shaking. Liquefaction of marginal marine sediments, which are known to occur at depths of ~15m below ground level at the valley entrance, is unlikely. It is noted that this information (i.e. geotechnical data showing the extent of the peat) was not available at the time of publication by Dellow et al. (2011) in late 2011. The concept of failure initiating at the toe of the slope is supported by the modelling carried out by Mulller and Martel (2000) on the initiation of translational sliding in hillslopes. The classification of the ground failure as 'incipient' is also considered to be accurate, based on the conclusions drawn in this chapter using the Muller and Martel (2000) and Petley et al. (2005) models of failure initiation.

Key failure mechanisms identified by Stephen-Brownie (2012) include a loss of lateral support (via the trampoline effect) to induce a lateral spreading type movement. Although Stephen-Brownie (2012) does not discuss the possible role of locally saturated layers and excess pore pressure, this is implied by the Cruden and Varnes (1996) definition of lateral spreading (see Chapter 2). As discussed in relation to the Dellow et al. (2011) model, the findings of this chapter are in agreement with the significance of the loss of toe support. Although the loss of support is likely to do with the peat, high vertical accelerations may also have played a role. Stephen-Brownie (2012) postulates the ground cracking has formed along steeply dipping joints within the hillslope loess, due to an outward-toppling motion. Based on the findings of geotechnical investigations not available to Stephen-Brownie (2012) at the time of writing, this is considered to be unlikely. The material overlying bedrock on the eastern side of the Hillsborough Valley is almost entirely loess-colluvium, which has been reworked downslope and lacks the 'vertical' structure of airfall loess. Stephen-Brownie (2012) concluded the 'incipient landsliding' model presented by Dellow et al. (2011) was the least likely mode of ground failure. It appears that features of ground damage associated with well-developed (i.e. not incipient) sliding were used to come to this conclusion.

Massey et al. (2013) identify the Vernon Terrace ground failure as a 'toe slump', a term coined by them. Although the Vernon Terrace area is not specifically discussed, toe slumping is considered to have resulted from undrained loading of locally saturated loess, colluvium, and alluvium (Massey et al. 2013). The interpretation of geotechnical data in this chapter, likely the same data considered by Massey et al., is in agreement with the undrained loading aspect of the 'toe slumping' model. It is noted that the term 'slump' is misleading, as it is normally used (in literature) to describe a rotational failure (Varnes 1978; Keefer 1984; Rib & Liang 1978), which the GNS cartoon (Figure 3.3) does not appear to imply. The generalised cartoon also implies movement having occurred along the top of the water table, which

is considered to be an oversimplification due to the layering and variability of moisture condition throughout the slope as shown by the borehole logs (Appendix A and Figure 5.4).

5.7 Discussion

5.7.1 Mechanisms of failure

The nature and distribution of ground damage in the Vernon Terrace area is characteristic of shallow, translational sliding. Fundamental to translational sliding is the presence of a planar or gently curved surface of rupture, however such a feature was not located during the logging of EQC boreholes drilled in the Vernon Terrace area (Stephen-Brownie 2012). In the absence of a throughgoing shear surface, it is hypothesised that movement has been accommodated by multiple slip surfaces of limited lateral and downslope extent, within the upper 10m of the slope. This hypothesis is supported by the inclinometer records for BH03, which recorded minor downslope movements following the June 2011 earthquake, at 3.5, 6.75 and 9.75m below ground. Movement has likely occurred within zones that have been logged as wet (and are possibly saturated or near-saturated).

Piezometric data shows evidence for increased pore pressure during the December 2011 earthquake. Although no movement was recorded by inclinometers for this event, it is inferred that the pore pressure increase would be significantly larger during the February 2011 and June 2011 earthquakes, facilitating slope movement by reducing effective stress within saturated or near-saturated layers. The variability of moisture condition throughout the slope is a result of colluvial layering (Figure 5.4). The limited lateral and downslope extent of colluvial units (inferred from poor correlation between BH08 and BH09 units in Figure 5.4), means there is no single, natural surface of weakness within the slope that can be exploited for the formation of a rupture surface. This may explain why displacements have been accommodated over such a wide zone (>6m for BH03).

5.7.2 State of failure summary

Overall, the factor of safety against sliding is considered to be lowered due to loss of tensile strength at the head of the feature and development of cracking within the slope (Petley et al. 2005). The modelling carried out by Muller and Martel (2000), together with comments made by Cruden and Varnes (1996) and Terzaghi (1950) indicate that cracking at the ‘head’ of a slope movement represents a relatively early, or ‘incipient’ stage of slope failure. This conclusion is supported by the model of progressive slope failure proposed by Petley et al. (2005), which shows distributed cracking within the slope to occur before development of a throughgoing rupture surface. The Petley et al. (2005) model may also help to explain how downslope movements (~0.3m) can be accommodated without a throughgoing shear surface. Modelling carried out by Muller and Martel (2000) shows cracking down the flanks of a slide, which is not observed in the Vernon Terrace area, to represent a later stage of failure.

5.7.3 Future slope behaviour

It seems unlikely that future slope movement could be triggered by increased pore-pressure resulting from infiltration of rainfall. A 1 in 10 year rainfall event was experienced in March 2014 and inclinometer readings taken following this event show no obvious response, with the possible exception of very minor (~2mm) movement recorded at 10m depth in BH08, although this is close to measurement error. Almost all of the slope displacements occurred in the February 2011 event, at which time the slope was subject to extremely high vertical and horizontal accelerations, together with (an inferred) pore pressure increase, which only resulted in ~0.3m of cumulative downslope movement. Given that the slope did not fail catastrophically at this time, it is probable that another large proximal earthquake, or a smaller event during unfavourable slope conditions (i.e. middle of winter) would be required to reactivate movement. The proximity of the Vernon Terrace area to the Port Hills fault on which the Christchurch earthquake occurred is considered to be a critical factor; the recurrence interval for an event on this fault is estimated to be ~7±1 k.y. (Mackey & Quigley 2014).

Currently, the toe of the movement is being buttressed by the valley floor. As pointed out by Massey et al. (2013), if further displacements were to occur and the slope fail completely, there is limited potential for runout or debris travelling a significant distance as the toe of the movement is already at the base of the relatively low-angle slope. It is unclear if the slope has previously failed in a similar fashion, although there is no discernible geomorphological evidence for this in the aerial photographs.

Although most of the ground cracks on the eastern hillslope have been infilled with a sand-bentonite mixture, Stephen-Brownie (2012) and Massey et al. (2013) both point out that the slope may be more prone to subterranean erosion (tunnel gullying), which is a widespread geotechnical issue encountered across the dispersive loess soils of the Port Hills.

6 Slope movement modelling

6.1 Introduction

Earthquakes are a major trigger of instability for both natural and engineered slopes, with earthquake magnitudes greater than 6.0 capable of generating widespread landsliding (Jibson 1993). Several approaches for evaluating co-seismic slope performance were developed during the twentieth century. These methods fall into three broad categories - pseudostatic analysis, stress-deformation analysis, and permanent displacement analysis - which output factor of safety, slope deformation, and slope displacement, respectively. The three types of analysis coexist in the engineering community and are summarised in this chapter.

Using permanent displacement analysis, this chapter compares modelled and actual slope displacements for the 2010-2011 CES to retrospectively determine an 'overall' critical acceleration for the eastern side of the Hillsborough Valley. The critical acceleration - above which downslope movement initiates - is then used to consider slope performance in the event of a future large earthquake. Slope displacements are modelled in SLAMMER (Jibson et al. 2013) using rigorous and simplified rigid sliding-block procedures.

6.2 Influence of earthquakes on the stability of soil slopes

Hillslope failure occurs when the shear stress across a potential failure surface is greater than the mobilised shear strength. The ability of earthquakes to trigger soil slope failure is variably due to:

- Ground accelerations adding to the destabilising forces acting on the soil mass (Hovius & Meunier 2012).
- Ground displacements rupturing bonds between soil particles, leading to loss of tensile strength and cohesion (Ishihara 1985).
- Seismic waves causing a cyclic loading effect on the soil, leading to compaction and a reduction of pore volume. Where pore water is unable to drain fast enough, pore pressure increases, reducing effective stresses between grains and consequently shear strength. Soils will liquefy if all shear strength is lost; slopes will 'fail' before shear strength is reduced to zero (Hack et al. 2007).

When considering slope failure, it is important to distinguish between triggers and causal factors. A trigger event is an external or internal process that initiates failure at a particular point in time, such as an earthquake or heavy rainfall; the causal factor in a landslide event is the process (or processes) that have made the slope susceptible to failure. Causal factors and triggers combine to create the landslide event, and it is important to consider all factors.

6.3 Methods for assessing the stability of slopes during earthquakes

6.3.1 Pseudostatic analysis

The simplest approach for evaluating seismic slope performance is the pseudostatic method. The procedure was first documented in the technical literature by Terzaghi (1950), following about two decades of use in industry. The pseudostatic method takes a conventional limit-equilibrium (factor of safety) analysis and adds an earthquake acceleration as a body force (Figure 6.1). Different earthquake accelerations are applied until the factor of safety is reduced to 1.0. The acceleration that lowers the factor of safety to 1.0 is called the yield acceleration, the exceedance of which is defined as failure. Pseudostatic analyses are quick and simple to perform, in part because they require no more information than is used in a standard static limit equilibrium analysis.

As is often the case for simple analysis methods, there are significant technical shortfalls. Applying an earthquake load as a static body force is extremely conservative, as it assumes the earthquake force is constant (i.e. not cyclic or transient), and acting only in a direction promoting slope instability. This limitation is partially addressed by use of a pseudostatic coefficient to reduce the applied earthquake load, however selection of a coefficient is often made solely on the basis of precedence or engineering judgement (Jibson 2011). Pseudostatic analysis can also be unconservative, in particular for slopes that lose more than 15% of their peak shear strength during shaking, and slopes that build up appreciable dynamic pore pressure during shaking (Jibson 2012). The pseudostatic method is unable to predict the consequences of failure, following exceedance of the yield acceleration, and also assumes that slip occurs simultaneously over the entire surface of rupture which does not model how actual slides develop (Muller & Martel 2000; Cruden & Varnes 1996).

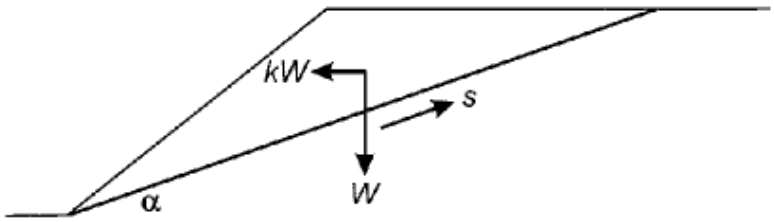

Figure 6.1: Simple pseudostatic force-body diagram, where k is the pseudostatic coefficient, W is the weight per unit length of the landslide, α is the slope angle, s is the shear resistance (Jibson 2011).

6.3.2 Finite element analysis (FEA)

The finite element method, initially developed for analysis of structural systems, was presented by Ray Clough at the 1960 ASCE Conference on Electronic Computation (Clough 1990). Finite element analysis is a computerised method for predicting how a two- or three-dimensional body or slope will deform in response to an applied load. The method works by breaking down the slope into a large number of node-bound elements (Figure 6.2). A load is applied and the response of each element is modelled by a set of mathematical equations. Unlike limit equilibrium methods, no assumptions need to be made regarding the shape or location of the failure surface (Griffiths & Lane 1999). The method can be applied to complex slope configurations and soil deposits to model virtually all types of failure mechanisms. The finite element method quickly came into use for analysing geotechnical problems in academia; its uptake by the engineering community was significantly slower (Griffiths & Lane 1999).

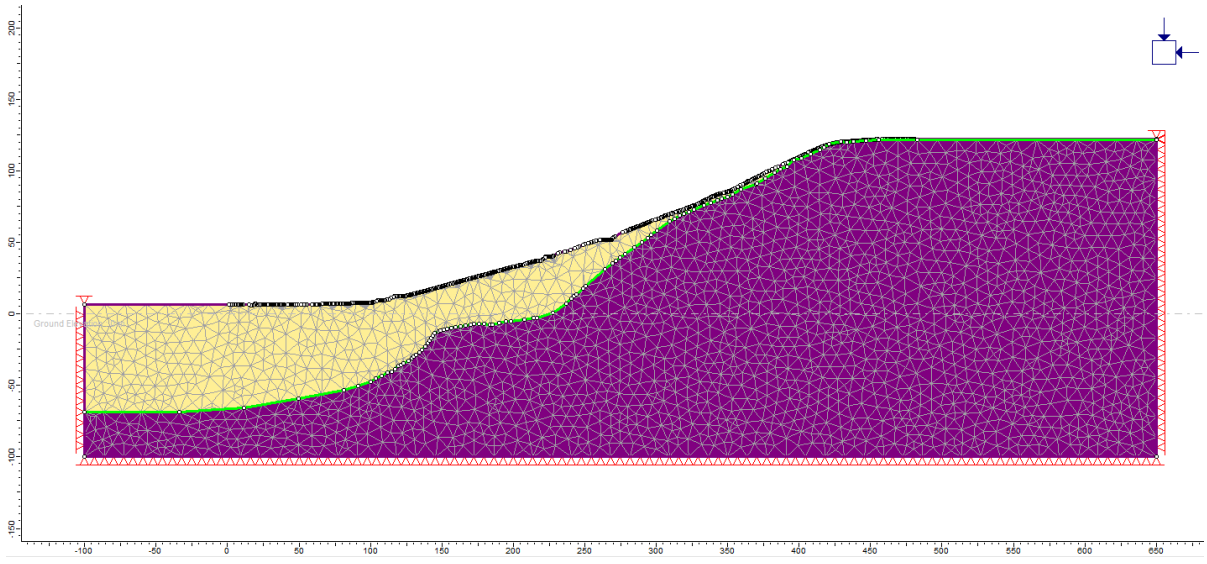

Figure 6.2: Preliminary two-dimensional finite element model prepared for the eastern side of the Hillsborough Valley using Phase2 modelling software. Note the grey mesh. Mesh nodes are not shown. Finite element modelling was not pursued for this research.

The two main limitations of finite element analysis are its complexity, and the quality and quantity of geotechnical data necessary to make the modelling worthwhile. While modern software is greatly contributing to the ease with which analyses can be performed, FEA is really only worthwhile if the quality of the geotechnical data and significance of the project warrants it. Detailed finite element analyses (which includes finite difference, discrete element and distinct element modelling) are usually reserved for critical projects such as tunnels, earth dams and slopes affecting structures and lifelines.

6.3.3 Permanent-displacement analysis

In his 1965 Rankine Lecture, Professor Nathan Newmark introduced a method for evaluating the seismic performance of dams and embankments, in which the cumulative downslope displacement of a sliding mass is calculated using strong motion records (Newmark 1965). Newmark's method models the sliding mass as a block on an inclined surface (Figure 6.3). A critical, or yield, acceleration (ky) is calculated for the block (as for pseudostatic analysis), which represents the horizontal acceleration at which basal resistance is overcome and permanent downslope movement initiates. Design or hazard-assessment criteria are used to select or create an appropriate earthquake strong motion record for use in the analysis. The parts of the record that exceed the critical acceleration are integrated to obtain a velocity-time history for the block. The velocity-time history is then integrated again to obtain the cumulative displacement of the block (Figure 6.4).

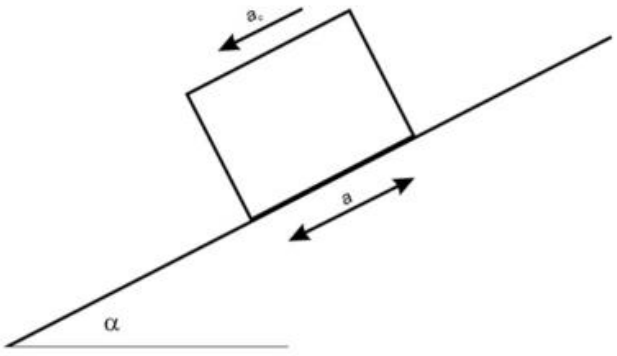

Figure 6.3: Conceptual model of a rigid sliding block analysis (Jibson 2011). Earthquake loading at the base of the block is denoted by a, ac is the critical acceleration of the block, and α is the slope angle.

The application of Newmark's method to landslides in natural slopes was first validated by Wilson and Keefer (1983), who analysed an earthquake-triggered slope failure that occurred in the vicinity of several strong-motion instruments. It has since been widely applied to evaluating the performance of slopes (Jibson 2011). Originally developed for earth dams, it is now considered best suited to modelling displacements of earthquake-triggered failure or deformation in natural slopes (Jibson 2012).

There are three types of sliding block analysis, known as rigid block, coupled and decoupled analysis. The original methodology developed by Newmark is known as rigid-block analysis. The assumption of rigid-plastic behaviour means that the dynamic response of the landslide mass can be ignored (i.e. no internal deformation is assumed), allowing block displacements to be modelled as plastic deformation along a discrete basal shear surface. These assumptions are generally reasonable for shallow translational slides in stiff or brittle material, but produce overly conservative displacements for deeper failures in softer materials (Jibson 2011).

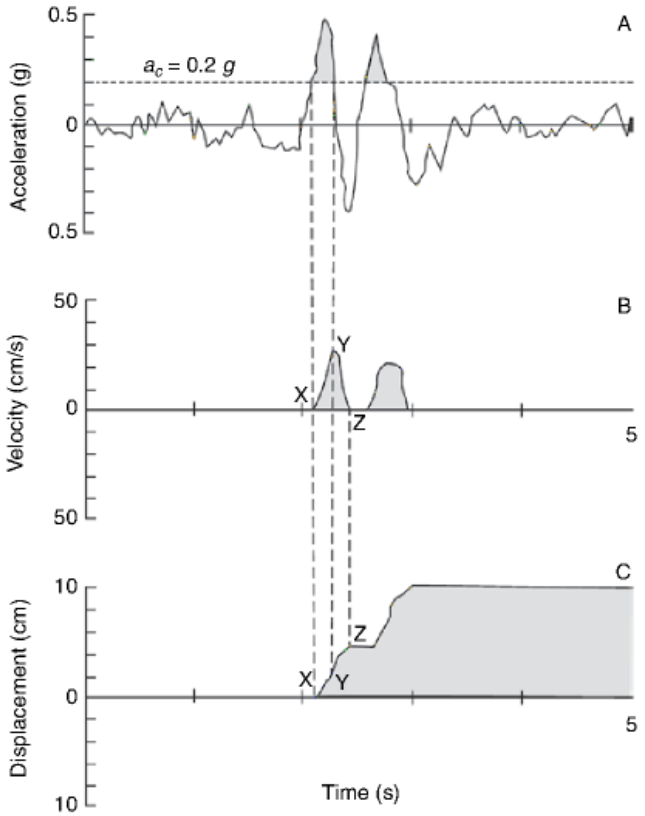

Figure 6.4: Double integration of acceleration-time history to compute permanent displacements (Jibson 2011). The point X marks the onset of sliding, Y is where shaking drops below the critical threshold, and Z is when the block stops moving (i.e. velocity returns to zero).

Decoupled analysis is a modification of the traditional Newmark procedure. The dynamic response of the block is independently computed, before being incorporated into a rigid block analysis. The simplified procedure developed by Makdisi and Seed (1978) is the most commonly used decoupled analysis method (Jibson 2012). A limitation of the decoupled approach is that it does not take into account the effects of sliding displacement on the ground motion, which can sometimes lead to overly conservative or extremely unconservative estimates of slope displacements.

Coupled analysis is an extension of decoupled analysis, where the dynamic response and permanent displacement are modelled together so that the influence of plastic sliding displacement on ground motions is taken into account (Jibson 2011). Coupled analysis is the most sophisticated form of sliding block analysis, and is also the most computationally intensive. The coupled approach provides the most accurate estimate of displacements for deeper failures in softer material.

6.4 Modelling approach and analysis selection

6.4.1 Modelling basis

Sliding block analyses are usually performed with a calculated yield acceleration to predict co-seismic slope displacements. The critical acceleration for the potential sliding mass is calculated using soil strength parameters (friction and cohesion), unit weight, thickness of the sliding mass, and slope angle (Bray et al. 1998). For the Hillsborough Valley research, earthquake shaking records, measured ground displacements and inclinometer data were instead used to back-analyse slope behaviour to determine a critical acceleration for the eastern side of the valley. Back-analyses were performed using simplified empirical models and actual earthquake shaking records from the nearby Cashmere High School (CMHS) and Heathcote Valley Primary Schools (HVSC), which were the nearest permanent recording stations (Figure 6.5). A table summarising strong-motion recordings for the four largest CES earthquakes is provided in Appendix E. The back-analysed critical acceleration was then used to consider how the slope may behave in a future Alpine Fault or Hope Fault earthquake, using the results of synthetic broadband modelling carried out by Holden (2014).

Permanent displacement analysis was selected because it made the best use of the software and geotechnical data available to the author, namely measured tension crack apertures (inferred to provide a lower-bound estimate for slope displacement) and inclinometer data. Performing back-analyses meant the suitability of the chosen method could be assessed through comparison of measured and modelled ground displacements. Sliding block analysis provided an opportunity to make use of time-acceleration records from nearby monitoring stations allowing the programme to capture and model the response of the sliding mass to unusually strong ground shaking in the CES.

6.4.2 Selection of rigid block analysis

Selection of a sliding block analysis is typically made on the basis of period ratio, T_s/T_m, which is the ratio of the fundamental site period (T_s) to the mean period of the earthquake motion (T_m) (Jibson 2011). Rigid-block analysis is generally used for period ratios of less than 0.1, and flexible (coupled or decoupled) analysis for period ratios of greater than 0.1. Rigid block models tend to give good results for relatively thin landslides in stiff or brittle material (Jibson 2012).

Ground damage on the eastern side of the Hillsborough Valley has likely resulted from incipient, shallow, translational movement within the loess colluvium (as discussed in Chapter 5). Although rigid-block analysis assumes displacements occur along a single rupture surface, shaking table modelling carried out by Wartman et al. (2005) demonstrated that rigid-block analysis can reasonably be applied to model deformation along multiple, distributed slip surfaces. In addition, a period ratio of 0.09 was calculated for the sliding mass, and rigid block analysis is generally considered suitable for the large majority of earthquake-triggered landslides (Jibson 2012).

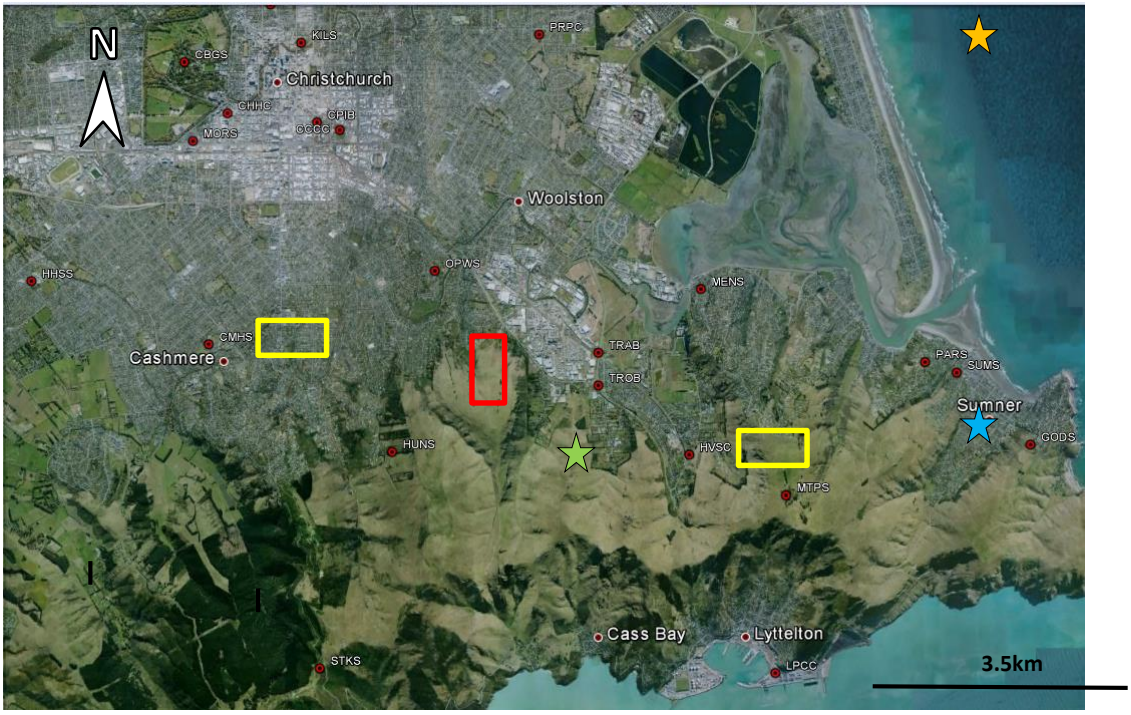

Figure 6.5: Recording station locations. The eastern side of the Hillsborough Valley is outlined in red. CMHS is outlined in yellow, west of the Hillsborough Valley. HVSC is outlined in yellow, east of the Hillsborough Valley. CMHS and HVSC were the two stations nearest to the Hillsborough Valley at the onset the of the CES. The green, blue and orange stars show the epicentres of the February, June and December 2011 earthquakes, respectively.

6.4.3 SLAMMER

SLAMMER (Seismic LAndslide Movement Modelled using Earthquake Records) is a Java program designed to carry out sliding block analyses for the evaluation of seismic slope performance. The software is available for free download from the United States Geological Survey (USGS) website (http://earthquake.usgs.gov/research/software/). Rigid, decoupled-flexible and coupled-flexible sliding block analyses can be carried out using user-specified ground motions or empirically calibrated equations. The former is referred to as 'rigorous' analysis and the latter as 'simplified' analysis.

Both rigorous and simplified rigid block analyses were carried out for the present research. Rigorous analyses were made possible due to the availability of strong-motion records for download from the GeoNet website, as discussed below.

6.4.4 Limitations and assumptions

A number of assumptions are made in order to carry out sliding block (and specifically rigid-sliding block) analyses, including:

- It is assumed that no permanent displacement occurs below the critical yield level.
- Vertical accelerations are assumed to be negligible. High vertical accelerations were a dominant feature of the Christchurch earthquake (<2.2g recorded in the adjacent Heathcote Valley). The possible role of high vertical accelerations in the observed displacements is not known, and is beyond the scope of this thesis.
- Dellow et al. (2011) allude to slope creep in the Vernon Terrace area occurring in the days to weeks following the Christchurch Earthquake. Displacements predicted by sliding block analyses do not account for this type of movement.
- It is assumed that the critical acceleration is not strain-dependent, and remains constant throughout the analysis.
- There is geotechnical evidence for pore water pressure increase during the December 2011 earthquake, by which time the slope had been fully instrumented. Strength loss associated with increased piezometric head is not directly accounted for or modelled by sliding block analysis.

6.5 Model input parameters

Simplified empirical analyses only require 2-4 numerical inputs. The Rathje and Saygili (2009) model used for this work uses PGA and earthquake magnitude. Rigorous analyses were performed using strong-motion records from instruments situated at the nearby Hillsborough Valley Primary School (4km to the southeast) and Cashmere High School (3km to the west), the locations of which are shown in Figure 6.5. Data and modelling input sources are described below.

6.5.1 Critical acceleration

Critical accelerations of 0.15, 0.2, 0.25 and 0.3 were selected for back analysis following preliminary, iterative modelling carried out in SLAMMER Comparison of results with estimated cumulative downslope displacements for the Vernon Terrace area (see section 6.5.4) indicated the critical acceleration for the Vernon Terrace area would likely fall within this range and it was therefore suitable for modelling.

6.5.2 Modelled PGAs for the eastern side of the Hillsborough Valley

PGAs for the eastern side of the Hillsborough Valley were obtained from PGA contour maps made available through the CGD (2015b). PGA contour maps were developed for the five largest earthquakes that occurred during the 2010 – 2011 CES (Figure 6.6). Modelled accelerations for the eastern side of the Hillsborough Valley vary from 0.18g (December 2011 earthquake A) to 0.64g (February 2011 earthquake), as shown in Table 6.1. Ground motion contours do not extend up ridges and hillslopes where topographic amplification may occur. While the ground damage being investigated did not occur on the valley floor, it is unlikely that topographic effects have amplified shaking. This is because ground damage occurred along the toe of a relatively low angle slope: guidelines set by the European Union for the design of structures for earthquake resistance (Eurocode 8, Part 5, Annex A) advise that for slope angles of less than 15°, topographic effects may be ignored, and goes on to recommend amplification factors for sites only near the top edge of isolated cliffs and slopes (Eurocode 2004). Horizontal acceleration estimates for the eastern side of the Hillsborough Valley were therefore not modified.

6.5.3 Strong-motion records

Corrected strong motion data from accelerograms at Cashmere High School (CMHS) and Heathcote Valley Primary School (HVSC) were downloaded for the Darfield, Christchurch, June 2011 and December 2011 (two events) earthquakes. These accelerograms were the closest instruments to the Hillsborough Valley during the 2010-2011 CES (Figure 6.5); additional instruments have since been installed across Christchurch. Data were downloaded as ASCII (text) files from ftp.geonet.org.nz/strong/processed/Proc. Ground accelerations were converted to g from mm/s^2 before being added to SLAMMER. Horizontal accelerations on the longitudinal and transverse axes were modelled separately, and the displacement results averaged. A summary table of strong motion records for the four largest 2010-2011 CES events is provided in Appendix E.

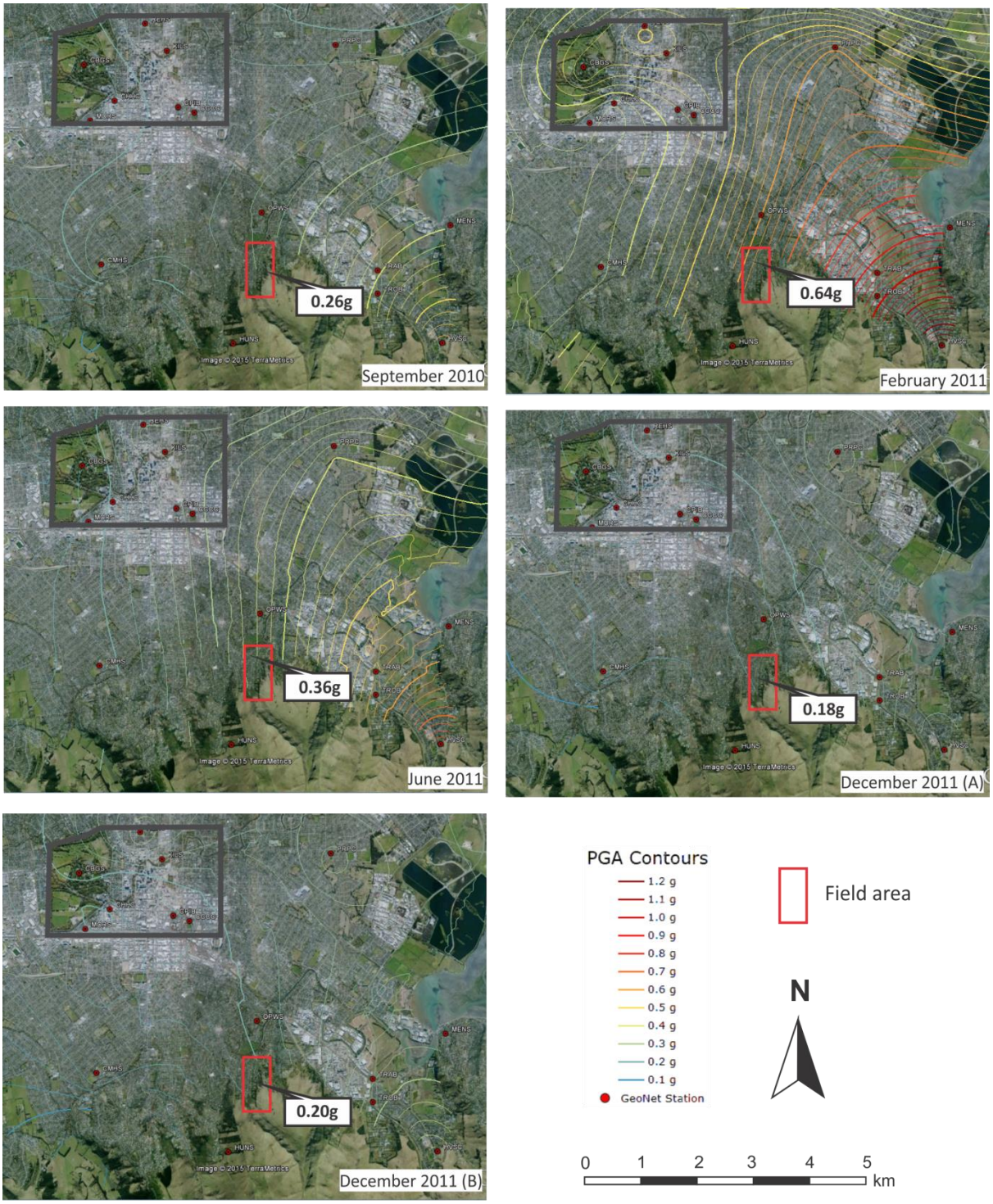

Figure 6.6: PGA contours for horizontal acceleration during the September 2010, February 2011, June 2011 and December 2011 earthquakes. Source: CGD (2015b). Central Christchurch is to the top left of the image, outlined in grey. Spatial distribution interpolated using ordinary kriging.

6.5.4 Tension crack apertures

Measured tension crack apertures were used to provide a lower-bound estimate for cumulative downslope displacement of the Vernon Terrace movement, on the assumption that this recorded permanent downslope displacement. Summing crack apertures along a line of section is considered to be a lower-bound estimate as it does not take into account strains within the slide mass (Petley et al. 2002). It is also possible that some cracks were not mapped. Cracks were mapped by GNS Science between October 2012 and January 2013. Crack location and aperture information were downloaded from the CGD 'Port Hills Mass Movements and Surface Deformations' map layer (CGD 2014). Examination of the map (Figure 2.2) indicates downslope displacements to vary from 0.2 - 0.3m, with 0.3m adopted as representative for this modelling. Massey et al. (2013) give cumulative displacements of 0.7 horizontal and 0.5m vertical for the Vernon Terrace area but it is unclear where these displacements were observed as they are not reflected in the mapping and have not been obtained using survey data. Although not stated, it is likely that the 0.7m figure is the maximum cumulative displacement measured or observed at one location and is therefore not representative of the whole slope.

6.5.5 Ground motion predictions for Alpine and Hope Fault earthquakes

Modelled magnitudes and PGAs for Alpine Fault and Hope Fault earthquake shaking were sourced from Holden (2014), who generated synthetic broadband strong-motion records for large Alpine and Hope Fault ruptures (M_w 8.2 and M_w 7.1, respectively). Synthetic records for soil (class D) and rock sites predict PGAs of 0.08 – 0.05g and 0.08 – 0.06g for Christchurch during Alpine and Hope Fault events, respectively (Table 6.1). Both faults are >100km from Christchurch City.

Table 6.1: Input parameters for simplified empirical rigid sliding block analyses. *For Class D soil sites.

	Earthquake	Earthquake magnitude (M_w)	Hillsborough Valley PGA (CGD 2015b)
CES	Darfield (September 2010)	7.1	0.26
	Christchurch (February 2011)	6.2	0.64
	June 2011	6	0.36
	December 2011 (A)	5.8	0.18
	December 2011 (B)	5.9	0.2
	Earthquake	**Modelled magnitude (M_w)**	**Christchurch PGA*, g (Holden 2014)**
Future	Alpine Fault	8.2	0.08
	Hope Fault	7.1	0.08

6.6 Back-analysis results

The results of back-analyses are presented as cumulative displacement step plots for each of the four critical accelerations (Figure 6.7), and are summarised in Table 6.2. The 'simplified' column gives the results of simplified empirical analyses carried out using the Rathje and Saygili (2009) model. The 'rigorous' column gives the results of analyses carried out using HVSC and CMHS strong-motion records. Tables showing individual calculated displacements for each critical acceleration and each earthquake event are provided in Appendix E.

Table 6.2: Predicted cumulative displacements of a sliding mass with k_y 0.15, 0.2, 0.25 and 0.3 subjected to shaking experienced at CMHS and HVSC during the five largest earthquakes of the 2010-2011 CES. Cumulative displacement for the Hillsborough Valley The simplified cumulative displacement is calculated using a simplified empirical model, using modelled PGAs for the eastern side of the Hillsborough Valley.

Critical acceleration (k_y)	**CMHS** cumulative displacement, m		**HVSC** cumulative displacement, m		**Simplified/Hillsborough Valley** cumulative displacement, m
	Rigorous	Simplified	Rigorous	Simplified	
0.15	0.07	0.04	1.01	1.60	0.24
0.2	0.02	0.01	0.66	1.01	0.11
0.25	0	0	0.45	0.82	0.05
0.3	0	0	0.31	0.48	0.03

Modelling predictions are presented as cumulative displacements, as the mapping on which slope displacement estimates are based was carried out following the 2010-2011 CES and are therefore cumulative. The predicted displacements presented in Table 6.2 are intended to provide an index of slope performance and should not be interpreted literally. The HVSC displacements are intended provide an upper estimate of slope performance for the Hillsborough Valley, as the accelerations recorded at HVSC were greater than those experienced in the Hillsborough Valley for the four earthquakes being considered. Similarly, the CMHS displacements provide a lower bound estimate. As the shaking records are being used as a guide only, the influence of site effects are ignored (CMHS is soil class D, HVSC and the Hillsborough Valley are on site class C; Bradley et al. 2014).

As critical acceleration of the theoretical landslide block is increased, the predicted displacements across all three sites (HVSC, CMHS and Hillsborough Valley) decrease. This is because critical acceleration must be exceeded to initiate sliding; a sliding mass with a higher k_y has greater resistance to sliding and therefore requires larger ground accelerations (magnitude and duration) to initiate sliding. Rigorous analyses performed using the HVSC shaking records predicted the highest slope displacements for all critical accelerations (~0.3 – 1.0m). Analyses performed using the CMHS records

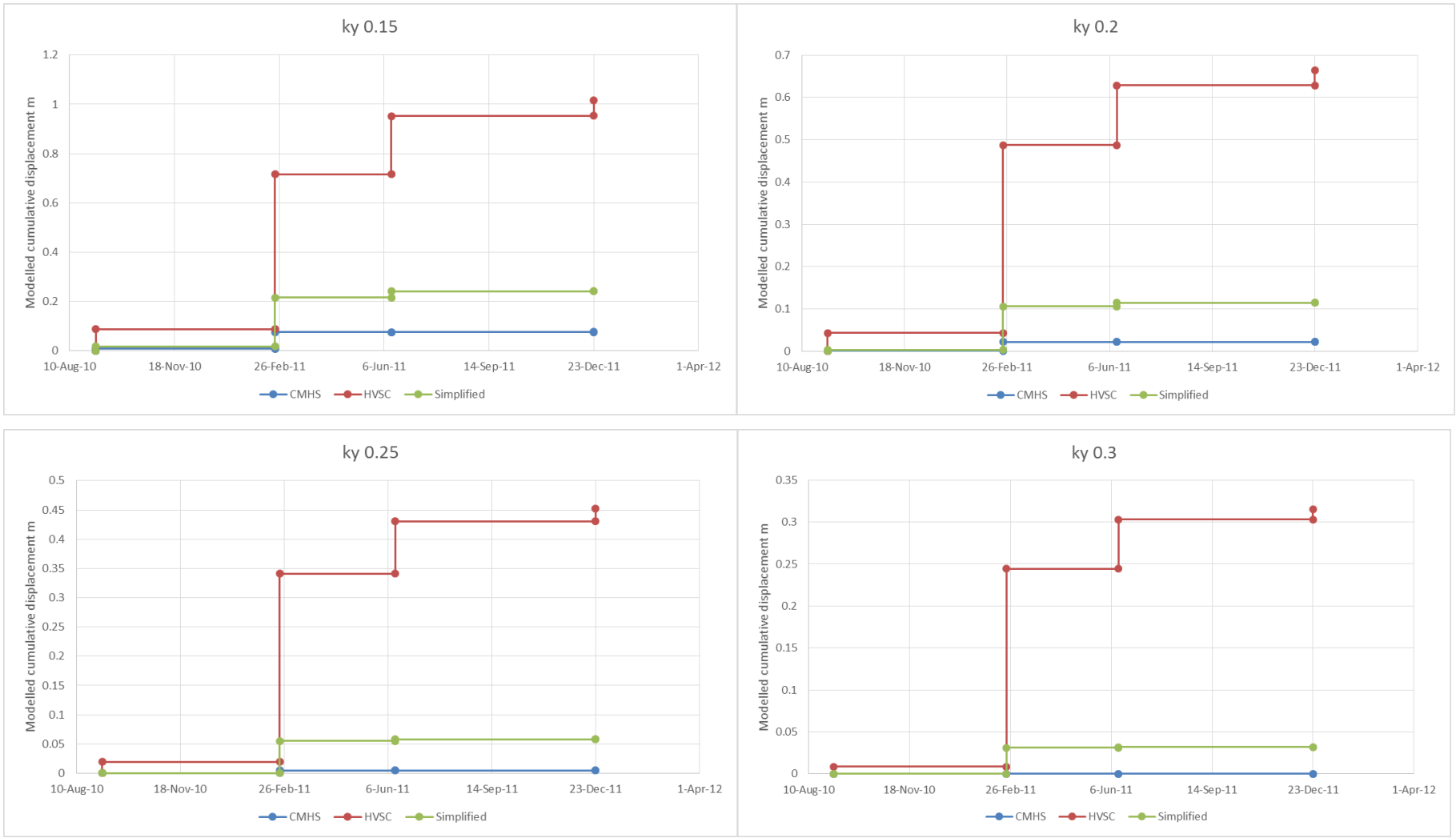

Figure 6.7: Modelled cumulative displacements for yield accelerations of 0.15, 0.20, 0.25 and 0.30. The four modelled earthquakes occurred on 4 September 2010 (Darfield), 22 February 2011 (Christchurch), 13 June 2011 and 23 December 2011.

predicted the smallest slope displacements across the range of assessed critical accelerations (~0 – 0.1m). The simplified analyses performed using modelled PGAs for the Hillsborough Valley predicted intermediate displacements (~0 – 0.15m). These predictions are consistent with the relative magnitude of ground accelerations recorded at each of the strong motion stations and modelled for the Hillsborough Valley. The PGA contour maps in Figure 6.6 show PGAs to be greatest at the HVSC station and smallest at the CMHS station for the September 2010, February 2011, June 2011 and December 2011 earthquakes.

Comparing the results of simplified and rigorous analyses carried out using CMHS and HVSC data, the simplified analyses have consistently predicted larger slope displacements for all of the modelled critical accelerations. It can reasonably be assumed that rigorous analyses conducted using actual strong-motion data for the Hillsborough Valley would predict smaller cumulative displacements than the simplified empirical analysis.

6.7 Interpretation of modelled displacements

In addition to the modelled predictions presented in the previous section, inclinometer records are available to help constrain the threshold acceleration for the slope (see Appendix D). Five inclinometers were installed above and below Vernon Terrace in May and June 2011 (see Chapter 5). One instrument was installed prior to the June earthquake at the northern end of the valley (in BH03) and showed small amounts of displacement (~50mm total) at 3.5, 6.75 and 9.75m depth. It is assumed that the central and southern parts of the slope also moved. All five inclinometers were installed by the time of the December earthquakes and no movement was detected. Given that PGAs for the eastern side of the Hillsborough Valley were in the order of 0.35 and 0.2g for the June and December earthquakes, respectively, the critical acceleration for the slope must be less than 0.35g and greater than 0.2g. Taking into account the modelled displacements (with the HVSC predictions known to be too high, and the CMHS predictions known to be too low), a critical acceleration of 0.2 – 0.25g is a reasonable assumption for the eastern side of the valley. This figure is considered to provide a lower-bound estimate for the slope as a whole, as some parts of the slope experienced zero displacements and would therefore have a higher k_y. Tables showing individual calculated displacements for each critical acceleration and each earthquake event are provided in Appendix E.

Considering future slope performance from a Newmark perspective, in order to cause the slope to move PGAs larger than the critical acceleration are required to initiate displacement of the sliding mass. A large magnitude earthquake (e.g. M_w 7.0-8.0) producing peak ground accelerations of 0.3 – 0.4g would cause the slope to move only very slightly (<0.1m), based on results of simplified empirical sliding

block analyses performed using the Rathje and Saygili (2009) method. The slope is not expected to move if the critical acceleration threshold is achieved – PGAs must be significantly greater than this threshold to initiate movement. It seems likely that it would require another proximal, shallow focus, large magnitude earthquake to reactivate slope movement.

Synthetic broadband modelling carried out by Holden (2014) for Alpine and Hope Fault earthquakes, predicts PGAs of 0.08g for soft soil sites (soil class D) in Christchurch City. Although the eastern side of the Hillsborough Valley is soil class C (i.e. stiffer; Kaiser et al. 2014), softer soils tend to amplify ground motions (Loye et al. 2013) so using ground motion modelled for a class D site is probably conservative. Using a PGA of 0.08g and an earthquake magnitude of 8.2 (Table 6.1) in a simplified block analysis predicts zero slope displacements for the Vernon Terrace area, as the PGA is significantly lower than the yield acceleration. Reactivation of the Port Hills fault on the which the Christchurch earthquake occurred is not considered here, given the long recurrence interval of 7±1 k.y (Mackey & Quigley 2014).

There are a number of modelling limitations that must be taken into account and there are significant characteristics of the Canterbury earthquake sequence that are not taken into account by sliding block analyses. Firstly, vertical accelerations, particularly during the February 2011 earthquake, were extreme. Acceleration in the vertical plane is not taken into account by sliding block analysis and it is very likely that vertical accelerations will have played a significant, but unknown, role in the observed slope displacements. Secondly, the role of dynamic pore pressure is not taken into account by the analyses. Piezometric data shows increased head of 0.5 – 1.5m in the Vernon Terrace area immediately following the December earthquakes (see Chapter 5 and Appendix D), which took up to seven days to dissipate. Although the PGAs for an Alpine or Hope Fault earthquake are insufficient to initiate block movement, displacements could still occur if the shaking is able to generate excess pore pressures in the wetter colluvial units. Any slope creep that may have occurred during the days following the earthquakes is not accounted for or captured by the analyses. It was also assumed that the four modelled events have accounted for the total slope displacements. If slope creep or aftershocks have made a significant contribution to the measured slope displacements, the actual yield acceleration the Vernon Terrace area could be higher than what has been estimated.

6.8 Synthesis

- Rigid-sliding block analysis was considered appropriate to model slope displacements in the Vernon Terrace area, based on the inferred failure mode (see Chapter 5) and calculated period ratio for the Vernon Terrace area.

- Rigid sliding block analyses were used to back-calculate a yield acceleration for the Vernon Terrace area. The results of back-analysis, together with inclinometer data, suggests a yield acceleration of 0.2 – 0.25 for the slope.
- Based on synthetic broadband modelling carried out by Holden (2014) for Alpine Fault and Hope Fault earthquakes, it is unlikely that ground motions generated by these earthquakes would reactivate movement of the Vernon Terrace area. This does not consider the possible role of dynamic pore pressure in slope movement.

7 Summary and conclusions

7.1 Project objectives

Following the 22 February 2011 earthquake, ground damage in the form of extensional cracking and compressional features were reported across the lower slope of the eastern side of the Hillsborough Valley. The aim of this thesis was to build an understanding of how different geological and geotechnical factors have collaborated to form the observed ground damage through field investigation, laboratory analysis and numerical modelling.

7.1.1 Engineering geological and geomorphological model for the eastern Hillsborough Valley

Site history was assessed through review of historical (1926-1973) and recent (2011) aerial photography. The valley was occupied by market gardens at the time of the 1926 aerial survey, with land-use changing from market-garden to mixed residential through the 1950s. The 1940 aerial images show severe gullying at the southern end of the valley, with fan debris extending across the lower slope and onto the valley floor. Overlaying the 2010-2011 CES ground damage onto the 1940 aerial photograph shows the ground cracking to follow the fan apices.

A seismic refraction survey was carried out in order to model the bedrock-colluvium interface. An accelerated weight drop and sledgehammer were used in conjunction to achieve excellent wave-path coverage directly below the geophone spread. Modelling indicates bedrock slopes relatively gently through the centre of the slope and is inferred to continue in a stepped fashion down to the valley floor. This ‘pattern’ is consistent with basalt lava outcrop patterns across the Port Hills.

Mapping was carried out using some 200 hand-auger, borehole and CPT records extracted from the CGD. Borehole records show the slope cover to be almost entirely loess colluvium, with lenses of in-situ loess preserved at depth. Tension cracking has occurred entirely within loess-colluvium, meaning there is no lithological/soil type change to explain the location of the cracking. The extent and thickness of a buried peat swamp at the base of the slope was mapped using CGD hand auger records. A zone of marked compression coincides with the thickest known extent of the peat deposits. Springs appeared during the 2010-2011 CES and these can be seen to approximately follow the periphery of the peat. Depth to bedrock at the centre of the valley is expected to be on the order of 100m.

7.1.2 Test methodology for measuring tensile strength of Port Hills loess-colluvium

Tensile strength testing of Port Hills loess-colluvium was undertaken to explore the significance of tensile failure of the eastern hillslope. A comprehensive review of the soil tensile testing literature was undertaken to find a suitable methodology that could be adapted for testing in the Engineering Geology Soil Mechanics Laboratory at the University of Canterbury.

A direct, mould-based approach was selected for testing, and a test procedure adapted from the work of Tamrakar et al. (2005) and Tamrakar et al. (2007). A figure-of-eight shaped mould was fabricated using available materials and testing was undertaken in a Wykeham Farrance shear rig. A workable test procedure was developed through trial and error over a period over several months. Test results showed remoulded loess-colluvium sampled from the Vernon Terrace area to possess tensile strength of 7 - 28 kPa across the range of tested moisture contents (10 – 15%) and dry densities (1650 -1900kg/m^3). Test results showed a negative correlation between moisture content and tensile strength and a positive correlation between density and tensile strength.

Prior to testing, it was not known if loess colluvium would possess measureable tensile strength. In the context of slope stability, if the soil (or rock) has tensile strength and tensile failure occurs, this contribution to stability is lost. Attempts to quantify the role of tensile strength using finite element modelling software did not produce reasonable results; more advanced modelling would be required to do so and was not further explored in this thesis.

7.1.3 Geomorphological and geotechnical aspects of ground damage

The type and distribution of surface damage in the Hillsborough valley is consistent with translational sliding, however drilling did not locate a surface along which sliding may have occurred. Inclinometer records for the borehole instrumented prior to the June 2011 earthquake show minor displacements at 3.5, 6.75 and 9.75m depth, suggesting that slope displacements have been accommodated by multiple shear surfaces, probably of limited lateral and downslope extent within the upper 10m of the slope. This arrangement is supported by the colluvial layering inherent within the slope. Piezometer records showed pore pressure increase due to the December 2011 earthquake; although no slope movements occurred at this time, elevated pore pressure may have facilitated slope movement during the February 2011 and June 2011 earthquake events.

The Vernon Terrace area is considered to be an ‘incipient failure’. From a geomorphological perspective, the scale of tension cracking and compression does not represent a late stage of failure, which would be implied by features such as cracking along the flanks of the slide and development of

a ‘true’ scarp. Geotechnically, distributed shearing within the upper 10m of the slope may indicate the early stages of rupture surface formation according to the Petley et al. (2005) crack propagation model.

7.1.4 Seismic slope performance through application of sliding block analyses

Sliding block analysis (also known as permanent displacement analysis) was utilised to understand how the Vernon Terrace area may perform in a future large earthquake. Sliding block analysis relies on calculation of a yield or critical acceleration, which must be overcome in order for sliding to occur. The known performance of the slope during the 2010-2011 CES was used in conjunction with strong-motion records for nearby stations to back-calculate the yield acceleration for the slope. This was done through comparison of modelled displacements with actual/measured displacements and inclinometer records, which indicate a range of 0.2 – 0.25g as a lower bound estimate for critical acceleration of the Vernon Terrace area. Recent synthetic broadband modelling carried out for Alpine Fault and Hope Fault events (>100km from Christchurch) indicate PGAs of 0.08g for the Christchurch area. From a Newmark perspective, in order for slope displacements to occur the yield acceleration must be exceeded. It is therefore unlikely that slope movement would be reactivated by an Alpine or Hope fault earthquake, given that the expected PGA (0.08g) is significantly less that the yield acceleration for the slope (0.2-0.25g). This conclusion does not take into account the duration of shaking, which is expected to be on the order of several minutes for an Alpine Fault rupture. Long duration shaking may influence the slope other ways, for example through the generation/build-up of excess pore pressure.

7.2 Principal conclusions

- It is hypothesised that the observed ground damage in the Vernon Terrace area has resulted from incipient, translational sliding which has occurred at a shallow depth (<10m) along multiple, discontinuous slip surfaces.
- Slope movement has occurred in response to very strong earthquake shaking during both the February 2011 and June 2011 earthquake events, with no movement recorded following the slightly more distal December 2011 earthquake event.
- The proximity of the valley to the Port Hills fault (subsurface) rupture is considered to be a critical factor in the triggering of movement. This is supported by the sliding-block modelling carried out for this research, which indicates large ground accelerations (>0.2 – 0.25g) are required to mobilise the slope. Alpine Fault and Hope Fault earthquakes are not expected to be able to produce these accelerations in Christchurch.

- It seems unlikely that slope movement could be reactivated by increased pore pressure resulting from rainfall infiltration, based on inclinometer data provided for the period June/July 2011 to May 2014.

7.3 Suggestions for future research

7.3.1 Trenching

The trenching carried out for this research was primarily for the purposes of soil sampling and did not reach the base of the tension crack. It is recommended that larger-scale trenching is carried out to attempt to locate the hypothesised multiple shear surfaces. Trenching should be carried out where the 'sliding mass' is likely to be thinner, such as at the northern or southern ends/extent of the ground damage, where the distance between extension and compression features is small.

7.3.2 Mapping

The presence of peat at the base of the hillslope is inferred to have played a role on the slope movement, through poor performance as a toe buttress during earthquake shaking. The mapped extent of the peat is based on shallow investigation records sourced from the CGD; investigations along the base of the slope at the southern end of the valley are limited and it is possible that the extent of the peat is greater (to the south) than what has been mapped for this thesis.

Research should also be undertaken to establish the presence or absence of peat in adjacent valleys that have exhibited similar deformation of the lower slope, such as Bowenvale Valley.

7.3.3 Failure mechanism modelling

It is recommended that finite element modelling is undertaken to investigate/establish the validity of the hypothesised mode of sliding for the Vernon Terrace area. The modelling carried out for this research assumes a failure mode (translational sliding) to calculate displacements and therefore does not provide any information on the development or progression of a failure surface. It is noted that strength and other geotechnical parameters for the Vernon Terrace area would need to be acquired in order for modelling to be undertaken.

7.3.4 Tensile strength testing

The tensile strength testing carried out for this thesis showed promising results. Test results showed repeatability and the measured strengths are considered reasonable for Port Hills loess colluvium, based

on the testing literature for silts with similar geotechnical properties. In addition to the possible contribution of tensile strength to hillslope stability, findings may also be applied to better understand the processes of creep movement and tunnel gullying in the Port Hills.

It is recommended that the indirect ‘double punch’ technique trialled for this research is revisited. The test is simple to carry out and is one of the few techniques which can easily measure tensile strength of undisturbed test specimens. Testing of undisturbed specimens will allow for comparison of undisturbed and remoulded tensile strengths of Port Hills loess colluvium.

For direct testing, it is recommended strain is measured using an LVDT. Future testing should also determine maximum dry density, optimum moisture content, unconfined compressive strength, matric suction and mineralogy of the clay fraction of the soil being tested, for greater understanding of how these elements influence tensile strength.

8 References

Ajaz, A. & Parry, R.H.G., 1974. An Unconfined Direct Tension Test for Compacted Clays. *American Society for Testing and Materials Journal of Testing and Evaluation*, 2(3), pp.163–172.

Ajaz, A. & Parry, R.H.G., 1975. Stress-strain behaviour of two compacted clays in tension and compression. *Geotechnique*, 25(3), pp.495–512.

Bannister, S. & Gledhill, K., 2012. Evolution of the 2010–2012 Canterbury earthquake sequence. *New Zealand Journal of Geology and Geophysics*, 55(3), pp.295–304.

Beavan, J., Motagh, M., Fielding, E.J., Donnelly, N. & Collett, D., 2012. Fault slip models of the 2010–2011 Canterbury, New Zealand, earthquakes from geodetic data and observations of postseismic ground deformation. *New Zealand Journal of Geology and Geophysics*, 55(3), pp.207–221.

Bell, D.H., 1980. *Detailed assessment of Lots 1-3, Stage VIIIA*, Christchurch, New Zealand.

Bell, D.H. & Trangmar, B.B., 1987. Regolith materials and erosion processes on the Port Hills, Christchurch, New Zealand. In *Fifth International Conference and Field Workshop on Landslides*. Christchurch, New Zealand, pp. 93 – 105.

Bradley, B.A. & Cubrinovski, M., 2011. Near-source strong ground motions observed in the 22 February 2011 Christchurch earthquake. *Bulletin of the New Zealand Society for Earthquake Engineering*, 44(4), pp.181–194.

Bradley, B.A., Quigley, M.C., Van Dissen, R.J. & Litchfield, N.J., 2014. Ground Motion and Seismic Source Aspects of the Canterbury Earthquake Sequence. *Earthquake Spectra*, 30(1), pp.1–15.

Bray, J.D., Rathje, E.M., Augello, A.J. & Merry, S.M., 1998. Simplified seismic design procedure for geosynthetic-lined, solid-waste landfills. , 5(1), pp.203–235.

British Geological Survey, How does BGS classify landslides? Available at: http://www.bgs.ac.uk/landslides/how_does_BGS_classify_landslides.html [Accessed September 11, 2015].

Brown, L.J., Beetham, R.D., Paterson, B.R. & Weeber, J.H., 1995. Geology of Christchurch, New Zealand. *Environmental & Engineering Geoscience*, 1(4), pp.427–488.

Brown, L.J. & Weeber, J.H., 1992. *Geology of the Christchurch Urban Area* M. B. Reay, ed., Lower Hutt, New Zealand: Institute of Geological and Nuclear Sciences Limited.

Brown, L.J. & Weeber, J.H., 1994. Hydrogeological implications of geology at the boundary of Banks Peninsula volcanic rock aquifers and Canterbury Plains fluvial gravel aquifers. *New Zealand Journal of Geology and Geophysics*, 37(2), pp.181–193.

Canterbury Geotechnical Database (CGD), 2014. Port Hills Mass Movements and Surface Deformations. *Map Layer CGD5180 - 30 October 2014*. Available at: https://canterburygeotechnicaldatabase.projectorbit.com/ [Accessed December 14, 2014].

Canterbury Geotechnical Database (CGD), 2015a. Geotechnical Investigation Data. *Map Layer CGD0010*. Available at: https://canterburygeotechnicaldatabase.projectorbit.com/ [Accessed July 14, 2015].

Canterbury Geotechnical Database (CGD), 2015b. Ground Motion. *Map Layer CGD5170 - 30 June 2015*. Available at: https://canterburygeotechnicaldatabase.projectorbit.com/ [Accessed July 14, 2015].

Carey, J.M. & Petley, D.N., 2014. Progressive shear-surface development in cohesive materials; implications for landslide behaviour. *Engineering Geology*, 177, pp.54–65. Available at: http://dx.doi.org/10.1016/j.enggeo.2014.05.009.

Christchurch City Council, 2013. *Christchurch City Fact Pack 2013*, Christchurch. Available at: http://resources.ccc.govt.nz/files/CityLeisure/statsfacts/FactPack2013.pdf.

Christchurch City Council, 2014. Class II mass movement area - information for property owners. Available at: http://www.ccc.govt.nz/assets/Documents/Environment/Land/PortHillsLandDamageClassIIInfo.pdf [Accessed February 2, 2015].

Christchurch City Libraries, Christchurch area showing swamps and vegetation cover - Compiled from "Black Maps" 1856. *Digital Maps*. Available at: http://christchurchcitylibraries.com/Heritage/Maps/433589.asp [Accessed February 12, 2015].

Clough, R.W., 1990. Original formulation of the finite element method. *Finite Elements in Analysis and Design*, 7(2), pp.89–101.

Crampton, N.A., Bell, D.H. & Pettinga, J.R., 1988. Predicted and Actual Foundation Conditions, Rapaki Point Section, Lyttelton-Woolston LPG Pipeline, Christchurch, New Zealand. In *Fifth Australia-New Zealand Conference on Geomechanics: Prediction versus Performance*. Sydney, NSW: The Institution of Engineers, Australia, pp. 273–277.

Cruden, D.M., Thomson, S. & Hoffman, B.A., 1991. Observation of graben geometry in landslides. In R. J. Chandler, ed. *Slope Stability Engineering: Developments and Applications*. London: Thomas Telford Ltd, pp. 33–36.

Cruden, D.M. & Varnes, D.J., 1996. Landslide types and processes. In A. K. Turner & R. L. Schuster, eds. *Landslides: Investigation and Mitigation*. Washington D.C.: Transportation Research Board, pp. 36–71.

Cubrinovski, M., Green, R. A., Allen, J., Ashford, S., Bowman, E., Brendon, Bradley, Cox, B., Hutchinson, T., Kavazanjian, E., Orense, R., Pender, M., Quigley, M. & Wotherspoon, L., 2010. Geotechnical reconnaissance of the 2010 Darfield (Canterbury) earthquake. *Bulletin of the New Zealand Society for Earthquake Engineering*, 43(4), pp.243–320.

Dellow, G., Yetton, M., Massey, C., Archibald, G., Barrell, D.J. a, Bell, D., Bruce, Z., Campbell, A., Davies, T., De Pascale, G., Easton, M., Forsyth, P.J., Gibbons, C., Glassey, P., Grant, H., Green, R., Hancox, G., Jongens, R., Kingsbury, P., Kupec, J., Macfarlane, D., McDowell, B., McKelvey, B., McCahon, I., McPherson, I., Molloy, J., Muirson, J., O'Halloran, M., Perrin, N., Price, C., Read, S., Traylen, N., Van Dissen, R., Villeneuve, M. & Walsh, I., 2011. Landslides caused by the 22 February 2011 Christchurch earthquake and management of landslide risk in

the immediate aftermath. *Bulletin of the New Zealand Society for Earthquake Engineering*, 44(4), pp.227–238.

Duncan, J.D. & Wright, S.G., 2005. *Soil strength and slope stability*, Hoboken, New Jersey: John Wiley & Sons, Inc.

Everett, M.E., 2013. *Near-Surface Applied Geophysics* 1st ed., New York: Cambridge University Press.

Fang, H. & Fernandez, J., 1981. Determination of Tensile Strength of Soils by Unconfined-Penetration Test. *American Society for Testing and Materials Special Technical Publication 740*, pp.130–144.

Fang, H.W. & Chen, W.F., 1970. *New method for determination of tensile strength of soils*, Bethlehem, Pennsylvania.

Forsyth, P.J., Barrell, D.J.A. & Jongens, R., 2008. *Geology of the Christchurch Urban Area*, Lower Hutt, New Zeaaland: Institute of Geological and Nuclear Sciences.

Fredlund, D.G. & Rahardjo, H., 1993. *Soil mechanics for unsaturated soils*, New York: John Wiley & Sons, Inc.

GeoNet, 2015. GeoNet Quake Search. Available at: http://quakesearch.geonet.org.nz/ [Accessed October 5, 2015].

Gibbons, C.R. & Kingsbury, P.A., 2013. Earthquake-induced slope instability: Data collection and management for future planning and development. In *New Zealand Society for Earthquake Engineering Technical Conference and AGM*. Wellington, New Zealand.

Gipprich, T.L., Snieder, R.K., Jibson, R.W. & Kimman, W., 2008. The role of shear and tensile failure in dynamically triggered landslides. *Geophysical Journal International*, 172, pp.770–778.

Glassey, P.J., 1986. *Geotechnical properties of lime stabilised loess, Port Hills, Canterbury*. University of Canterbury.

GNS Science, 2014. Recent aftershock map. Available at: http://www.gns.cri.nz/gns/Home/Our-Science/Natural-Hazards/Recent-Events/Canterbury-quake/Recent-aftershock-map [Accessed October 10, 2015].

Goldwater, S., 1990. *Slope failure in loess: A detailed investigation, Allendale, Banks Peninsula.* Univeristy of Canterbury.

Greaves, G.N., Greer, a. L., Lakes, R.S. & Rouxel, T., 2011. Poisson's ratio and modern materials. *Nature Materials*, 10(11), pp.823–837.

Green, M., (in prep). *Hydrogeological investigation of earthquake related springs in the Hillsborough Valley, Christchurch, New Zealand*. University of Canterbury.

Griffiths, 1973. Loess of Banks Peninsula. *New Zealand Journal of Geology and Geophysics*, 16(3), pp.657–675.

Griffiths, D. V. & Lane, P.A., 1999. Slope stability analysis by finite elements. *Geotechnique*, 49(3), pp.387–403.

Hack, R., Alkema, A., Kruse, G.A.M., Leenders, N. & Luzi, L., 2007. Influence of earthquakes on the stability of slopes. *Engineering Geology*, 91, pp.4–15.

Hampton, S., 2010. *Growth, Structure and Evolution of the Lyttleton Volcanic Complex, Banks Peninsula, New Zealand*. University of Canterbury.

Hasegawa, H. & Ikeuiti, M., 1964. On the tensile strength of disturbed soils. In J. Kravtdrenco & P. M. Sirieys, eds. *Symposium on Reology and Soil Mechanics*. Berlin: Springer, pp. 405–412.

Holden, C., 2014. *Ground motion modelling of an Alpine fault earthquake and a hope fault earthquake for main South Island cities (NZ)*, Avalon, Wellington.

Hovius, N. & Meunier, P., 2012. Earthquake ground motions and patterns of seismically induced landsliding. In J. J. Clague & S. Douglas, eds. *Landslides: Types, Mechanisms and Modeling*. Cambridge: Cambridge University Press, pp. 24 – 34.

Hughes, T.J., 2002. *A detailed study of Banks Peninsula loess*. University of Canterbury.

Ishihara, K., 1985. Stability of natural deposits during earthquakes. In *Proceedings 11th International Conference on Soil Mechanicsand Foundation Engineering*. San Francisco, pp. 321 – 376.

Ives, D., 1973. Nature and distribution of loess in Canterbury, New Zealand. *New Zealand Journal of Geology and Geophysics*, 16(3), pp.587–610.

Jessberger, H.L. & Stone, K.J.L., 1991. Subsidence effects on clay barriers. *Géotechnique*, 41(2), pp.185–194.

Jibson, R.W., 2011. Methods for assessing the stability of slopes during earthquakes-A retrospective. *Engineering Geology*, 122(1-2), pp.43–50.

Jibson, R.W., 2012. Models of the triggering the landslides during earthquakes. In J. J. Clague & D. Stead, eds. *Landslides: Types, Mechanisms and Modeling*. Cambridge: Cambridge University Press, pp. 196 – 206.

Jibson, R.W., 1993. Predicting Earthquake-Induced Landslide Displacements Using Newmark's Sliding Block Analysis. In *Transportation Research Record*. Washington D.C.: Transportation Research Board, pp. 9–16.

Jibson, R.W., Rathje, E.M., Jibson, M.W. & Lee, Y.W., 2013. SLAMMER - Seismic LAndslide Movement Modelled using Earthquake Records (ver 1.1).

Kaiser, A., Holden, C., Beavan, J., Beetham, D., Benites, R., Celentano, A., Collett, D., Cousins, J., Cubrinovski, M., Dellow, G., Denys, P., Fielding, E., Fry, B., Gerstenberger, M.C., Langridge, R.M., Massey, C., Motagh, M., Pondard, N., McVerry, G., Ristau, J., Stirling, M., Thomas, J., Uma, S. & Zhao, J., 2012. 6.2 Christchurch earthquake of February 2011: preliminary report. *New Zealand Journal of Geology and Geophysics*, 55(February 2015), pp.67–90. Available at: http://www.tandfonline.com/doi/pdf/10.1080/00288306.2011.641182.

Kaiser, A., Massey, C. & Holden, C., 2014. *Site amplification, polarity and topographic effects in the Port Hills during the Canterbury earthquake sequence*, Lower Hutt, New Zeaaland.

Keefer, D.K., 1984. Landslides caused by earthquakes. *Geological Society of America Bulletin*, 94(April), pp.406–421.

Kelzieh, A., 1991. *The tensile strength of soils and its importance*. Arizona State University.

Kim, T.H., Kim, T.H., Kang, G.C. & Ge, L., 2012. Factors Influencing Crack-Induced Tensile Strength of Compacted Soil. *Journal of Materials in Civil Engineering*, 24, pp.315–320.

Krishnayya, A.V.G. & Eisenstein, Z., 1974. Brazilian Tensile Test for Soils. *Canadian Geotechnical Journal*, 11(4), pp.632–642.

Krishnayya, A.V.G., Eisenstein, Z. & Morgernstern, N., 1974. Behaviour of compacted soil in tension. *Journal of the Geotechnical Engineering Division*, 100, pp.1051–1061.

Leavell, D.A. & Peters, J.F., 1987. *Uniaxial Tensile Test For Soil*, Vicksburg, Mississippi, USA.

Leonards, G.A. & Narain, J., 1963. Flexibility of clay and cracking of earth dams. *Journal of the Soil Mechanics and Foundations Division*, 89, pp.47–98.

Loye, K., Evans, S.J., Lin, S.L. & Dhakal, R.P., 2013. Effect of soil type on seismic demand. In *Proceedings of the 2013 New Zealand Society Earthquake Engineering Technical Conference and AGM*. Wellington, New Zealand.

Lu, N. & Godt, J., 2013. *Hillslope Hydrology and Stability*, Cambridge: Cambridge University Press.

Lu, N. & Likos, W.J., 2006. Suction Stress Characteristic Curve for Unsaturated Soil. *Journal of Geotechnical and Geoenvironmental Engineering*, 132, pp.131–142.

M. Quigley, R. Van Dissen, P. Villamor, N. Litchfield, D. Barrell, K. Furlong, T. Stahl, B. Duffy, E. Bilderback, D. Noble, D. Townsend, J. Begg, R. Jongens, W. Ries, J. Claridge, A. Klahn, H. Mackenzie, A. Smith, S. Hornblow, R. Nicol, S. Cox, R. Langrid, K.P., 2010. Surface rupture of the Greendale fault during the Mw 7.1 Darfield (Canterbury) Earthquake, New Zealand: Initial findings. *Bulletin of the New Zealand Society for Earthquake Engineering*, 43(4).

Mackey, B.H. & Quigley, M.C., 2014. Strong proximal earthquakes revealed by cosmogenic 3 He dating of prehistoric rockfalls, Christchurch, New Zealand. *Geology*, 42(11), pp.975–978.

Makdisi, F.I. & Seed, H.B., 1978. Simplified procedure for estimating dam and embankment earthquake-induced deformations. *ASCE Journal of the Geotechnical Engineering Division*, 104, pp.849–867.

Massey, C.I., Lukovic, B., Mcverry, G., Yetton, M.D., Litchfield, N., Carey, J. & Ries, W., 2013. *Canterbury Earthquakes 2010/11 Port Hills Slope Stability: Stage 1 report on the findings from investigations into areas of significant ground damage (mass movements), GNS Science Consultancy Report 2012/317*, Available at: http://www.ccc.govt.nz/assets/Documents/Environment/Land/CR2012-317Stage1.pdf.

McDowell, B., 1989. *Site investigation for residential development on the Port Hills, Christchurch*. University of Canterbury.

McKenzie, N.J., Coughlan, K.J. & Cresswell, H.P. eds., 2002. *Soil physical measurement and interpretation for land evaluation*, Collingwood, Victoria: CSIRO Publishing.

Muller, J.R. & Martel, S.J., 2000. Numerical Models of Translational Landslide Rupture Surface Growth. *Pure and Applied Geophysics*, 157, pp.1009–1038.

Nahlawi, H., Chakrabarti, S. & Kodikara, J., 2004. A direct tensile strength testing method for unsaturated geomaterials. *Geotechnical Testing Journal*, 27(4), pp.356–361.

Newmark, N.M., 1965. Effects of earthquakes on damns and embankments. *Geotechnique*, 15, pp.139 – 159.

NZ Herald, 2011. Christchurch earthquake: Aerial photos, day two. Available at: http://www.nzherald.co.nz/christchurch-earthquake-photos/news/image.cfm?c_id=1503036&gal_cid=1503036&gallery_id=116939#7382536 [Accessed October 10, 2015].

NZ Police, 2012. List of deceased. Available at: http://www.police.govt.nz/major-events/previous-major-events/christchurch-earthquake/list-deceased [Accessed October 17, 2015].

O'Rourke, T.D., Jeon, S.S., Toprak, S., Cubrinovski, M. & Jung, J.K., 2012. Underground Lifeline System Performance during the Canterbury Earthquake Sequence. In *Proceedings of the 15th World Congress on Earthquake Engineering (15WCEE)*. Lisbon, Portugal.

Ogilvie, G., 2009. *The Port Hills of Christchurch* 3rd ed., Christchurch, New Zealand: Phillips and King Publishers.

Peron, H., Laloui, L., Hu, L.B. & Hueckel, T., 2009. Desiccation Cracking of Soils. *European Journal of Civil and Environmental Engineering*, 13(7), pp.869–888.

Petley, D., 2011. Boulder vs house – landslide losses in the Christchurch earthquake. *AGU Blogosphere*. Available at: http://blogs.agu.org/landslideblog/2011/02/26/boulder-vs-house-landslide-losses-in-the-christchurch-earthquake/ [Accessed October 10, 2015].

Petley, D.N., 2004. The evolution of slope failures: mechanisms of rupture propagation. *Natural Hazards and Earth System Sciences*, 4, pp.147–152.

Petley, D.N., Bulmer, M.H.K. & Murphy, W., 2002. Patterns of movement in rotational and translational landslides. *Geology*, 30, pp.719–722.

Petley, D.N., Higuchi, T., Petley, D.J., Bulmer, M.H. & Carey, J., 2005. Development of progressive landslide failure in cohesive materials. *Geology*, 33(3), pp.201–204.

Raeside, J.D., 1964. Loess deposits of the South Island, New Zealand, and soils formed on them. *New Zealand Journal of Geology and Geophysics*, 7, pp.811–838.

Ranjan, G. & Rao, A.S.R., 2007. *Basic and Applied Soil Mechanics*, New Age International.

Rathje, E.M. & Saygili, G., 2009. Probabilistic assessment of earthquake-induced sliding displacements of natural slopes. *Bulletin of the New Zealand Society for Earthquake Engineering*, 42(1), pp.18–27.

Rib, H.T. & Liang, T., 1978. Recognition and Identification. In R. L. Schuster & R. J. Krizek, eds. *Landslides - Analysis and Control: National Academy of Sciences Transportation Research Board Special Report 176*. Washington D.C.: Transportation Research Board, pp. 34–79.

Ring, U. & Hampton, S., 2012. Faulting in Banks Peninsula: tectonic setting and structural controls for late Miocene intraplate volcanism, New Zealand. *Journal of the Geological Society, London*, 169, pp.773–785.

Rohdewald, S., 2014. Rayfract [software]. Available at: http://rayfract.com/.

Roylance, D., 2008. Mechanics of materials. Available at: http://web.mit.edu/course/3/3.225/book.pdf [Accessed October 27, 2015].

Sandmeier, K.J., 2014. Reflex 2D-Quick [software]. Available at: http://www.sandmeier-geo.de/Reflex2DQuick.html.

Satyanarayana, B. & Rao, K.S., 1972. Measurement of tensile strength of compacted soil. *Geotechnical Engineering: Journal of the Southeast Asian Geotechnical Society*, 3(1), pp.61–66.

Snyder, V.A. & Miller, R.D., 1985. Tensile strength of unsaturated soils. *Soil Science Society of America Journal*, 49, pp.58–65.

Sowers, G.F. & Royster, D.L., 1978. Field Investigation. In R. L. Schuster & R. J. Krizek, eds. *Landslides - Analysis and Control: National Academy of Sciences Transportation Research Board Special Report 176*. Washington D.C.: Transportation Research Board, pp. 81–111.

Stark, T.D. & Choi, H., 2008. Slope inclinometers for landslides. *Landslides*, 5(3), pp.339–350. Available at: http://link.springer.com/10.1007/s10346-008-0126-3.

Stephen-Brownie, C., 2012. *Earthquake-Induced Ground Fissuring in Foot-Slope Positions of the Port Hills, Christchurch*. University of Canterbury.

Stirling, M., Gerstenberger, M., Litchfield, N., Mcverry, G., Smith, W., Pettinga, J. & Barnes, P., 2008. Seismic hazard of the Canterbury region, New Zeland: New earthquake source model and methodology. *Bulletin of the New Zeland Society for earthquake engineering*, 41(2), pp.51–67.

Suklje, L., 1969. *Rheological aspects of soil mechanics*, London: John Wiley & Sons, Inc.

Tamrakar, S.B., Mitachi, T. & Toyosawa, Y., 2007. Measurement of soil tensile strength and factors affecting its measurement. *Soils and Foundations*, 47(5), pp.911–918.

Tamrakar, S.B., Toyosawa, Y., Mitachi, T. & Itoh, K., 2005. Tensile strength of compacted and saturated soils using newly developed tensile strength and measuring apparatus. *Soils and Foundations*, 45(6), pp.103–110.

Tang, G. & Graham, J., 2000. A Method for Testing Tensile Strength in Unsaturated Soils. *Geotechnical Testing Journal*, 23, p.377.

Tehrani, B.H., 1988. *Chemical stabilisation of Whaka Terrace Loess, Christchurch*. University of Canterbury.

Terzaghi, K., Peck, R.B. & Mesri, G., 1996. *Soil mechanics in engineering practice* 3rd ed., New York: Wiley.

Tschebotarioff, G.P., Ward, E.R. & DePhilippe, A.A., 1953. The tensile strength of disturbed and recompacted soil. In *Proceedings of the 3rd International Conference on Soil Mechanics and Foundation Engineering*. Zurich, pp. 207–210.

Uchida, I. & Matsumoto, R., 1961. On the test of the modulus of rupture of soil samples. *Soil and Foundation*, 2(1), pp.51–55.

Eurocode 8 EN 1998-5., 2004. Design of structures for earthquake resistance Part 5: Foundations, retaining structures and geotechnical aspects.

Vaníček, I., 2013. The importance of tensile strength in geotechnical engineering. *Acta Geotechnica Slovenica*, 10, pp.5–17.

Varnes, D.J., 1978. Slope movement types and processes. In R. L. Schuster & R. J. Krizek, eds. *Landslides - Analysis and Control: National Academy of Sciences Transportation Research Board Special Report 176*. Washington D.C.: Transportation Research Board, pp. 12–33.

Wartman, J., Seed, R.B. & Bray, J.D., 2005. Shaking Table Modeling of Seismically Induced Deformations in Slopes. *Journal of Geotechnical and Geoenvironmental Engineering*, 131(5), pp.610–622.

White, C., in prep. *Untitled MSc thesis.* Univeristy of Canterbury.

Wilson, H.D., 1994. Regeneration of Native Forest on Hinewai Reserve, Banks Peninsula. *New Zealand Journal of Botany*, 32, pp.373–383.

Wilson, R.C. & Keefer, D.K., 1983. Dynamic analysis of a slope failure from the 6 August 1979 Coyote Lake, California, earthquake. *Bulletin of the Seismological Society of America*, 73(3), pp.863–877.

Win, S., 2006. *Tensile Strength of Compacted Soils subject to Wetting and Drying*. University of New South Wales.

Yetton, M.D., 1986. *Investigation and remedial methods for subsurface erosion control in Banks Peninsula Loess*. University of Canterbury.

Zhang, B., Li, Q., Yuan, H. & Sun, X., 2015. Tensile Fracture Characteristics of Compacted Soils under Uniaxial Tension. *Journal of Materials in Civil Engineering*, 27(10).